AD-A040 056 TERRA TEK INC SALT LAKE CITY UTAH F/G 8/7
CONSTITUTIVE PROPERTY INVESTIGATIONS IN SUPPORT OF FULL-SCALE P--ETC(U)
APR 77 D K BUTLER, R R NIELSEN, R K DROPEK DNA001-75-C-0177
UNCLASSIFIED WES-TR-S-77-3 NL

1 OF 2
AD
A040056

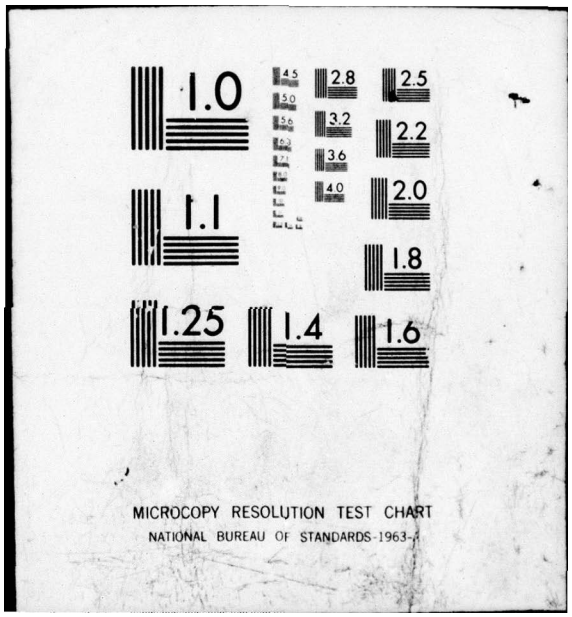
1.0
1.1
1.25
1.4
1.6
1.8
2.0
2.2
2.5
2.8
3.2
3.6
4.0
4.5
5.0
5.6
6.3
7.1
8.0
9.0
MICROCOPY RESOLUTION TEST CHART
NATIONAL BUREAU OF STANDARDS-1963-A

TECHNICAL REPORT S-77-3

CONSTITUTIVE PROPERTY INVESTIGATIONS IN SUPPORT OF FULL-SCALE PENETRATION TESTS IN DAKOTA SANDSTONE, SAN YSIDRO, NEW MEXICO

by

D. K. Butler

Soils and Pavements Laboratory
U. S. Army Engineer Waterways Experiment Station
P. O. Box 631, Vicksburg, Miss. 39180

and

R. R. Nielsen, R. K. Dropek, S. W. Butters
Terra Tek, Inc.
University Research Park, 420 Wakara Way
Salt Lake City, Utah 84108

April 1977
Final Report

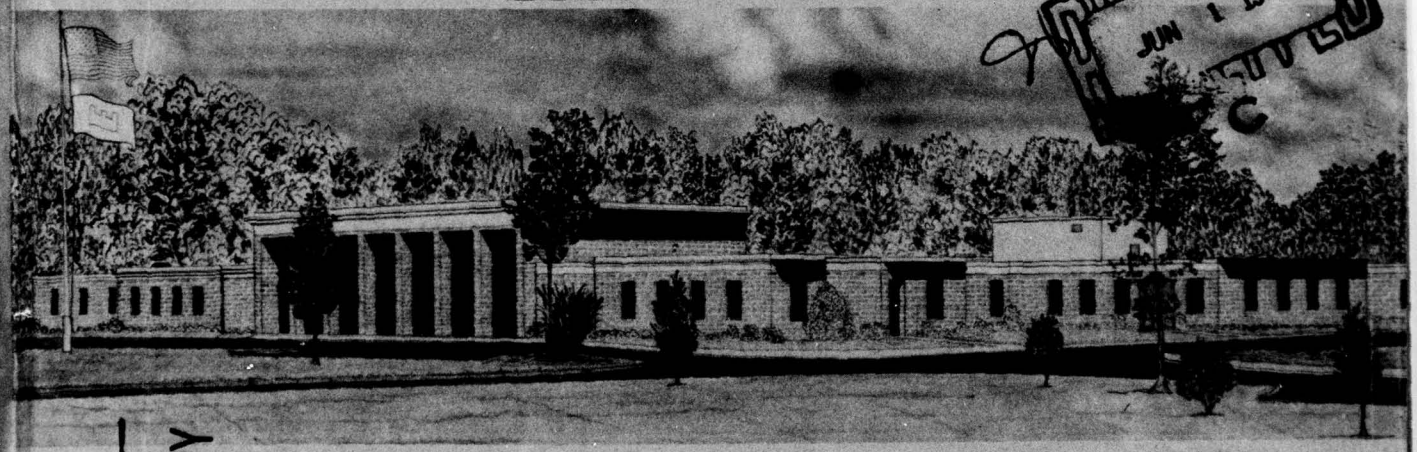

Prepared for Defense Nuclear Agency
Washington, D. C. 20305

Under DNA Subtask SB211, Work Unit 11
Field Firing Material Testing, and
Contract No. DNA 001-75-C-0177

Destroy this report when no longer needed. Do not return it to the originator.

Unclassified

SECURITY CLASSIFICATION OF THIS PAGE (When Data Entered)

REPORT DOCUMENTATION PAGE

READ INSTRUCTIONS BEFORE COMPLETING FORM

1. REPORT NUMBER: Technical Report S-77-3

2. GOVT ACCESSION NO.

3. RECIPIENT'S CATALOG NUMBER

4. TITLE (and Subtitle): CONSTITUTIVE PROPERTY INVESTIGATIONS IN SUPPORT OF FULL-SCALE PENETRATION TESTS IN DAKOTA SANDSTONE, SAN YSIDRO, NEW MEXICO

5. TYPE OF REPORT & PERIOD COVERED: Final report Apr 75-Apr 76

6. PERFORMING ORG. REPORT NUMBER

7. AUTHOR(s): Dwain D. K. Butler, R. K. Dropek, R. R. Nielsen, S. W. Butters

8. CONTRACT OR GRANT NUMBER(s): Contract No. DNA 001-75-C-0177

9. PERFORMING ORGANIZATION NAME AND ADDRESS: U. S. Army Engineer Waterways Experiment Station, Soils and Pavements Laboratory, P. O. Box 631, Vicksburg, Miss. 39180 (Continued)

10. PROGRAM ELEMENT, PROJECT, TASK AREA & WORK UNIT NUMBERS: DNA Substask SB211, Work Unit 11

11. CONTROLLING OFFICE NAME AND ADDRESS: Defense Nuclear Agency, Washington, D. C. 20305

12. REPORT DATE: April 1977

13. NUMBER OF PAGES: 149 (12) 145 p.

14. MONITORING AGENCY NAME & ADDRESS (if different from Controlling Office): (18) WES (19) TR-S-77-3

15. SECURITY CLASS. (of this report): Unclassified

15a. DECLASSIFICATION/DOWNGRADING SCHEDULE

16. DISTRIBUTION STATEMENT (of this Report)

Approved for public release; distribution unlimited.

17. DISTRIBUTION STATEMENT (of the abstract entered in Block 20, if different from Report)

18. SUPPLEMENTARY NOTES

This research was sponsored by the Defense Nuclear Agency under Subtask SB211, Work Unit 11, "Field Firing Material Testing," and Contract No. DNA 001-75-C-0177.

389 155

19. KEY WORDS (Continue on reverse side if necessary and identify by block number)

Constitutive models
Projectile penetration
Sandstones
Soil penetration tests
Stress-strain relations (Rock)

20. ABSTRACT (Continue on reverse side if necessary and identify by block number)

Results of a field and laboratory investigation of a proposed site for full-scale field projectile penetration tests are presented. The tests are part of the Defense Nuclear Agency's Earth Penetrating Weapon (EPW) Research Program. The site is located near San Ysidro, New Mexico, and the proposed target for the penetration tests is a large, exposed outcrop of Dakota sandstone. Results of the overall investigation will be used to construct

(Continued)

DD FORM 1 JAN 73 1473 EDITION OF 1 NOV 65 IS OBSOLETE

Unclassified

SECURITY CLASSIFICATION OF THIS PAGE (When Data Entered)

Copy

9. PERFORMING ORGANIZATION NAME AND ADDRESS (Continued)

Terra Tek, Inc.
University Research Park
420 Wakara Way
Salt Lake City, Utah 84108

20. ABSTRACT (Continued)

contitutive models of the sandstone for use in calculational studies of the in situ penetration events and of reverse ballistic tests that will employ large-diameter sandstone core obtained from the site during the course of the investigation.

The field investigation was designed to provide information about the in situ condition in the rock, and the laboratory test program was designed to study the mechanical behavior of the rock under a variety of stress and strain boundary conditions. The results of the laboratory program are analyzed and recommended constitutive properties are presented.

Appendix A discusses the in situ seismic survey. Appendix B presents the data plates for the dynamic tests conducted in the laboratory test program. The compression wave velocity measurements on large-diameter cores are listed in Appendix C, and Appendix D presents the results of the Terra Tek laboratory testing program.

PREFACE

This investigation was conducted during the period April 1975 - April 1976 by personnel of the Soil Dynamics Division (SDD) of the Soils and Pavements Laboratory (S&PL), U. S. Army Engineer Waterways Experiment Station (WES); Terra Tek, Inc. (TT), Salt Lake City, Utah; and Systems, Science and Software (S^3), La Jolla, California. The S^3 work will be reported separately. However, by direction from the Defense Nuclear Agency (DNA), the TT studies have been included in this report. The WES work was sponsored by DNA under Subtask SB211, Work Unit 11, "Field Firing Material Testing." The TT effort was funded by DNA, Contract No. DNA 001-75-C-0177, with MAJ Todd D. Stong as Contracting Officer's Representative.

This investigation was planned and the report prepared by Mr. D. K. Butler, SDD. Technical consultation and guidance were provided by Dr. P. F. Hadala, SDD. Messrs. L. L. Steen, A. L. Peeples, B. F. Wright, P. L. Collins, and R. A. Hammack, SDD, assisted with the various phases of the WES laboratory testing program. Messrs. J. R. Curro, Jr., E. Gomez, and D. H. Douglas of the Earthquake Engineering and Vibrations Division, S&PL, conducted the field geophysical survey. Appendix A, summarizing the geophysical survey, was prepared by Mr. Curro. The TT portion of the investigation is described in Appendix D, which was prepared by Messrs. R. R. Nielsen, R. K. Dropek, and S. W. Butters. The WES work was performed under the general supervision of Dr. J. G. Jackson, Jr., Chief, SDD, and Mr. J. P. Sale, Chief, S&PL.

COL G. H. Hilt, CE, and COL John L. Cannon, CE, were Directors of WES and Mr. F. R. Brown was Technical Director during the conduct of this investigation and the preparation and publication of this report.

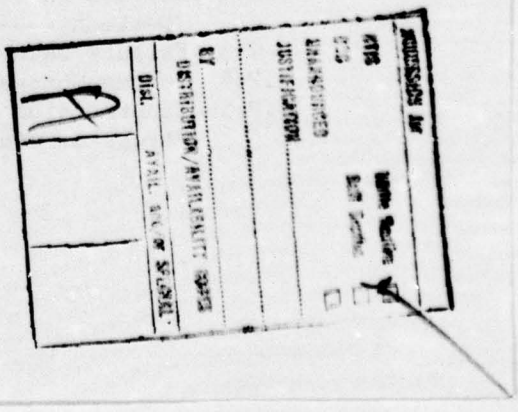

CONTENTS

CHAPTER 1

INTRODUCTION

1.1 BACKGROUND

The current Defense Nuclear Agency (DNA) Earth Penetrating Weapon (EPW) Research Program is concerned with assessing the survivability of candidate EPW's following impact and penetration into hard earth targets. Little is known regarding penetrator survivability as a function of impact velocity and target material properties for "hard" targets. Three targets, which may qualitatively be described as being low- to medium-strength rocks, were selected for full-scale field penetration tests to elucidate this area of terradynamics and to provide data to aid in future penetrator design considerations. The three targets were large outcrops of welded tuff, sandstone, and siltstone.

An outcrop of Thirsty Canyon welded tuff at a site located near Mount Helen on the Tonopah Test Range (TTR), Nevada, was selected as the first target. This is the strongest of the three rocks considered and, presumably, for a given impact velocity, a penetrator which survives penetration into the welded tuff would also survive in sandstone and siltstone. An outcrop of Dakota sandstone at a site near San Ysidro, New Mexico, was selected as the second target, and the siltstone site selected is located near Los Lunas, New Mexico. At each of these sites, Sandia Laboratories, Albuquerque (SLA), is scheduled to fire a series of instrumented 16.5-cm-diam, 182-kg penetrators into the in situ rock. The purposes of these tests are to assess survivability of the penetrators, determine depth of penetration and stresses in the target, and determine strains and accelerations in the penetrator. In addition, Avco Corporation will conduct a series of reverse ballistic tests using heavily instrumented penetrators and 38.1-cm-diam sandstone core from the San Ysidro site. For all three sites, pretest penetration predictions, posttest analyses, and detailed finite difference and finite element analyses of selected penetration tests will be performed by various agencies. To

support the analytical studies of the penetration tests, constitutive property investigations of the target materials are required. This report deals with such an investigation for the San Ysidro sandstone site which was conducted by the U. S. Army Engineer Waterways Experiment Station (WES), Terra Tek, Inc. (TT), and Systems, Science and Software (S^3).

1.2 PURPOSE

The purposes of this report are (1) to present the results of field investigations at the sandstone site near San Ysidro, New Mexico, (2) to present the results of laboratory tests on sandstone core from the site, and (3) to recommend constitutive properties for the sandstone based on the results of the field investigations and laboratory tests (for both the in situ condition and the large-diameter core). The constitutive properties are intended for use in developing constitutive models of the target materials.

1.3 SCOPE

The sandstone site field investigation (including the drilling and sampling program and field geophysical surveys) is described in Chapter 2. Chapter 3 presents the results of the laboratory test program on intact core specimens from the site and also gives the results of tests on the sandstone in a comminuted state. Constitutive property analyses for the sandstone are discussed in Chapter 4 and, finally, conclusions and recommendations are presented in Chapter 5.

CHAPTER 2

SITE INVESTIGATIONS AND RESULTS

2.1 SITE DESCRIPTION

The sandstone penetration test site is located about 19 km southwest of San Ysidro, New Mexico, and 80 km northwest of Albuquerque, New Mexico. A large and fairly massive outcrop of Cretaceous Dakota sandstone at the site will be the target for the field penetration tests. The outcrop is a cuesta with a gentle surface slope (dip slope) of about 10 degrees to the south, and the maximum height of the north scarp face is about 10 metres above the base. The outcrop is exposed on three sides, although there is considerable rubble about the base, and the surface disappears under overburden to the south.

The outcrop is a good penetration test site due to its remoteness from houses or major roads, its good vehicular access, and its relatively large surface area (≈100 metres by 100 metres) of completely exposed sandstone. Also, major fractures across the outcrop (striking approximately 30 degrees south of east) are spaced about 12 metres apart. There is a smaller, irregular "hexagonal-shaped" jointing pattern in the top surface of the sandstone with a typical scale dimension of about 1 metre. Some weathering has occurred along the major fractures, particularly near the sides of the outcrop, but the smaller scale joints are very tight.

The Dakota sandstone at the site is a light tan colored, fine- to medium-grained, calcite cemented quartzose sandstone. It is uniform in appearance on both the surface and the exposed portions of the sides of the outcrop, with the exception of a zone about 0.5 metre thick and 3 metres below the surface which is slightly lighter in color, harder, and exhibits a reaction with hydrochloric acid (HCℓ). All other sandstone at the site exhibits no reaction with HCℓ.

2.2 FIELD DRILLING AND SAMPLING PROGRAM

In April 1975, WES conducted a drilling program at the site described in Section 2.1. The purposes of the drilling program were:

(1) To determine the rock quality at the site (hence, the suitability of the site for the earth penetrator experiments).

(2) To obtain NX (4.5-cm-diam) core samples and 12.7-cm-diam steel tube samples to support laboratory material property investigations at WES and TT and sandstone-steel friction tests at S^3.

(3) To obtain two 0.38-m-diam by 0.62-m-long core samples for use in reverse ballistic tests at Avco Corporation.

(4) To select two penetrator impact points and drill seven instrumentation holes for SLA.

Figure 2.1 shows the site boring layout. Boreholes NX-1 and NX-3 are positioned approximately midway between two of the major E-W striking fractures, and a line joining boreholes NX-2 and U-1 is approximately perpendicular to a line joining NX-1 and NX-3. Logs and pertinent comments for the NX boreholes are given in Figure 2.2. Rock Quality Designation (RQD)[1] values for the three NX borings ranged from 63 to 100 percent with a weighted average for all the core runs of 82 percent. Boring U-1 was made with a 12.7-cm-diam steel tube sampler to a depth of 3.72 m (jar samples were taken at the end of each steel tube run). The NX core samples were coated with wax in the field to preserve the in situ water content, and the ends of the steel tubes were sealed with "O-ring" packers.

The sandstone varied from light tan (buff) color to nearly white with light gray to black marbling for the majority of the core recovered. A nominal 0.7-m-thick layer of bluish gray, "shaly" sandstone with black marbling was encountered at a depth of 8.32 m in NX-1 and at a depth of 6.91 m in NX-3. The light tan sandstone was encountered again at a depth of 7.61 m in NX-3. Yellow to orange staining (hematite or limonite coating) was present in some of the core, making it difficult to

determine at times whether core breaks were natural fractures with surface stains or a mechanical break through a pervasive stain region.

2.3 LARGE-DIAMETER SAMPLES

In addition to the small-diameter samples described in Section 2.2, two 0.38-m-diam by 0.62-m-long core samples were obtained at the site. These large-diameter sandstone samples will be used for reverse ballistic testing of instrumented penetrators by Avco Corporation. The samples were obtained completely intact with no evidence of either natural fractures or mechanical breaks. The condition of these large-diameter cores, the RQD values in boreholes NX-2 and NX-3, and the results of radiographic examination of the steel tube samples from borehole U-1 (which showed no fractures in the upper 2.2 m) suggest that there are no fractures in the sandstone for at least the upper metre of the site in the immediate vicinity of the proposed projectile impact points.

2.4 PENETRATOR IMPACT POINTS AND INSTRUMENTATION HOLES

Two penetrator impact points were selected (I and II in Figure 2.1) along a line joining borings NX-1 and NX-3. For each impact point, three 9.84-cm-diam holes were drilled. These will be used by SLA for the installation of in situ pressure gages prior to the planned penetration tests. Impact point II was located such that borehole NX-3 could also be used as an instrumentation hole. Specifications for the location of the instrumentation holes were supplied by SLA. In addition, an 18.7-cm-diam by 9.1-m-deep hole was drilled for SLA; the penetrators will be suspended in this hole for pretest checks of on-board telemetry systems.

2.5 GEOPHYSICAL SURVEYS

The WES Earthquake Engineering and Vibrations Division conducted a geophysical investigation of the site. The survey consisted of a surface seismic refraction survey, a downhole compressional (P)- and

shear (S)- wave velocity survey, and a crosshole P- and S-wave velocity survey. Figure 2.3 is a plan view of the seismic test layout. The surface refraction lines were 36 m long. Figures 2.4 and 2.5 are interpreted P- and S-wave velocity profiles between borings NX-2 and U-1, and Figures 2.6 and 2.7 are the corresponding profiles between borings NX-1 and NX-3. The P-wave profile indicates a two-layer structure at the center of the boring pattern. The S-wave profile, however, indicates a three-layer structure with velocity interfaces at 1.8 m and 4.6 m. P-wave velocities indicated by the downhole method average about 13 percent larger than the corresponding crosshole values, while the crosshole and downhole S-wave velocities are essentially the same. Comparison of surface refraction and crosshole P-wave velocities indicates that there is no horizontal direction dependence for compression waves. Appendix A contains the complete set of data from the seismic surveys.

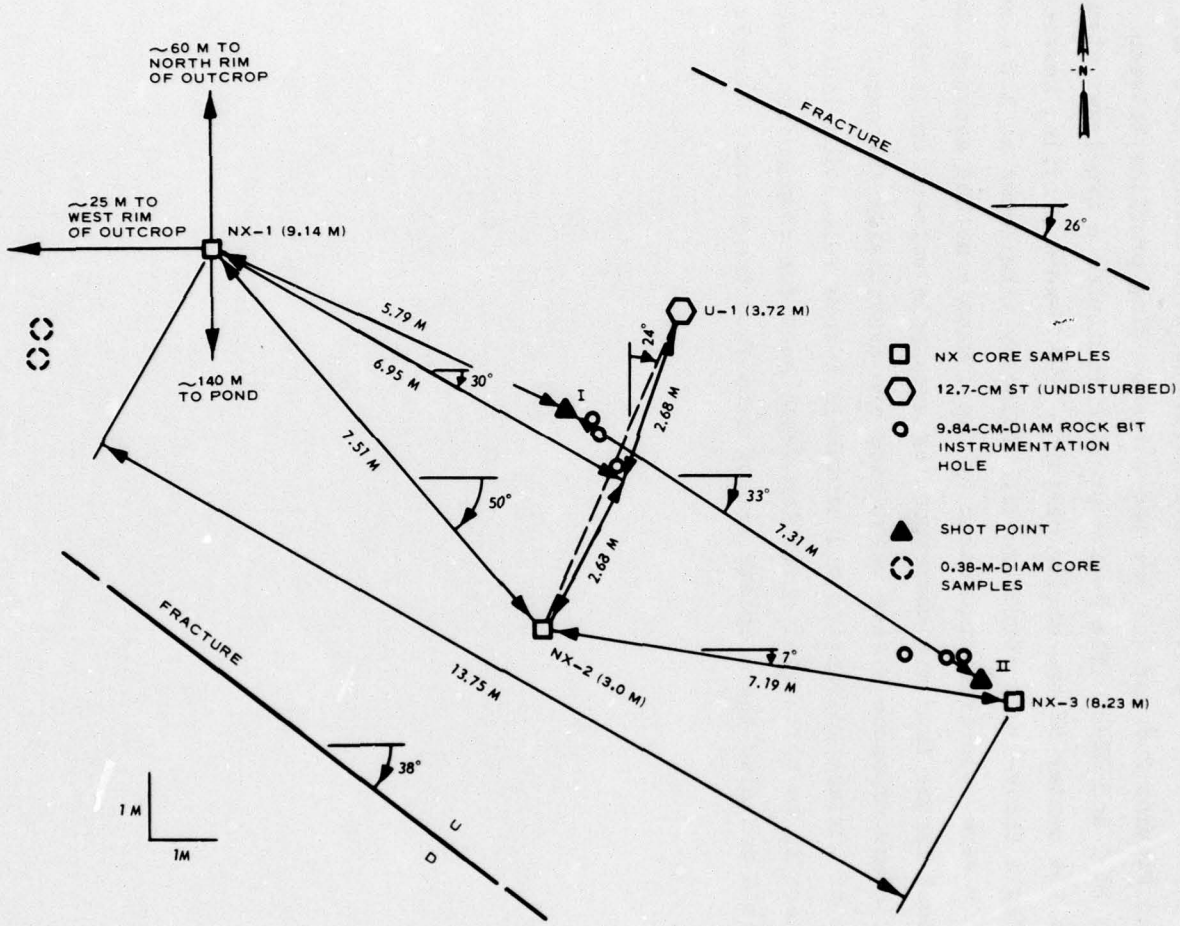

Figure 2.1. Sandstone site boring plan.

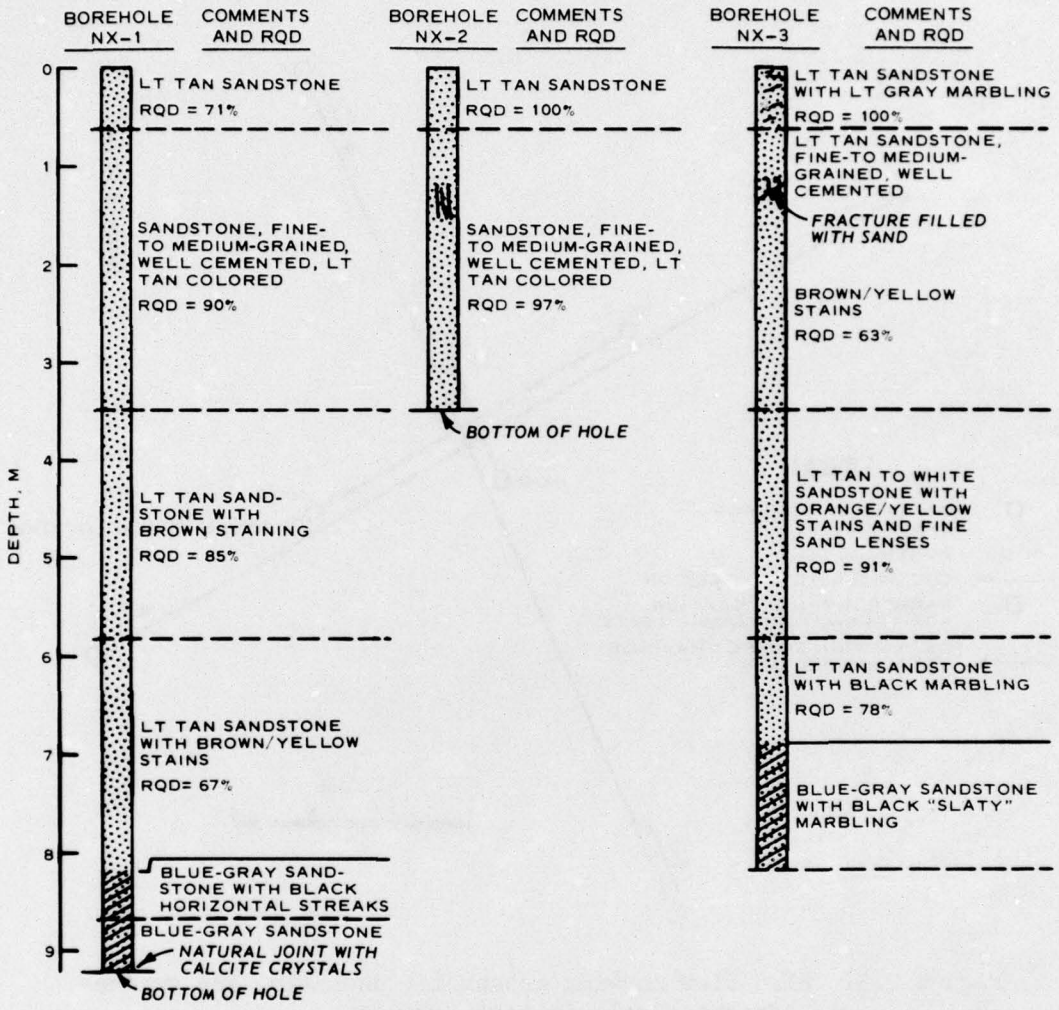

Figure 2.2. Boring logs for NX-1, NX-2, and NX-3.

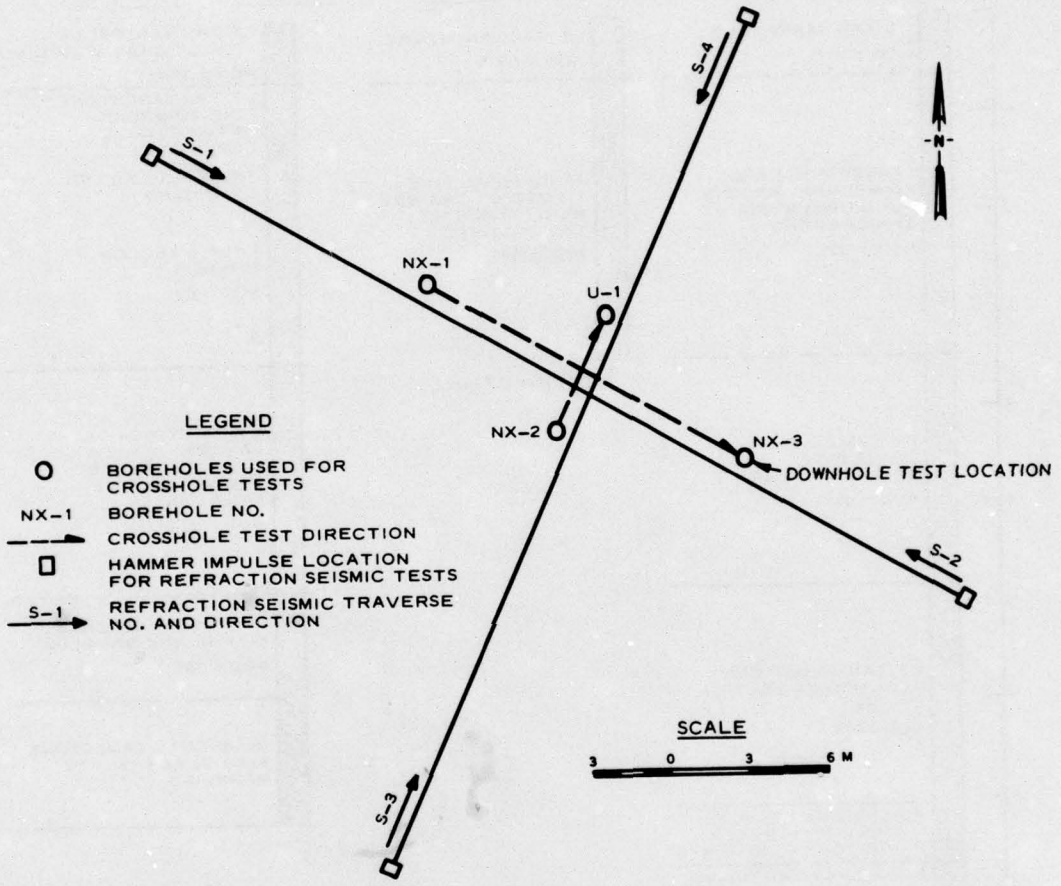

Figure 2.3. Plan view showing crosshole, downhole, and surface refraction seismic test layouts.

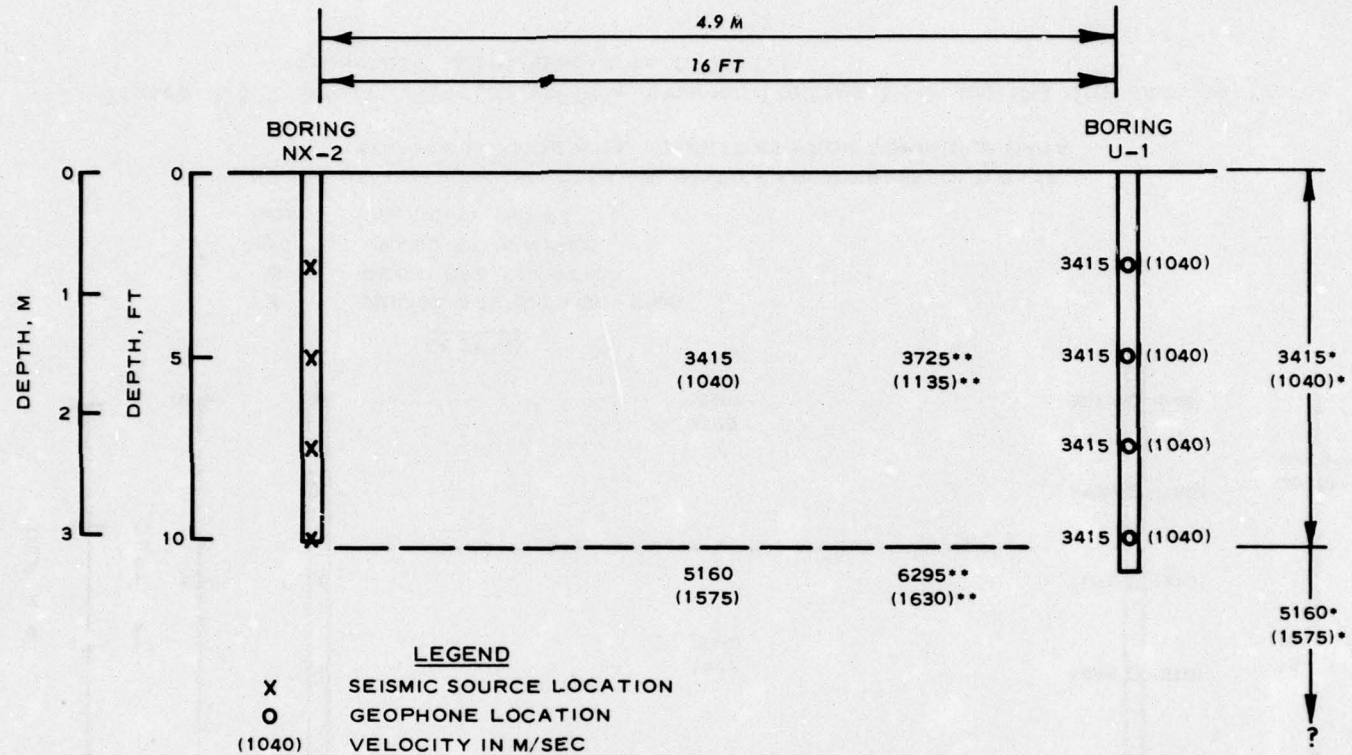

Figure 2.4. P-wave velocity profile between borings NX-2 and U-1 interpreted from surface refraction seismic, crosshole, and downhole test data.

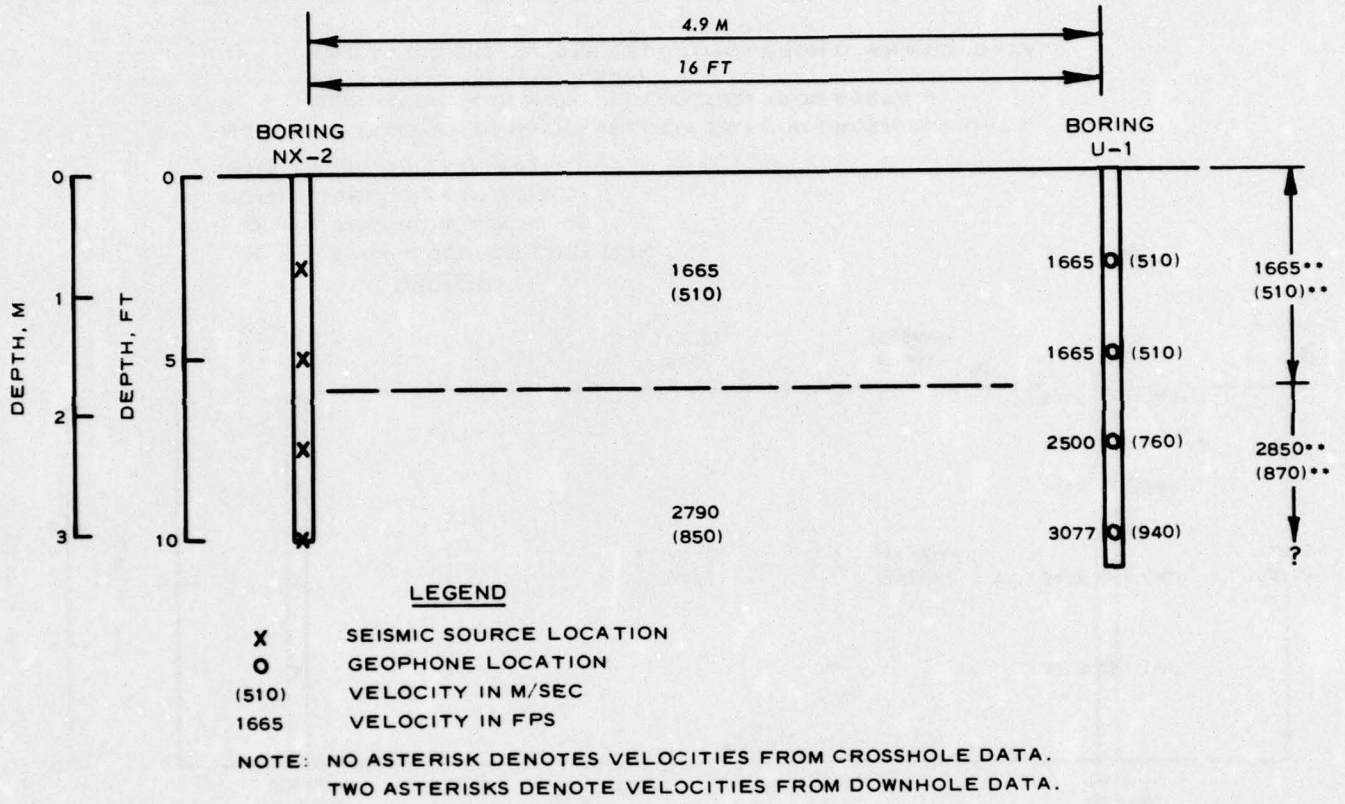

Figure 2.5. S-wave velocity profile between borings NX-2 and U-1 interpreted from crosshole and downhole test data.

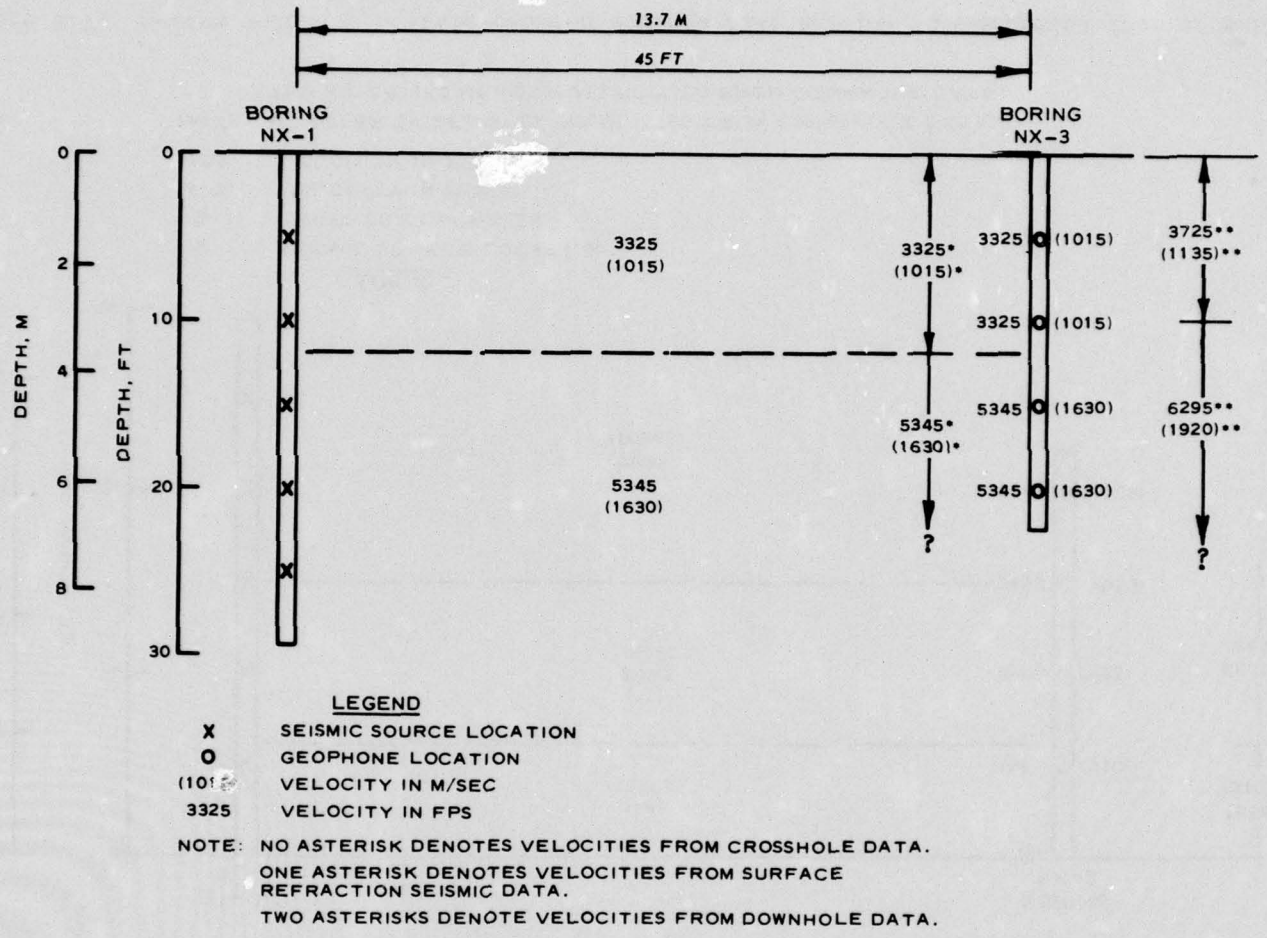

Figure 2.6. P-wave velocity profile between borings NX-1 and NX-3 interpreted from surface refraction seismic, crosshole, and downhole test data.

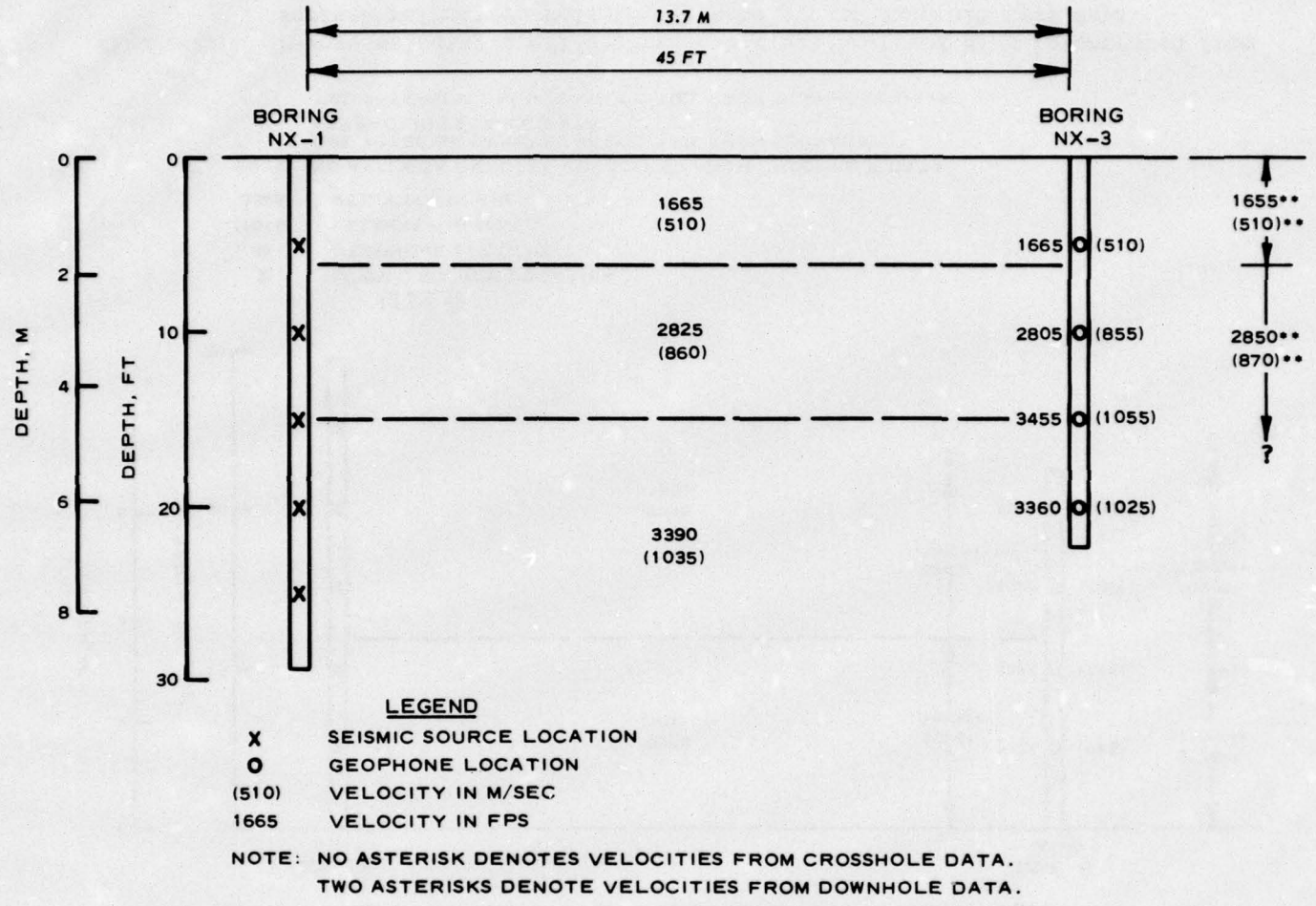

Figure 2.7. S-wave velocity profile between borings NX-1 and NX-3 interpreted from crosshole and downhole test data.

CHAPTER 3

LABORATORY TEST PROGRAM AND RESULTS

3.1 PHILOSOPHY OF TEST PROGRAM

The objective of the laboratory test program was to determine the behavior of the sandstone under a variety of stress and strain boundary conditions. Results of the test program will be used to develop temperature-independent constitutive models of the sandstone for pretest and posttest analyses and calculational studies of both the field penetration tests and the reverse ballistic tests into the large-diameter core. Since the constitutive models will be of varying degrees of sophistication, the test program was designed to supply data to support sophisticated modeling efforts.

Three agencies participated in the sandstone testing program: WES, TT, and S^3. WES conducted static (S)* and dynamic (D)* unconfined compression (UC) tests, uniaxial strain (UX) tests, undrained stress-controlled triaxial compression (TX) tests, direct pull tensile (T) tests, Brazilian tensile (BT) tests, hollow cylinder (HC) tests, and isotropic compression (IC) tests, as well as numerous tests to determine physical composition data as a function of depth for the site. TT conducted undrained static, strain-controlled triaxial compression (TX) tests, strain-controlled triaxial extension (TE) tests, uniaxial strain (UX) tests, and isotropic compression (IC) tests. S^3 conducted sandstone-on-steel friction tests at varying sliding velocities. Since most of the detailed calculational studies of the penetration tests will concentrate on the early time portions of the field penetration events and the reverse ballistic tests, the primary effort in the laboratory

---

* For purposes of this study, static tests are defined as those with strain rates of 10^{-4}/sec or a stress rate of approximately 1 kbar/min. Dynamic tests are defined as tests in which the stress rate is approximately 0.3 kbar/msec and in which inertial stresses are negligible.

test program involved core samples from the upper 3 to 4 m of the sandstone test site. In addition to determining the mechanical properties of the sandstone in an intact state, it is desirable to know the mechanical behavior of the sandstone in a mechanically altered or comminuted state.* Thus, a limited number of laboratory tests were conducted on mechanically crushed sandstone from the site.

3.2 TEST PROGRAM FOR INTACT SAMPLES AND RESULTS

Tables 3.1 and 3.2 list the laboratory tests conducted at WES and TT to characterize the mechanical properties of the Dakota sandstone from the penetration site. The test number scheme used in this report for the WES tests identifies the test type, whether static or dynamic, the borehole number, and the in situ depth of the sample in feet (1 m = 3.281 ft); for example, DTX-NX1-7.6 indicates a dynamic triaxial shear test on a sample from borehole NX-1 at a depth of 7.6 ft (2.3 m).

3.2.1 Classification and Composition Tests. Standard laboratory composition and classification tests were performed on selected specimens of the core samples (as received in the laboratory) from boreholes NX-1, NX-2, NX-3, and U-1 to determine wet density (γ_w), water content (w), and specific gravity of solids (G_s) of the sandstone. Results of these tests are plotted versus depth in Figure 3.1. Calculated values of dry density (γ_d), volume of voids (V_v), and volume of air (V_a) for each of the data points in Figure 3.1, assuming a constant value for G_s of 2.68, are plotted in Figure 3.2.

Figures 3.1a and 3.1b indicate that a wet density of about 2.08 g/cm^3 and a water content of 3 percent are representative of the

---

* Observations following full-scale field penetration tests have revealed concentric zones of rock failure: a comminuted zone adjacent to the penetrator grading into a brecciated zone which in turn grades into a zone of radial shear fractures. Detailed constitutive models of the target during impact often include a simulation of the degradation of the impact target properties to that of the comminuted target material and, therefore, data are required for both conditions.

upper 3 m of the site; below the 3-m depth, both γ_w and w appear to increase. The specific gravity of solids (grain density) appears to be relatively constant at about 2.68 to a depth of 9 m (Figure 3.1c). From Figure 3.2c, a value of 18 percent for the volume of air appears to be representative for the upper 3 m of the site; and from Figure 3.2a, a value of 2.02 g/cm^3 is representative for the dry density of the upper 3 m of the site.

3.2.2 Specimen Preparation for Intact Laboratory Testing. NX test specimens were cut from core segments with a diamond blade saw and then finished to the desired specimen length with a precision surface grinder. The greatest departure from planeness of any of the specimen ends was 0.015 cm, while the average value of the maximum departures from planeness for all the specimen ends was 0.008 cm. The specimen ends were perpendicular to the lateral surfaces within 0.4 degree, and the ends of the specimens were parallel within 0.4 degree. The exposure time of each end of the specimens to air was about five minutes.

3.2.3 Sources of Error and Estimated Error Levels. There are three types of measurement systems and functions in the laboratory IC, TX, and UX tests: pressure, load, and deformation. In these measurements, the three sources of random error are calibration error, output error, and operator error. Pressure cells (for determining confining pressures in IC and TX tests) are calibrated with a precision dead load tester and, in general, pressure values are considered accurate within ± 2 percent on the average. Load cells are calibrated with precision proving rings and are considered accurate within ± 3 percent (including possible pressure effects). In data analysis, however, it is not loads but stresses which are required (utilizing the deformed specimen cross-sectional area). Deformation measurements are made with linear variable differential transformers (LVDT's) and bonded strain gages. For LVDT measurements, all sources of random error (including nonlinearity, electronic instrumentation errors, reading errors, etc.) are considered to be small compared to those systematic errors associated with specimen irregularities (see Section 3.2.2) and apparatus

compressibility. For vertical deformation, this is sometimes referred to as a "seating error" and 0.008 cm can be taken as the worst case deformation error for vertical deformation (or 0.06 percent strain for a 12.7-cm-high specimen) due to these sources. For lateral deformation measurements, the LVDT probes contact the rubber membranes and a further source of error may be the compression of the membranes; however, the membranes also smooth out specimen irregularities and, in general, the error for lateral deformation measurements should be no greater than the worst case error for vertical measurements. Since the maximum strains in the IC and UX tests were less than 2 percent and the maximum principal strain differences in the TX tests were 4 percent, the percent error due to this source could be as high as 15 percent. When this measurement system is used on more compliant specimens, the percent error would, of course, decrease. Sources of error for strain gage measurements of strains include nonlinearity, imperfect bonding to specimen, air bubbles between gage and specimen, cross-axis sensitivity, hysteresis, imperfect temperature compensation, etc. Experience has shown that, with careful attention to details of application, strain gages are both precise and accurate when not strained beyond their intended range and when test times are not so long that creep and fatigue must be considered. The levels of error are comparable to those in the pressure measurements (2 to 3 percent). Indeed strain gage measurements are commonly used to check and even correct LVDT measurements.

Only the "seating error" and other errors due to specimen irregularities, membrane compressibility, and apparatus compressibility are readily identified as being cumulative errors (as contrasted with random errors). These cumulative errors tend to bias somewhat the deformation data (hence, calculated strain data) to larger values of calculated volumetric strain. Volumetric strains in this report have been calculated assuming that the specimens deform as right circular cylinders and this, in turn, defines the cross-sectional areas to be used for vertical stress calculations. For the small strains ($\approx$2 percent maximum strain) experienced by the sandstone specimens in the WES tests, errors caused

by this particular deformed shape assumption compared, for example, with the assumption of two truncated cones, are very small (≈0.1 percent strain at maximum). These comments on possible errors are intended to cause readers to view test data with a "healthy caution." The possible effects of errors on interpreted data and recommended properties are discussed further in Chapter 4.

3.2.4 Unconfined Compression Tests and Sonic Velocities. Twelve NX (5.4-cm-diam by 12.7-cm-long) specimens were selected for unconfined compression tests and sonic velocity determination. The 12 specimens were air-dried for 48 hours prior to measuring sonic velocities and were then tested in unconfined, uniaxial compression. Both compression wave velocity (V_p) and shear wave velocity (V_s) were determined in the axial direction of the core specimens using ceramic transducers. Results of the sonic velocity measurements are plotted versus depth in Figure 3.3, and Figure 3.4 presents the unconfined compressive strength of the specimens versus depth. The symbols with a slash through them indicate that prior to testing the specimens represented by these symbols were observed to have a tight horizontal crack. The presence of the cracks in the specimens does not appear to have had a significant effect on the measured sonic velocities and unconfined strengths. For the unconfined compression tests on the specimens without cracks, axial deformation was measured; and, for these cases, the tangent modulus of elasticity at 50 percent of the unconfined compressive strength (E_{T50}) is plotted versus depth in Figure 3.5.

3.2.5 Isotropic (Hydrostatic) Compression Tests. Both static and dynamic isotropic compression (IC) tests were conducted on NX-diameter specimens which were nominally 7.6 cm in length. The specimens were jacketed in a 0.064-cm-thick rubber membrane immediately after removing the wax coating. The deformations during loading were measured with both lateral and vertical LVDT's and bonded strain gages. The strain gage deformation measurements were used to confirm and possibly correct the LVDT deformation measurements. For the static IC tests, the maximum pressure attainable was about 0.7 kbar, with intermediate load-unload

cycles. The maximum pressure attainable in the dynamic IC tests was about 1.0 kbar, with no intermediate load-unload cycles. Descriptions of the test device used for the static and dynamic IC tests (also for the triaxial shear tests to be discussed later) can be found in Reference 2. In addition to the IC tests on NX core samples, one IC test was performed on a 12.7-cm-diam by 25.4-cm-long sandstone specimen to a maximum pressure of 0.3 kbar (test SIC-U1-4.9).

Figure 3.6 presents pressure versus engineering volumetric strain for three static IC tests. Only one of the intermediate load-unload cycles is shown. Also given in Figure 3.6 for comparison are data from the IC loading phase of the static TX tests discussed in the next section. The curves are essentially parallel above a pressure of 0.15 kbar. The pressure versus volumetric strain curves stiffen with increasing pressure up to mean normal pressures of at least 0.5 kbar. Permanent compaction following unloading from 0.7 kbar appears to be about 0.45 percent volumetric strain for the static IC case.

The dynamic IC results are presented in Figure 3.7 (along with results of the IC phase of a dynamic TX test). The rate of application of pressure to the specimens in these tests was of the order of 0.1 kbar/msec. Scatter in the results for these four tests is quite small ($\approx$0.15 percent volumetric strain at a pressure of 0.1 kbar). The curves stiffen with increasing pressure to the maximum level experienced in the tests (1.0 kbar). Permanent compaction following unloading from 1.0 kbar is about 0.35 percent volumetric strain. Data plates for individual tests are contained in Appendix B.

Comparison of the static and dynamic IC test results (Figures 3.6 and 3.7) shows the scatter in the two sets of test results to overlap. In general, the dynamic mean normal pressure versus volumetric strain curves have larger initial slopes than the static curves, although the slopes are comparable at pressures above about 0.15 kbar. The exception is the curve for static test SIC-U1-4.9 (12.7-cm-diam specimen), which has an initial slope as large as any of the dynamic curves. Hysteresis is somewhat more pronounced in the static test results. If

the static and dynamic results are considered as a composite set of data, the scatter in the results is not unreasonable for test specimens from different boreholes and varying depths. In general, the dynamic IC curves define the upper bound of the scatter band, and rate effects in IC (at least for a rate of loading of the order of 0.1 kbar/msec) appear to be limited to a larger initial loading bulk modulus and slightly less hysteresis.

3.2.6 Triaxial Compression Tests. Static and dynamic triaxial compression (TX) tests were conducted on NX-diameter specimens 12.7 cm long. As in the IC tests, the specimens were jacketed in rubber membranes prior to testing and no drainage was allowed during the test. For the TX tests, a confining pressure was first applied to the specimen (IC phase); then the specimen was loaded axially in compression to failure while holding the confining pressure constant (shear phase). Deformation measurements were made primarily with LVDT's although vertical strain gages were also used in some of the static TX tests. Results of the TX tests can be interpreted to yield loading and unloading shear moduli, deviatoric stress-strain behavior, shear strengths, failure relations, Poisson's ratio, and information regarding compaction or expansion (dilatation) of the specimen in shear.

Results of the static TX tests are presented in Figure 3.8. Several important facts can be deduced from a cursory examination of these results: the slope of the deviatoric stress-strain curves (twice the loading shear modulus) increased with increasing confining pressure; the strengths of the specimens (the maximum deviatoric stress attained in a test) increased with increasing confining pressure; average deviatoric strain to failure was approximately 1.4 percent for all the tests; and dilatation occurred for all the tests, the amount of dilatation decreasing with increasing confining pressure. Figure 3.9 presents the results of a static special stress path (SSP) test (test STX-NX2-7.5) in which the specimen was (1) loaded in IC to 0.3 kbar, (2) loaded axially to a deviatoric stress somewhat below the expected strength for that confining pressure, and then (3) subjected to a constant axial load

at that magnitude as the confining pressure was decreased until failure occurred. The specimen was observed to change in its deviator stress-strain response immediately upon decreasing the confining pressure and exhibited a more ductile response. Also, upon decreasing the confining pressure, the specimen first unloaded on the loading mean normal pressure-volumetric strain and then dilated prior to failure at a deviator stress consistent with the failure envelope defined by the standard TX test results.

The dynamic TX test results are presented in Figure 3.10. These curves are smoothed versions of the test results; individual test data plates (unsmoothed) and time history plates are presented in Appendix B. A cursory examination of Figure 3.10 reveals that: loading shear modulus increased with confining pressure; shear strength increased with confining pressure; dilatation occurred in shear prior to failure (for test DTX-NX1-8.0, the specimen first dilated and then compacted prior to failure*); and average deviatoric strain to failure was about 1.2 percent. It should be noted that failure did not occur in test DTX-NX1-9.6A; the same specimen was later tested and failed at a lower confining pressure (test DTX-NX1-9.6B). The average rate of deviatoric stress increase for the tests was 0.15 kbar/msec. Also, due to the dynamic nature of the tests, the loading device was able to "follow" the deformation of the specimens into the postfailure region of behavior. For the three tests with confining pressure, a "residual" strength was defined which was one-third to one-half of the peak strength.

Comparison of the static and dynamic TX test results indicated no significant rate effects: strengths (peak deviator stresses) were comparable at similar confining pressures; initial loading shear moduli were comparable at similar confining pressures; and deviator strains to failure were comparable for all the tests. Dilatation occurred in both the static and dynamic test shear phases, but in the dynamic tests the

---

* This type of response can be due to a fortuitous location of one or more of the lateral LVDT's in relation to the failure region, and thus the response may not represent true material behavior.

amount of dilatation did not appear to decrease with increasing confining pressure as it did in the static tests.

3.2.7 Uniaxial Strain Tests. Two static and one dynamic uniaxial strain (UX) tests were conducted on specimens 6.4 cm in height by 12.7 cm in diameter from borehole U-1. The specimens were tested in vertical compression with a rigid lateral constraint, i.e., essentially no lateral strains.* Details regarding the testing method and the UX test device are given in References 3 and 4. Results of the UX tests are presented in Figure 3.11 in the form of vertical stress versus vertical strain plots. One of the static curves and the dynamic curve agree closely, while the other static curve exhibits smaller slopes (larger strains) in loading. The unloading curves for all three curves agree substantially in slope. An unsmoothed data plate for the dynamic UX test is presented in Appendix B.

3.2.8 Tensile Strength Tests. Three types of tests were conducted to obtain information about the strength of the sandstone in tension: direct pull tensile tests, Brazilian tensile tests, and hollow cylinder tests. The direct pull tensile test method (ASTM Designation: D2936-71) consists of attaching metal end caps to the test specimens (NX by 12.7 cm) with epoxy and then applying a tensile force to the end caps until the specimen fails in uniaxial tension, usually along a plane perpendicular to the specimen axis. The tensile strength σ_T in the direct pull test is then calculated by dividing the maximum applied tensile force by the specimen cross-sectional area. In the Brazilian tensile test (ASTM Designation: C496-71), a line load is applied to the lateral surface of a cylindrical specimen (diameter D and length L) parallel to the specimen axis. Although the distribution of stresses in the Brazilian test is complicated, rupture usually occurs along the main diameter, and in the center of the specimen the compressive and tensile stresses, σ_1 and σ_3, respectively, on the plane of rupture are easily calculated. The hollow cylinder test uses a thick-walled cylinder configuration

---

* With the WES dynamic UX test device, the condition of zero lateral strain may not be realized for tests on rock.

and determines the internal pressure P required to rupture the test specimens. This method produces a radial compressive stress ($\sigma_1 = \sigma_r$) and a circumferential tensile stress ($\sigma_3 = \sigma_\theta$), and failure commonly occurs on a plane containing a specimen diameter and the specimen axis. A simpler interpretation of the hollow cylinder test is to assume only a uniform tensile stress σ_T to exist perpendicular to the failure plane.

Results of the three types of tensile tests are summarized in Table 3.3. These results will be used later in specifying a failure envelope for the sandstone. The sandstone is observed to be considerably weaker in tension than in compression. It is noteworthy that tensile strengths computed by using the simpler interpretation of the hollow cylinder test are comparable to tensile strengths observed in the direct pull tests.

3.2.9 Size Effect Study. In order to determine if the measured mechanical response of the sandstone is dependent on test specimen size, a very limited size effect study was conducted. This study was intended to give guidance in the specification of constitutive properties for the large-diameter core and was not intended as an exhaustive size effect study. The results of a static IC test on a 12.7-cm-diam by 27.2-cm-long test specimen are presented in Figure 3.6 and briefly discussed in Section 3.2.5. Also, in addition to the 12 static UC tests on NX by 12.7-cm test specimens, four static UC tests were conducted on 3.6-cm-diam by 7.1-cm-long specimens and one test was conducted on a 12.7-cm-diam by 27.2-cm-long specimen (see Table 1). Figure 3.12 presents the results of the UC size effect study. The one data point for a 12.7-cm-diam specimen is interpreted as a lower bound on the strength since, due to nonplanarity of one specimen end, failure was initiated as a progressive "crumbling" at the loading platen specimen contact.

3.2.10 Compression Wave Velocity Measurements on Large Core. The only nondestructive laboratory test which could conveniently be conducted

on the two pieces of large-diameter sandstone core was the measurement of wave velocities in the specimens. It was desirable to obtain velocity measurements using both an impulsive source (corresponding to the type of source used in the field seismic survey) and a vibratory source (1-MHz piezocrystal corresponding to the laboratory ultrasonic method). It proved to be impossible to detect a signal (at the receiver) using a piezocrystal source; so, as a substitute, a device called a "soniscope," which uses a 20-kHz vibratory source, was utilized. Two types of impulsive sources were used: a hammer impacting a steel rod and a Schmidt hammer. Table 3.4 summarizes the results of axial compression wave-velocity measurements on the first core and both axial and radial measurements on the second core. A complete listing of test results using impulsive sources is presented in Appendix C. Comparison of the radial and axial measurements on core No. 2 reveals no significant anisotropic, geometric, or path length effect on the compression wave velocity. Comparison of values (2) and (3) in Table 3.4 for core No. 2 reveals no measurement dependence on receiver response frequency for a two decade change. However, comparison of values (3) and (4) indicates a velocity dependence on the type of impulsive source, although this conclusion is obscured by the fact that a simple contact switch was used as an oscilloscope trigger for the hammer source and an accelerometer was used as a trigger for the Schmidt hammer source.

3.2.11 Terra Tek Test Results for Intact Specimens. WES shipped the majority of the core from boring NX-3 to TT to support their portion of the laboratory testing program (as presented in Table 3.2). The results of the TT test program are presented in Appendix D. Three figures from Appendix D are presented in this section also. Figure 3.13 is the hydrostatic compression (IC) response to 8 kbar for the sandstone. Notable in this response is the pronounced softening in the hydrostat about 1 kbar and a permanent set (compaction) of approximately 4 percent on unloading from 8 kbar. Figure 3.14 presents the results of static, strain-controlled TX compression tests at confining pressures of 0, 0.5,

1, and 3 kbar; the data plotted here in deviatoric stress-strain space were obtained from Figure 1 of Appendix D. Failure data from the TX tests (from the TX compression tests of Figure 3.14 and also two TX extension tests (Figure 3, Appendix D)) are plotted in Figure 3.15.

3.2.12 S^3 Sandstone-on-Steel Interface Friction Testing Program. WES supplied S^3 with 3.5-cm-diam by 4.5-cm-long specimens of the sandstone to support their sandstone-on-steel interface friction test program. The purpose of the program was to determine the friction coefficient of the sandstone on steel as a function of relative interface velocity and normal stress. These data will be used to support the development of friction rules to apply to the penetrator-target interface during analytical calculations of the penetration events. Descriptions of the test apparatus and test procedure are given in Reference 5, and the results of interface friction tests on air-dry specimens of the sandstone are presented in Reference 6.

3.3 TEST PROGRAM FOR COMMINUTED MATERIAL AND RESULTS

The WES and TT laboratory test program for comminuted sandstone is outlined in Table 3.5. Sandstone core from the site was mechanically crushed to sand-sized particles and a portion of the original batch of crushed material was shipped to TT. Figure 3.16 is a gradation curve for the crushed sandstone prior to testing. The tests were conducted on specimens of air-dried material. The specimens were remolded on the specimen base cap of the TX test device in rubber membranes surrounded by a forming jacket for the WES tests. A vacuum was maintained in the specimens after removing the forming jacket and prior to testing to prevent the cohesionless specimens from slumping under their own weight. The average density of the specimens was 1.6 g/cm^3 or 77 percent of the intact sandstone density.

Four static stress-controlled TX tests were conducted on the crushed material at WES. Both the IC and the shear phases of the tests were cycled in order to obtain load-unload information. Figures 3.17 and

3.18 present the results of the IC and shear phases, respectively, of the four tests. Posttest gradation analyses were performed on the specimens; the results are plotted in Figure 3.16. The results of the gradation analyses do not indicate a consistent trend of additional grain crushing occurring as a result of the tests.

Results of the two TT tests on the comminuted material are discussed in Appendix D. The failure data points from the TT triaxial compression tests are included in Figure 3.15. Gradation analyses were conducted following isotropic compression to 1 and 4 kbar and the results are presented in Figure 9 of Appendix D.

TABLE 3.1 WES LABORATORY TEST PROGRAM FOR INTACT SPECIMENS

Test Type	Static (S) or Dynamic (D)	Number of Tests	Specimen Size	Remarks
IC	S	3	NX* by 7.6 cm	Cycled isotropic (hydrostatic) compression tests to ≈1 kbar. Both LVDT's and bonded strain gages used to measure strains.
IC	S	1	12.7 cm diam by 27.2 cm	Isotropic compression test (loading only) to ≈1/4 kbar.
IC	D	3	NX by 7.6 cm	Isotropic compression (load-unload) tests to ≈1 kbar.
TX	S	6	NX by 12.7 cm	Triaxial compression tests. Confining pressures of 0, 0.05, 0.15, 0.28, and 0.48 kbar and a special stress path test. LVDT's used to measure strains. Some tests also employed vertical bonded strain gages.
TX	D	5	NX by 12.7 cm	Triaxial compression tests. Confining pressures of 0, 0.05, 0.15, and 0.35 kbar.
UX	D	1	12.7 cm diam by 6.4 cm	Uniaxial strain test to 0.14 kbar.
UX	S	2	12.7 cm diam by 6.4 cm	Cycled uniaxial strain to 0.14 kbar.
BT	S	3	NX by 12.7 cm	Brazilian tensile tests.
T	S	3	NX by 12.7 cm	Direct pull tensile tests.

(continued)

* NX specimens are 5.4 cm in diameter

TABLE 3.1 (CONCLUDED)

Test Type	Static (S) or Dynamic (D)	Number of Tests	Specimen Size	Remarks
HC	S	2	NX OD by 0.66 cm ID by 7.6 cm long	Hollow cylinder tensile tests.
UC	S	12	NX by 12.7 cm	Unconfined, uniaxial stress tests. Air-dried specimens.
UC	S	4	3.6 cm diam by 7.1 cm	Unconfined, uniaxial stress tests. Air-dried. Part of limited size effect study.
UC	S	1	12.7 cm diam by 27.2 cm	Unconfined, uniaxial stress test. Air-dried. Part of limited size effect study.
V_S	-	12	NX by 12.7 cm	Sonic velocities, compression and shear. Conducted on specimens prior to the UC tests.
Composition	-	Numerous	-	Numerous standard physical property tests such as wet and dry density, grain specific gravity, and water content, to determine composition properties as a function of depth.

TABLE 3.2 TT LABORATORY TEST PROGRAM FOR INTACT SPECIMENS*

Test Type	Number of Tests	Specimen Size	Remarks
TX	9	NX by 10.2 cm	Strain-controlled. Confining pressures of 0, 0.5, 1, and 3 kbar. Strain-gaged, cantilevered, spring arms used to measure strains.
TC	3	NX by 10.2 cm	Strain-controlled. Confining pressures of 1 and 2 kbar.
IC	3	NX by 10.2 cm	To 8 kbar.
UX	3	NX by 10.2 cm	

* See Appendix D.

TABLE 3.3 TENSILE STRENGTH TEST RESULTS

Test Type	Individual Test Results kbar				Mean Values
	Test No.	σ_1	σ_3	σ_T	
Direct pull	T-NX2-6.4	-	-	-0.0058	σ_T = -0.0063 kbar
	T-NX1-8.8	-	-	-0.0045	
	T-NX2-8.5	-	-	-0.0086	
Brazilian tensile	BT-NX2-6.0	0.0342	-0.0114	-	σ_1 = 0.0369 kbar
	BT-NX2-5.5	0.0393	-0.0131	-	σ_3 = -0.0123 kbar
	BT-NX2-9.0	0.0372	-0.0124	-	
Hollow cylinder	HC-1	0.0690	-0.0710	-0.0096	σ_1 = 0.0669 kbar
	HC-2	0.0648	-0.0668	-0.0089	σ_3 = -0.0689 kbar
					σ_T = -0.0092 kbar

TABLE 3.4 SUMMARY OF COMPRESSION WAVE VELOCITY MEASUREMENTS ON LARGE-DIAMETER CORE

Average Measured Compression Wave Velocity			
Axial m/sec	Radial m/sec	Source	Receiver
		Core No. 1	
(1) 1180	-	Hammer	10-kHz accelerometer
		Core No. 2	
(2) 1100	-	Hammer	10-kHz accelerometer
(3) 1090	-	Hammer	1-MHz piezocrystal
(4) 1330	-	Schmidt hammer	1-MHz piezocrystal
(5) -	1090	Hammer	10-kHz accelerometer
(6) 1050	-	20-kHz vibrator (soniscope)	20-kHz receiver

TABLE 3.5 WES AND TT LABORATORY TEST PROGRAM ON CRUSHED DAKOTA SANDSTONE

Laboratory	Test Type	Number of Tests	Specimen Size	Remarks
WES	Static TX	4	3.45 cm diam by 7.5 cm long	Confining pressures of 18, 35, 70, and 105 bars. Confining pressure cycled at one-half maximum. Deviator stress cycled at one-half estimated maximum.
TT	Static TX	2	1.91 cm diam by 3.81 cm long	Confining pressures of 1 and 3.2 kbar. Obtained peak deviator stress and strains.

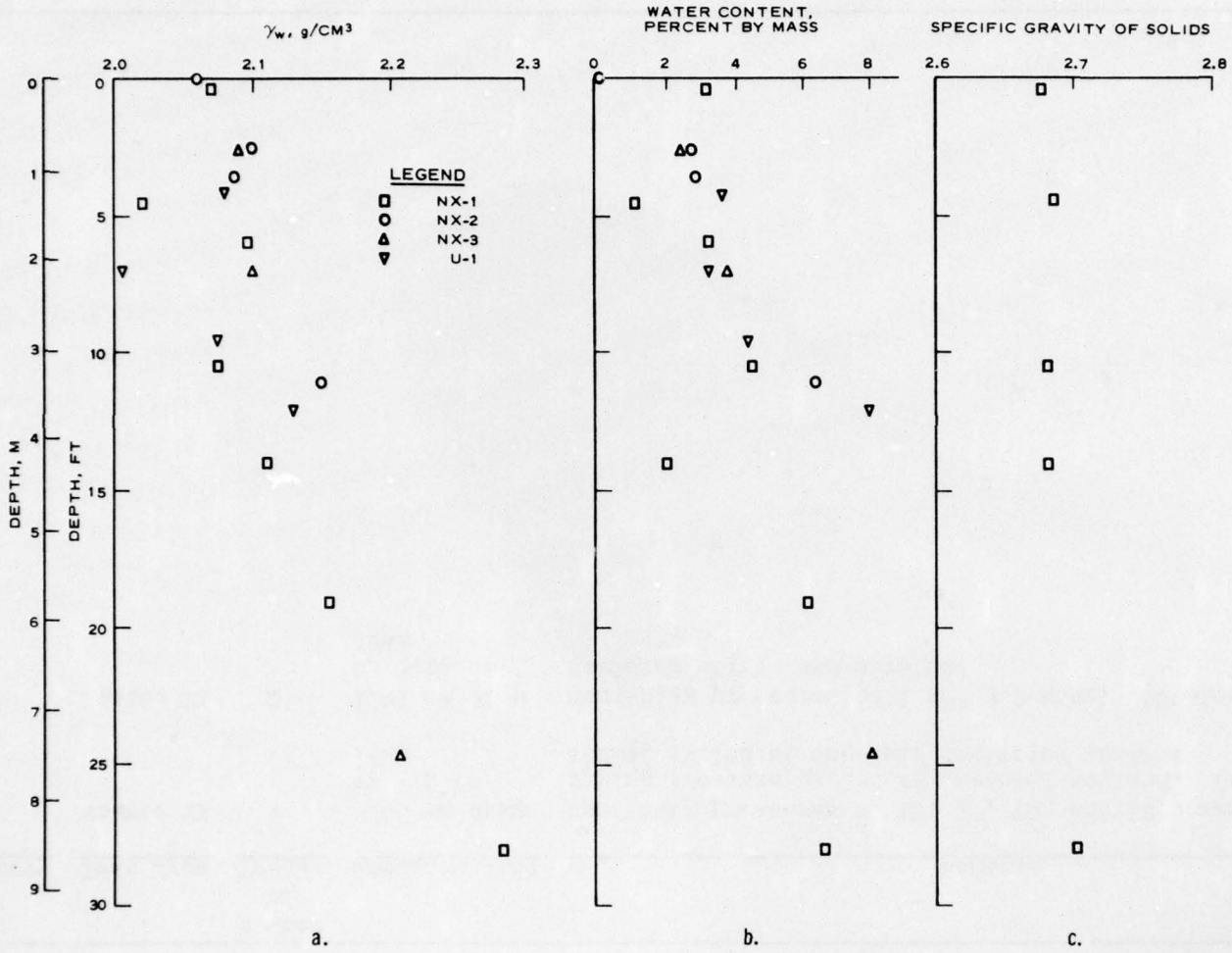

Figure 3.1. Classification and composition data, Dakota sandstone, San Ysidro, N. Mex.

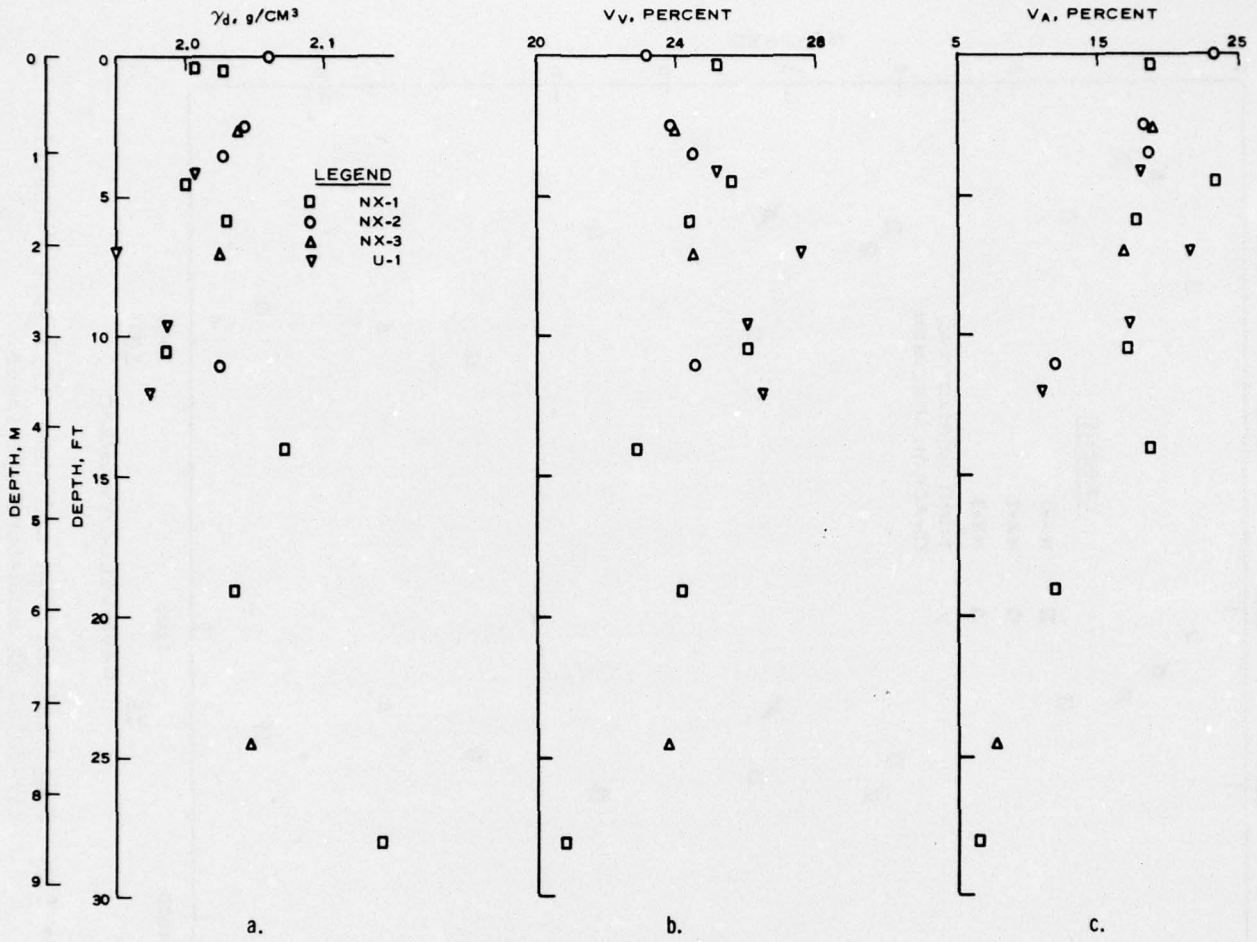

Figure 3.2. Classification and composition parameters computed from data in Figure 3.1.

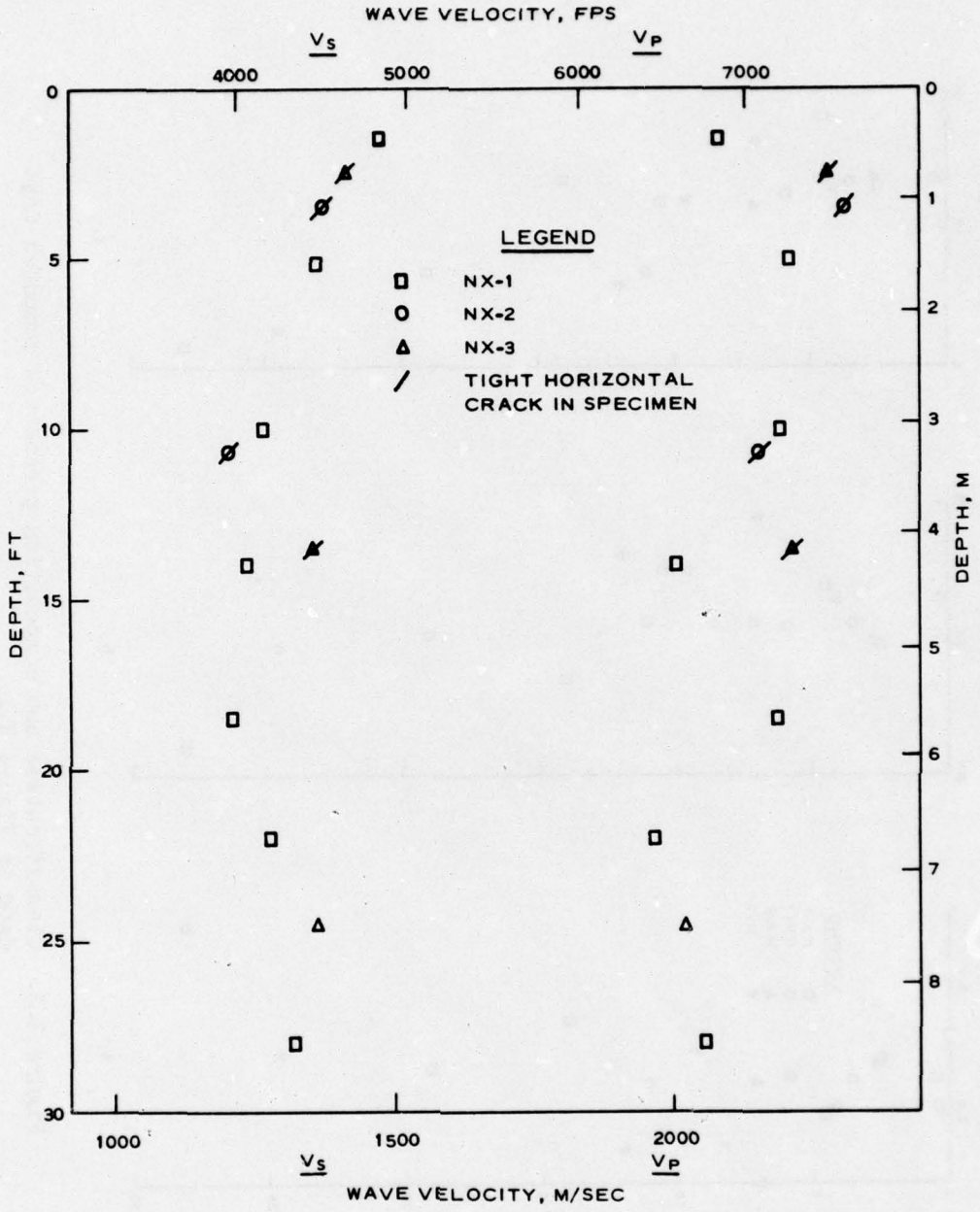

Figure 3.3. Compressional (V_p) and shear (V_s) wave velocities of air-dried NX sandstone specimens.

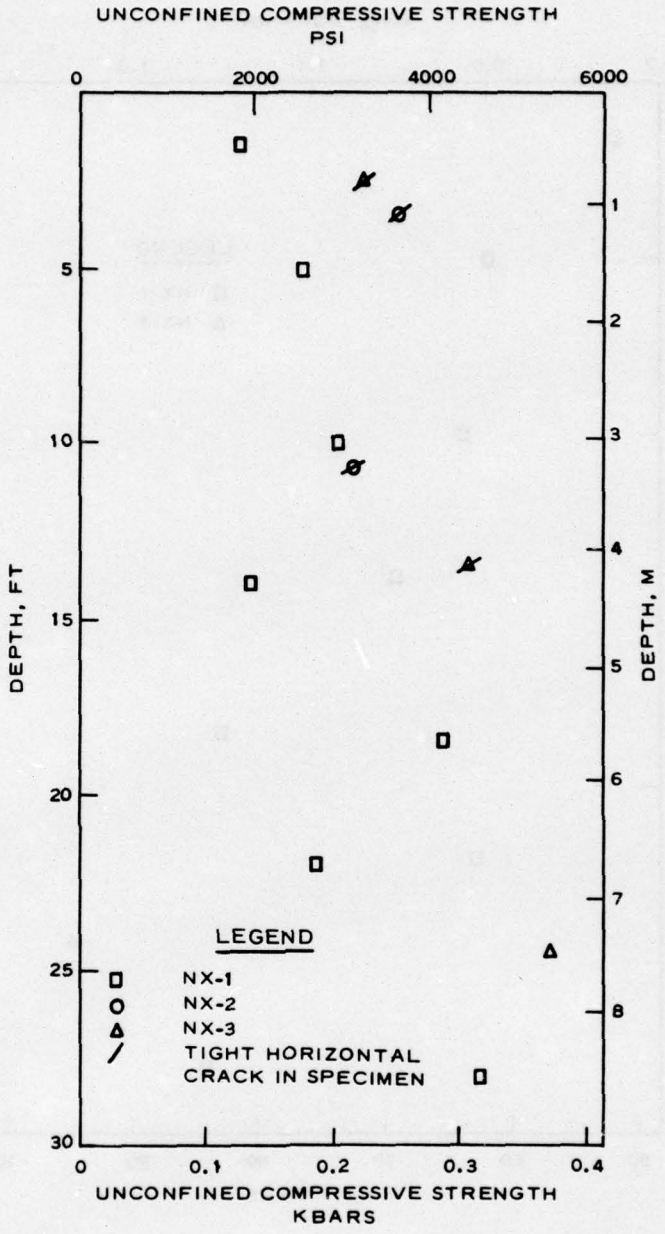

Figure 3.4. Unconfined compressive strength of air-dried NX sandstone specimens.

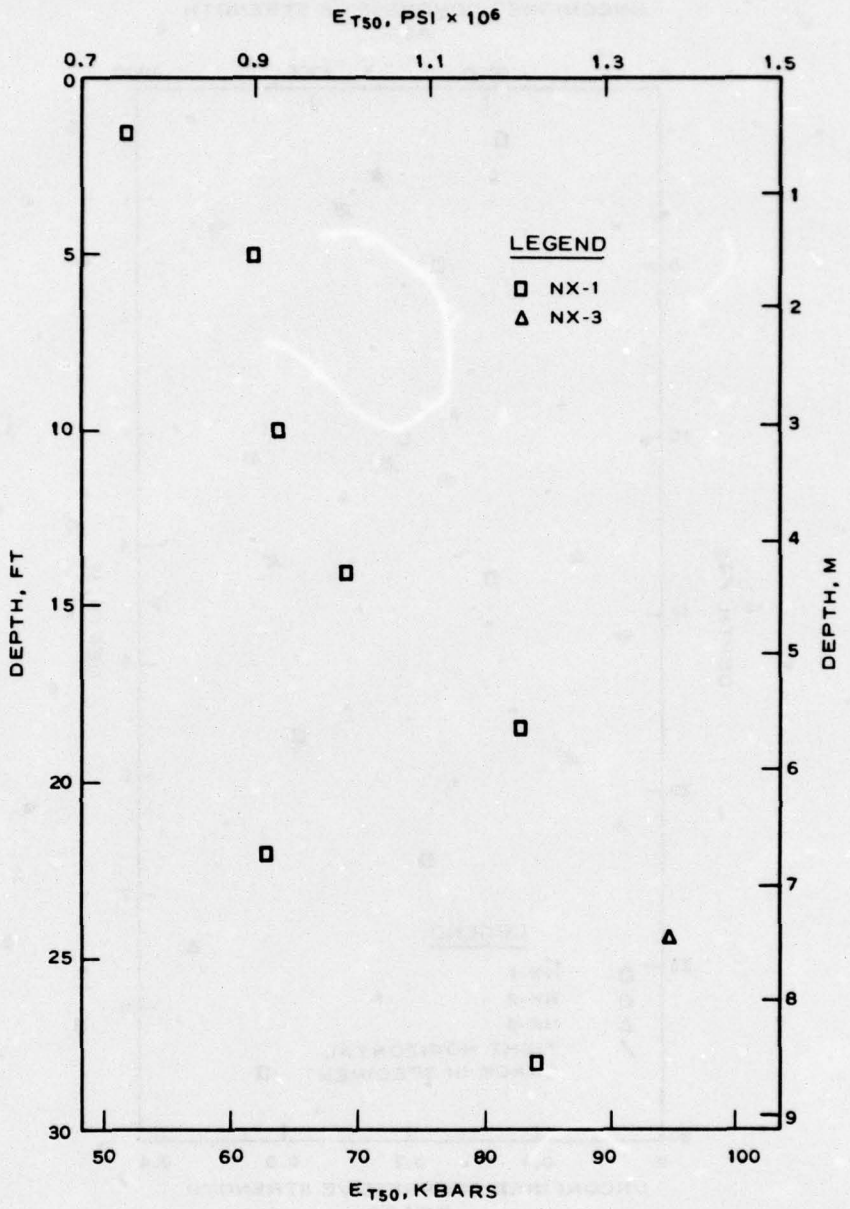

Figure 3.5. Tangent modulus of elasticity at 50 percent of the unconfined compressive strength for the air-dried NX specimens without cracks.

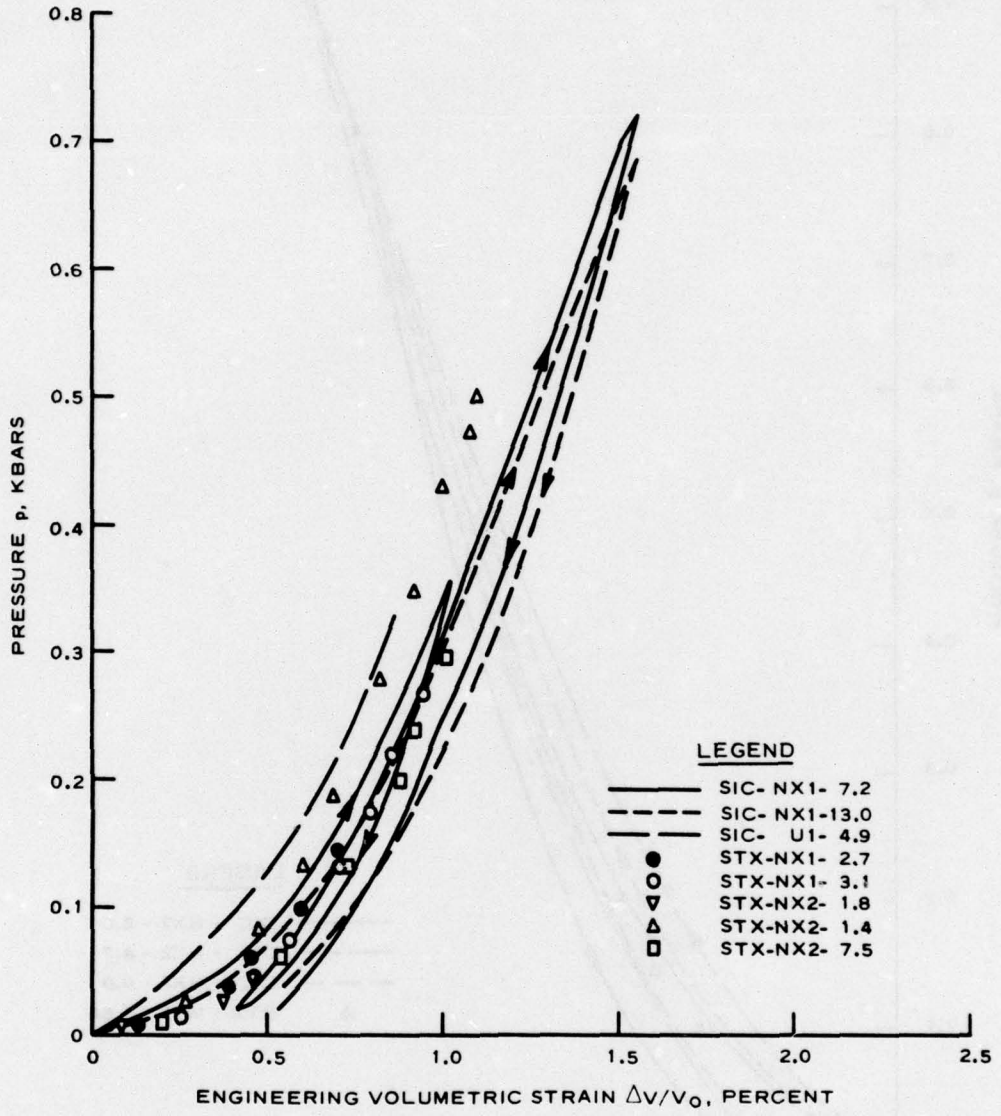

Figure 3.6. Static isotropic compression tests, Dakota sandstone, San Ysidro, N. Mex.

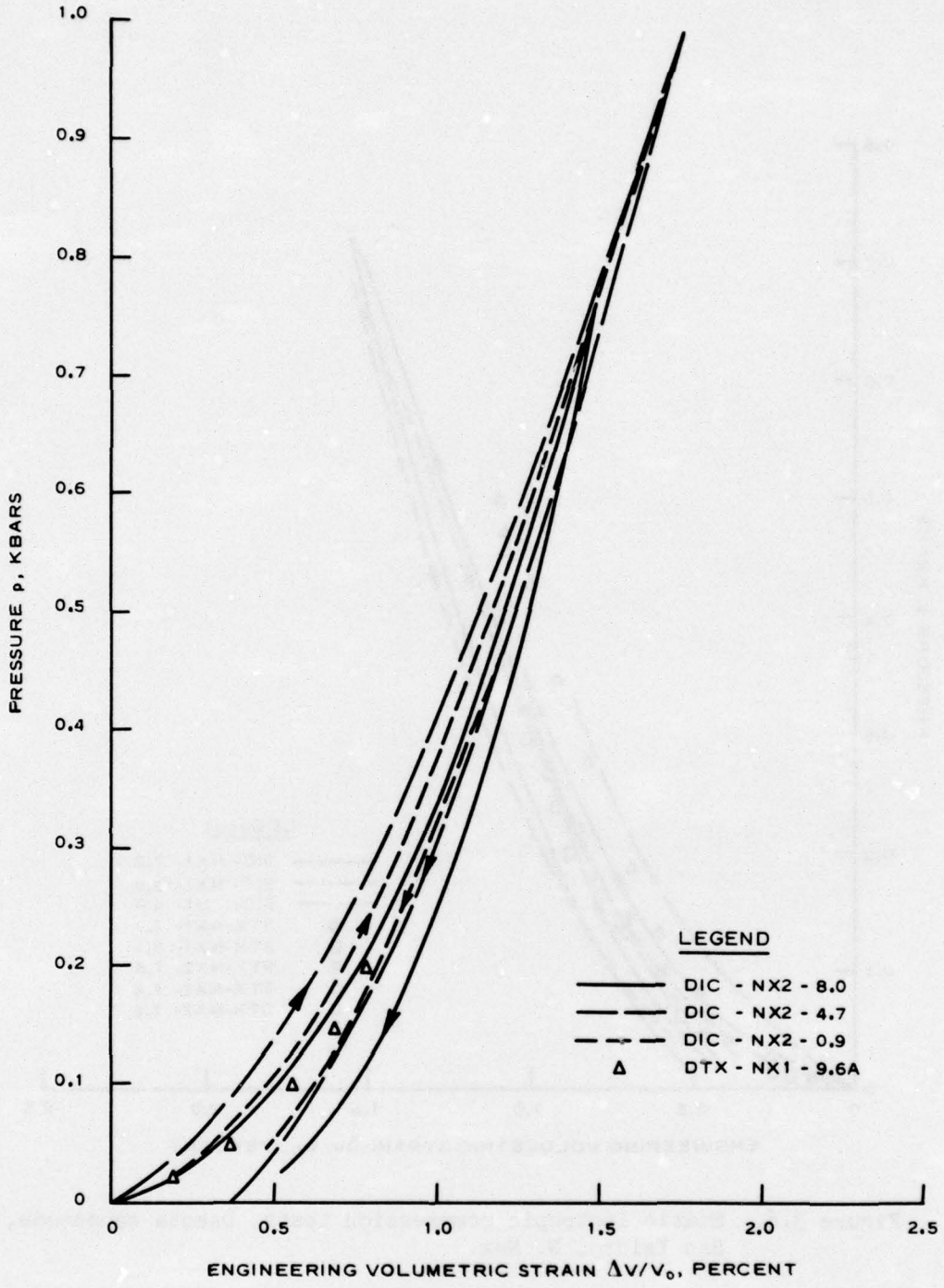

Figure 3.7. Dynamic isotropic compression tests, Dakota sandstone, San Ysidro, N. Mex.

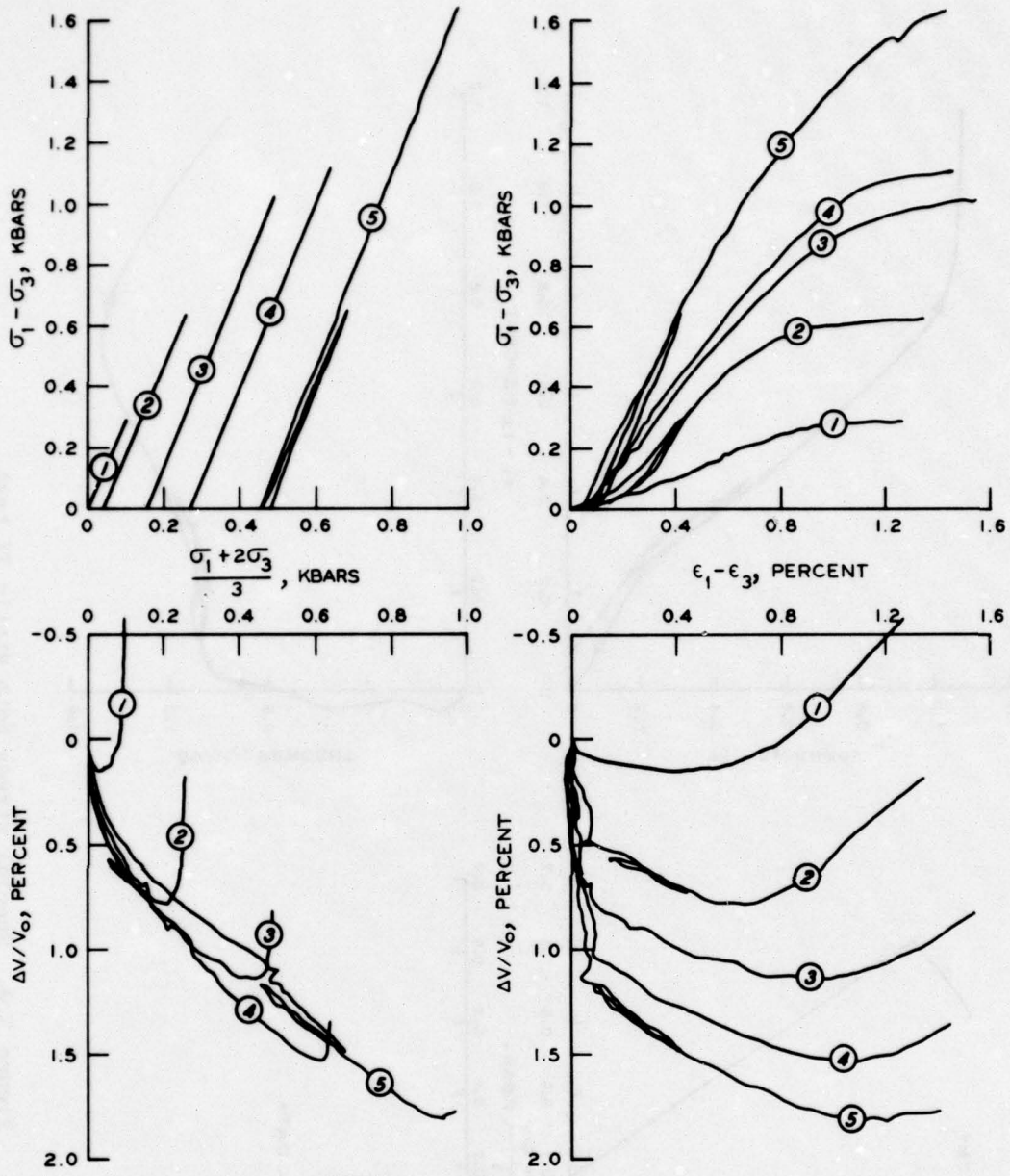

LEGEND

	σ_3, KBARS	γ_w, g/CM^3	w, %	V_A^*, %
①	0	2.086	3.0	18.4
②	0.06	2.081	2.8	18.8
③	0.162	2.072	3.0	18.9
④	0.276	2.080	3.0	18.6
⑤	0.455	2.079	2.8	18.9

* $G_s = 2.68$

Figure 3.8. Static triaxial shear tests, Dakota sandstone, San Ysidro, N. Mex.

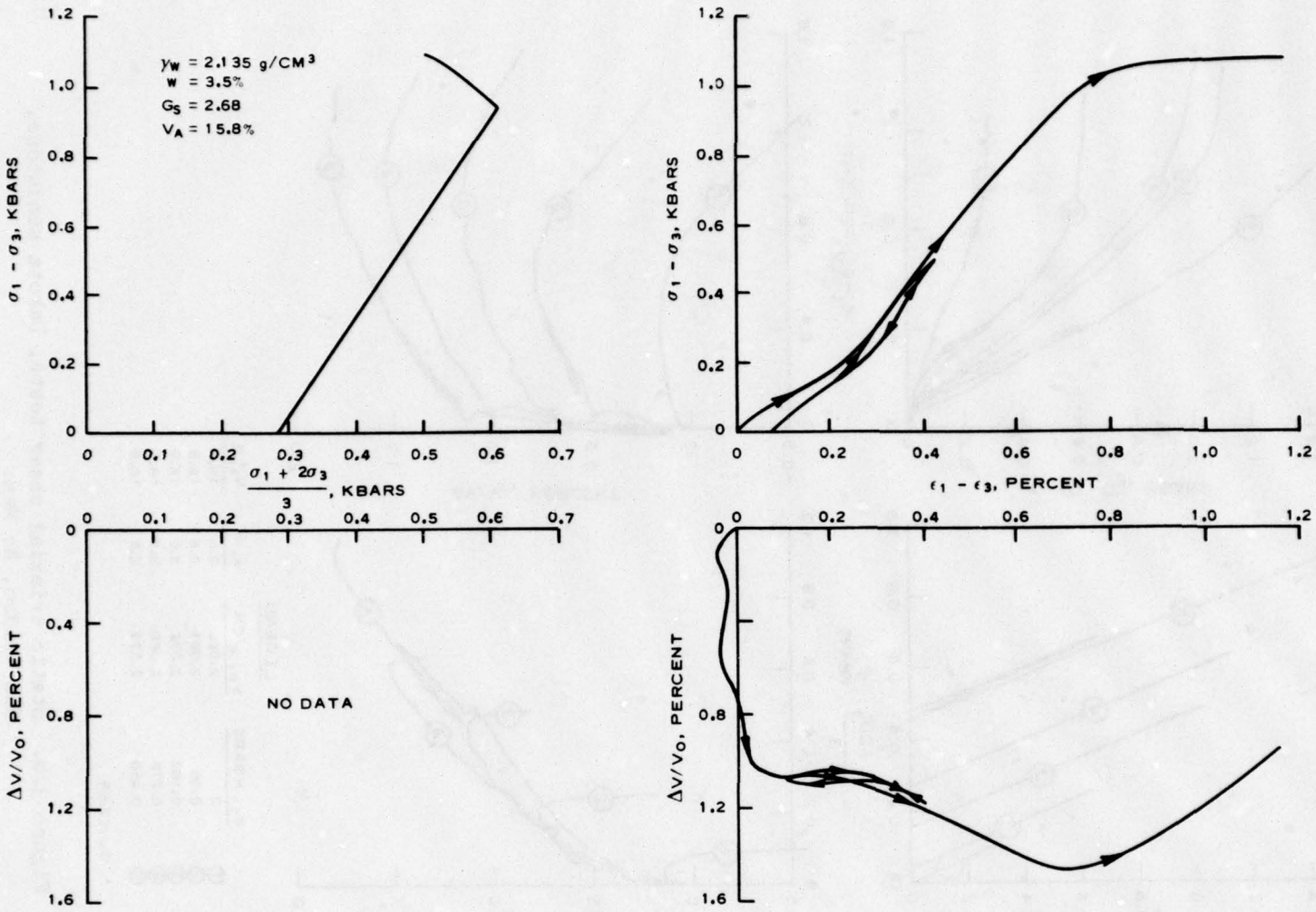

Figure 3.9. Special stress path static TX test.

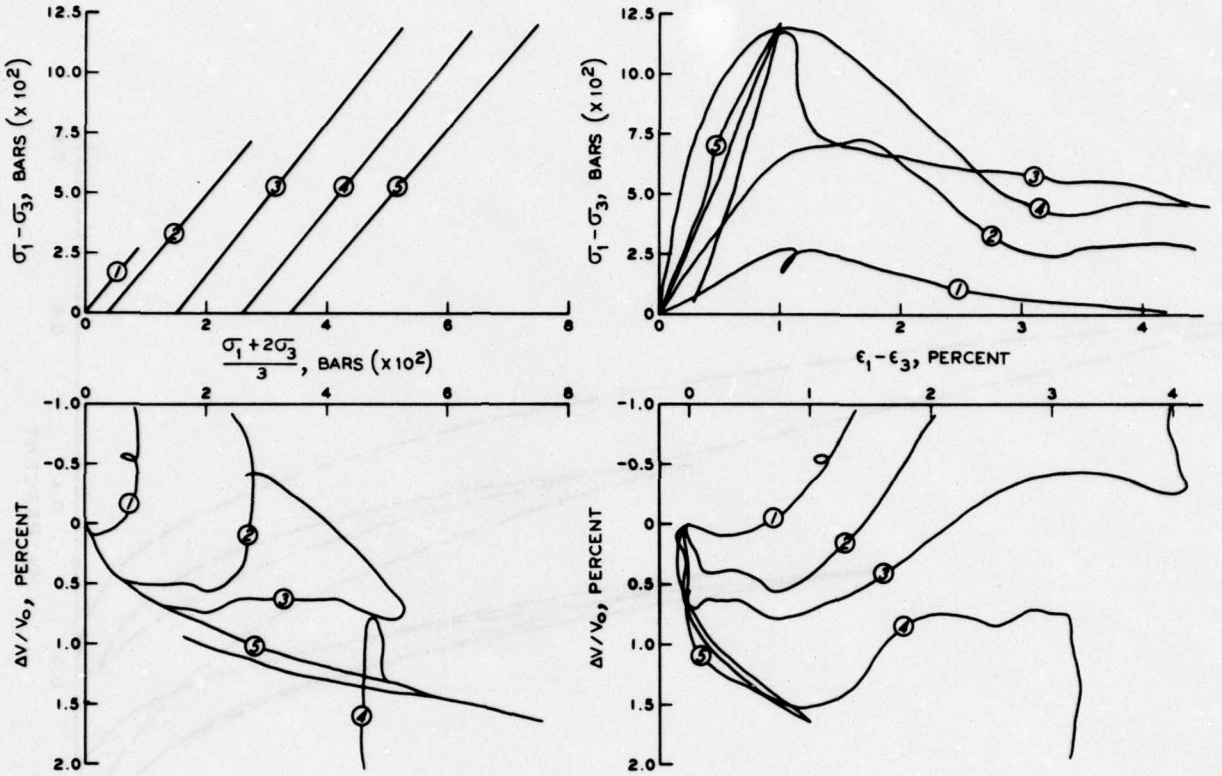

Figure 3.10. Dynamic triaxial shear tests, Dakota sandstone, San Ysidro, N. Mex.

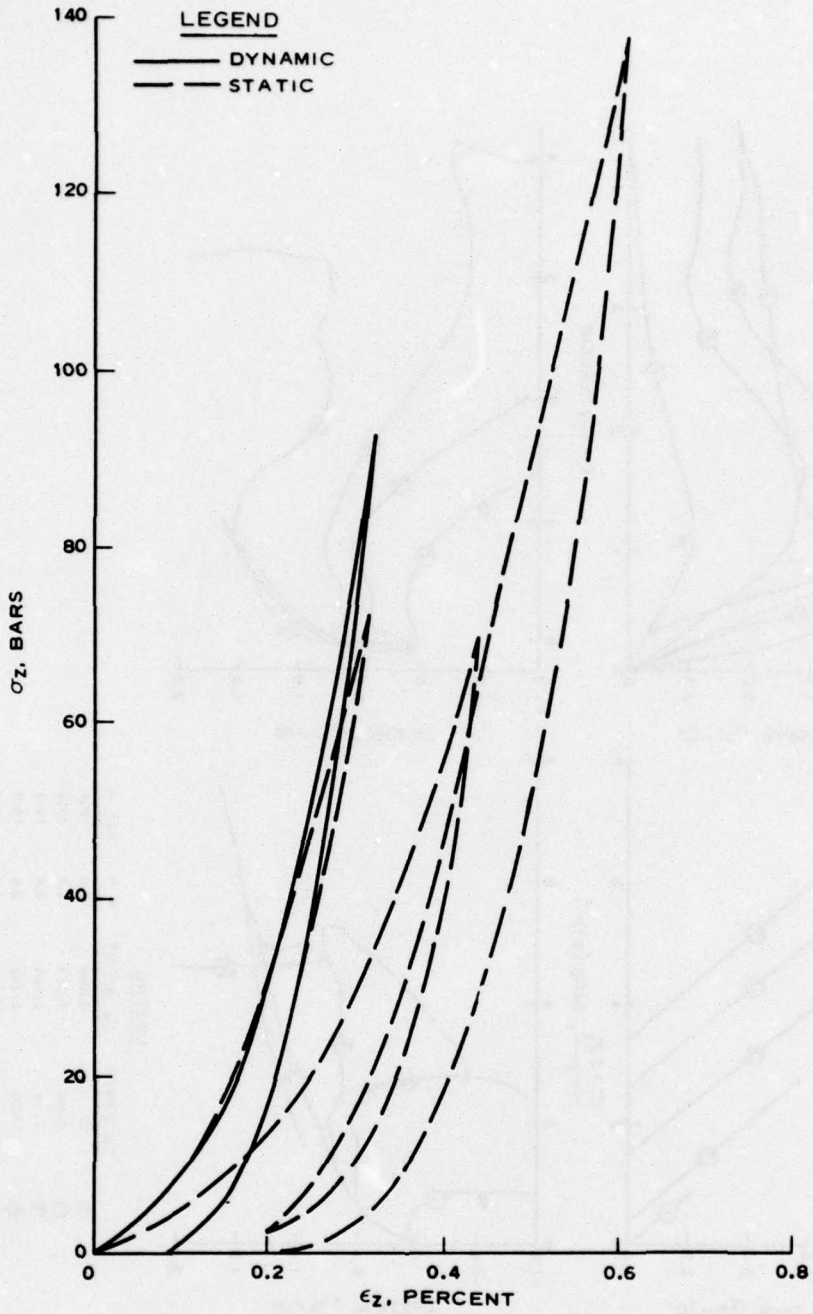

Figure 3.11. Static and dynamic uniaxial strain response for intact Dakota sandstone.

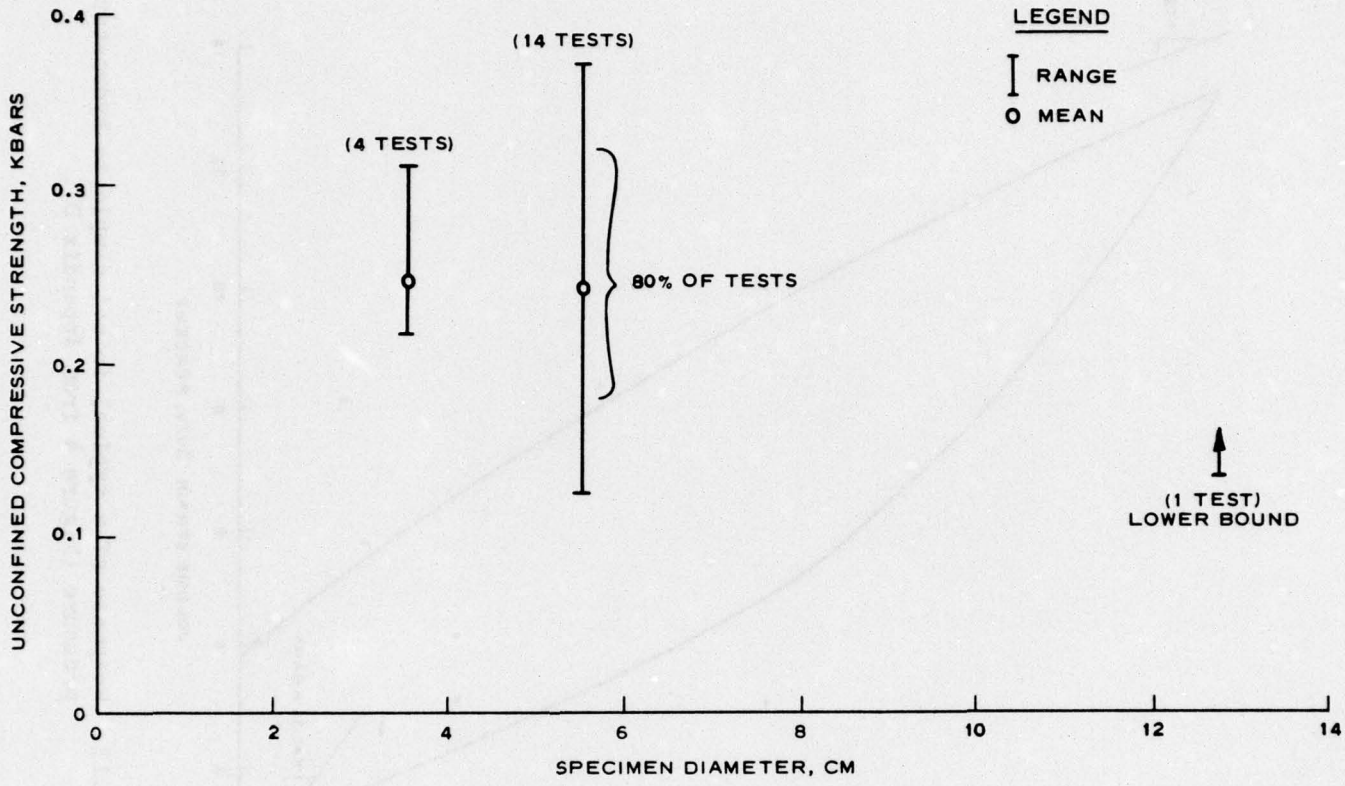

Figure 3.12. Effect of specimen diameter on unconfined compressive strength.

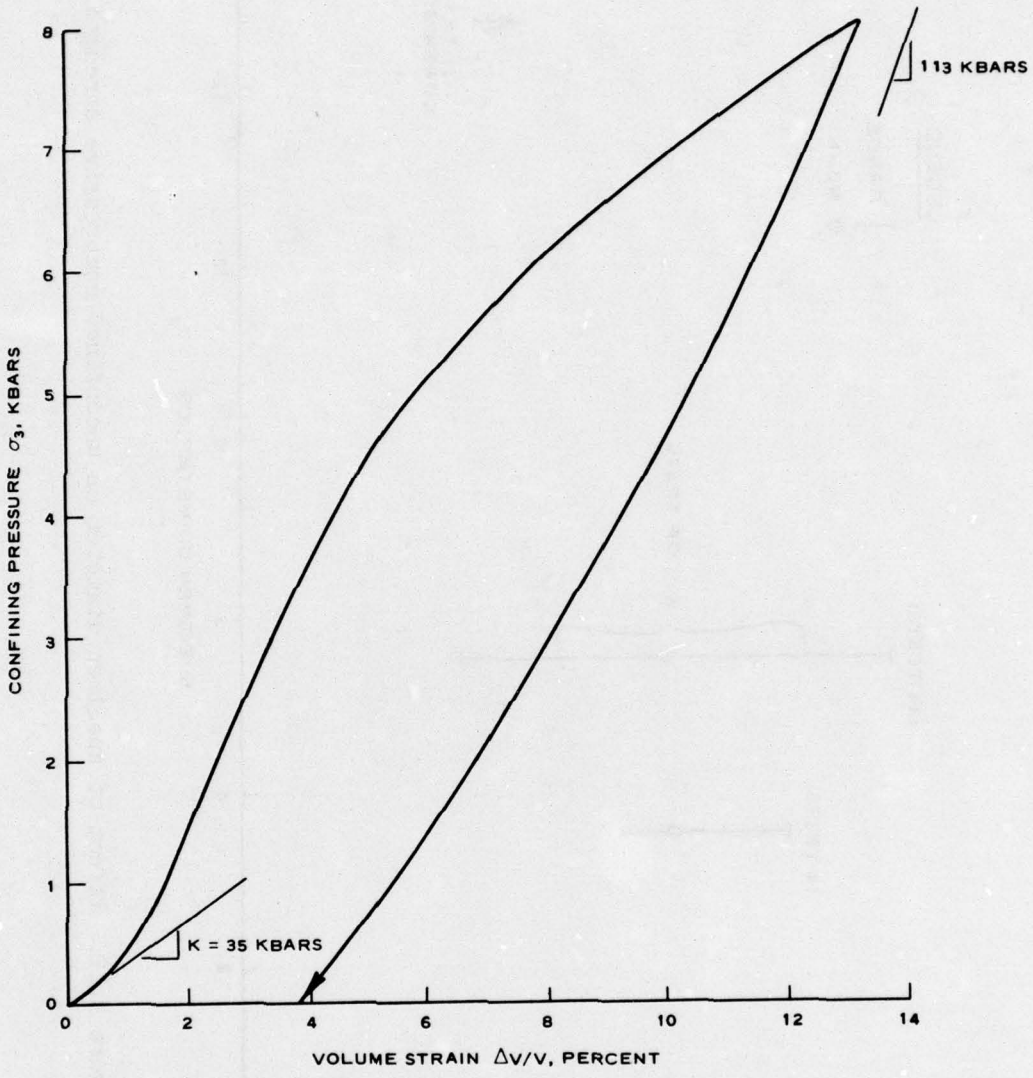

Figure 3.13. Response of a typical intact sample to hydrostatic pressure (Figure 4 from Appendix D).

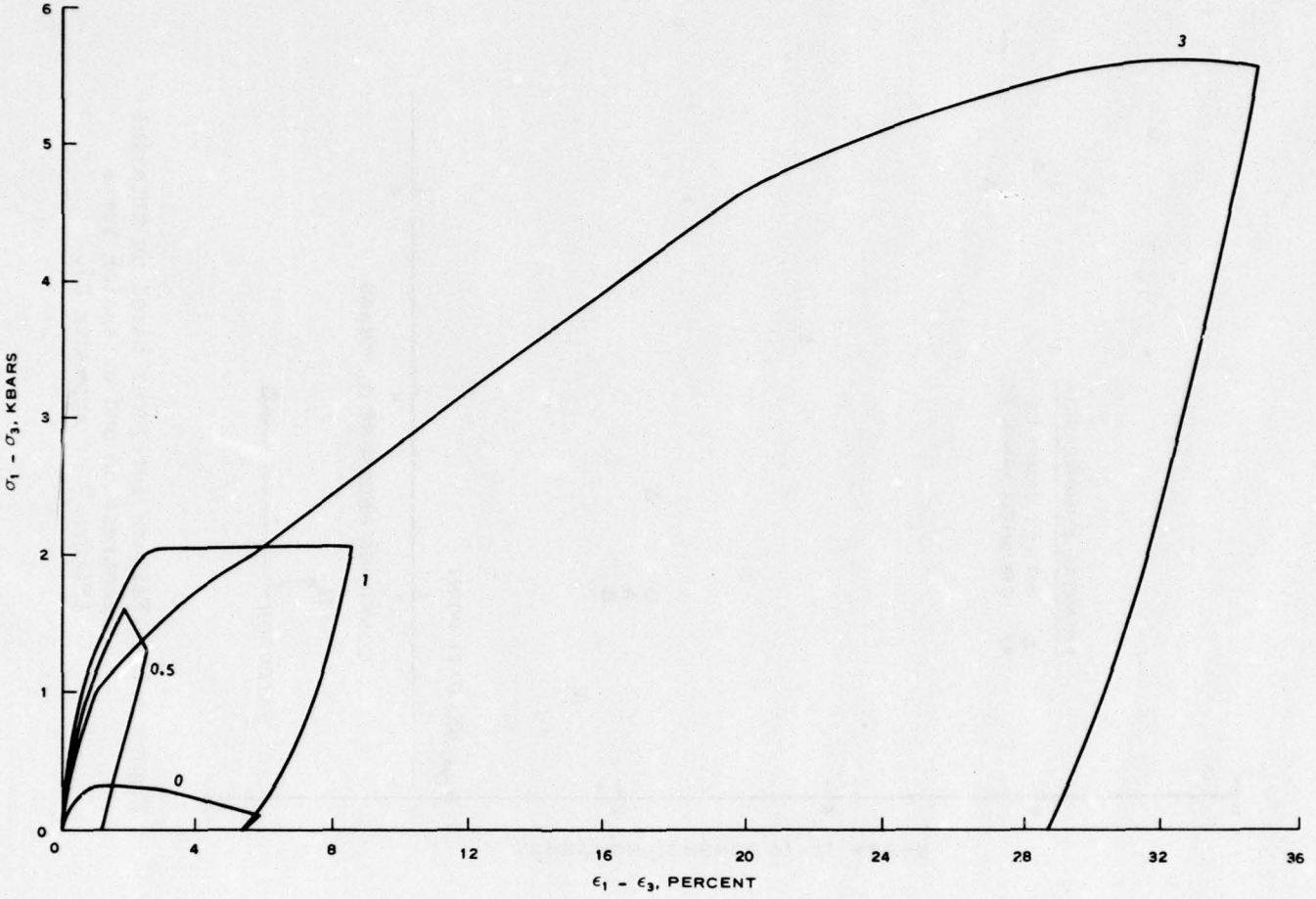

Figure 3.14. Deviator stress-strain response for TX compression tests on intact sandstone specimens (adapted from Figure 1 of Appendix D).

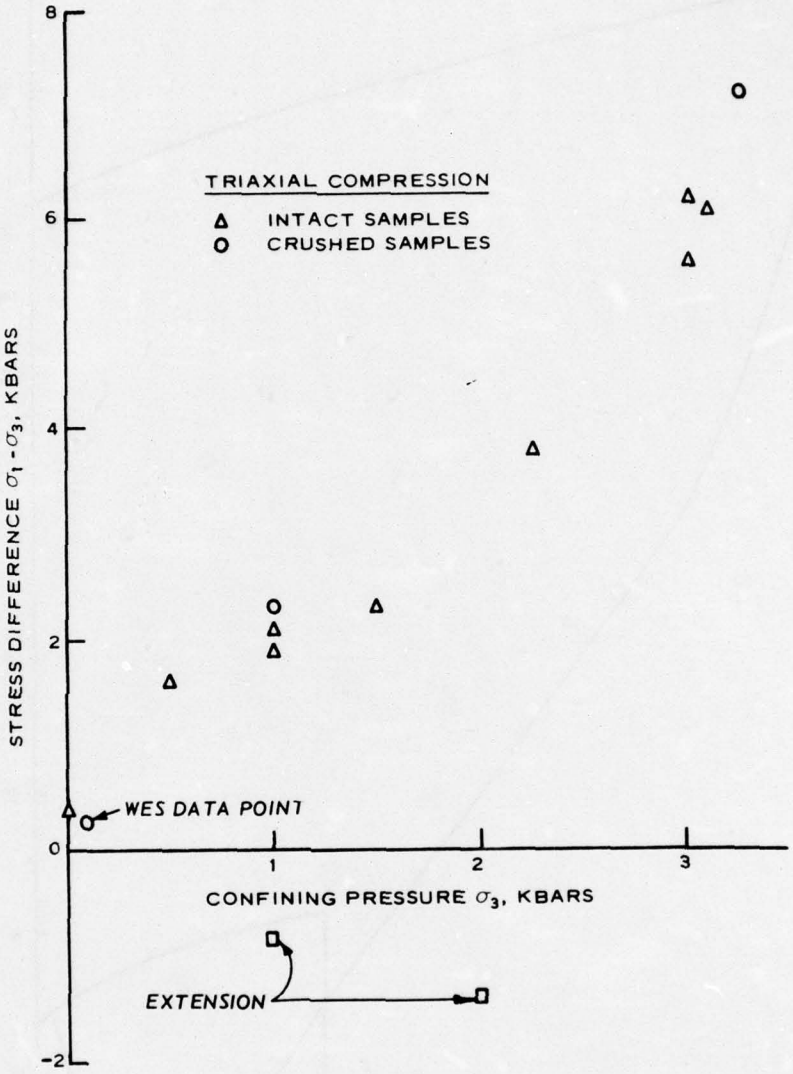

Figure 3.15. Failure envelopes based on triaxial compression and extension tests (Figure 3 of Appendix D).

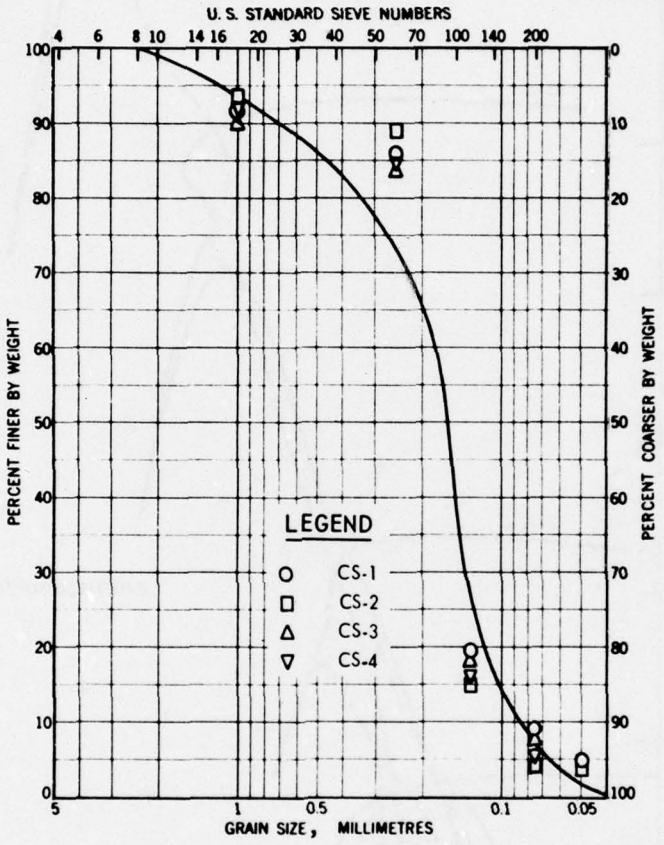

Figure 3.16. Gradation curve for crushed Dakota sandstone specimens.

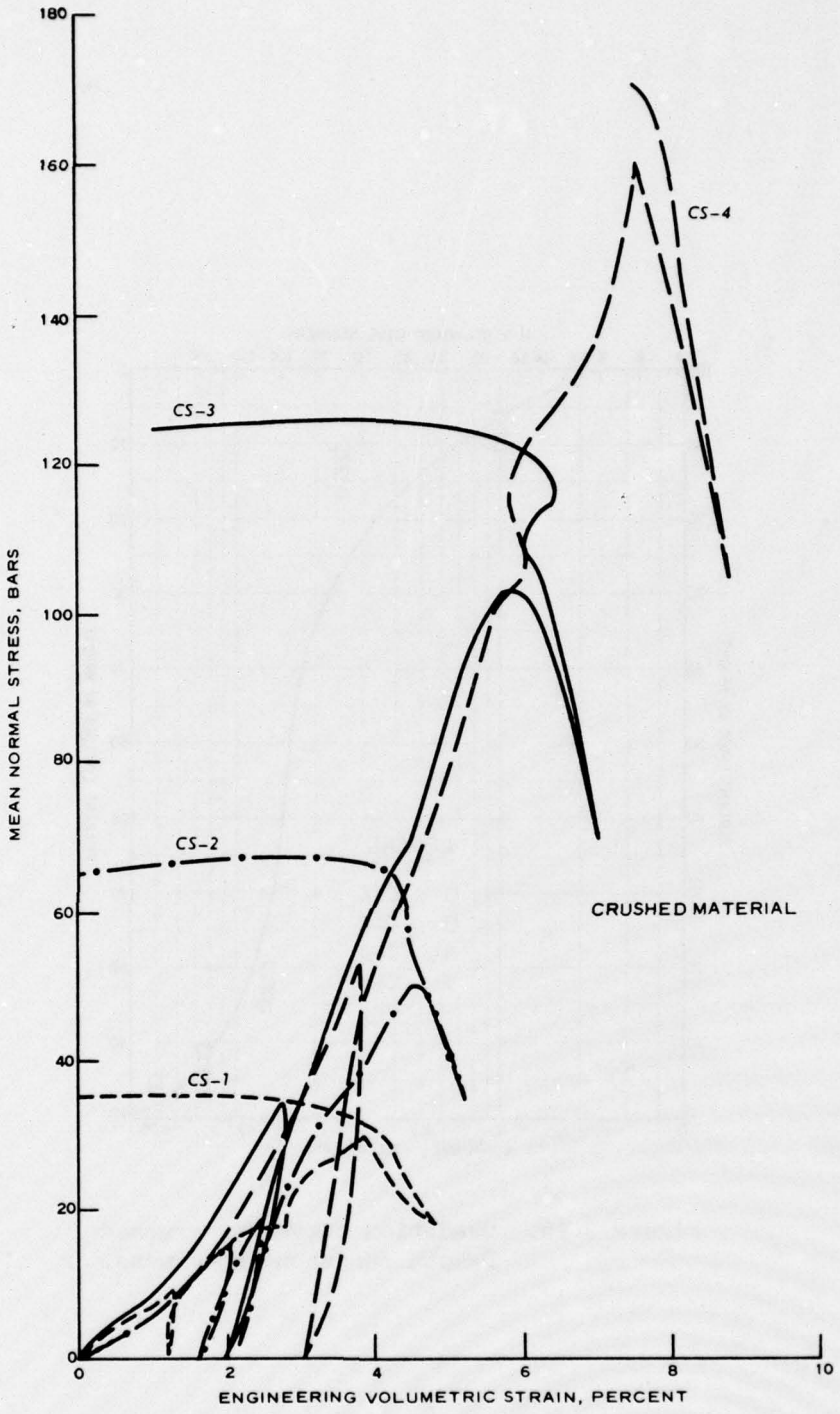

Figure 3.17. Mean normal stress versus volumetric strain response of crushed sandstone specimens during TX tests.

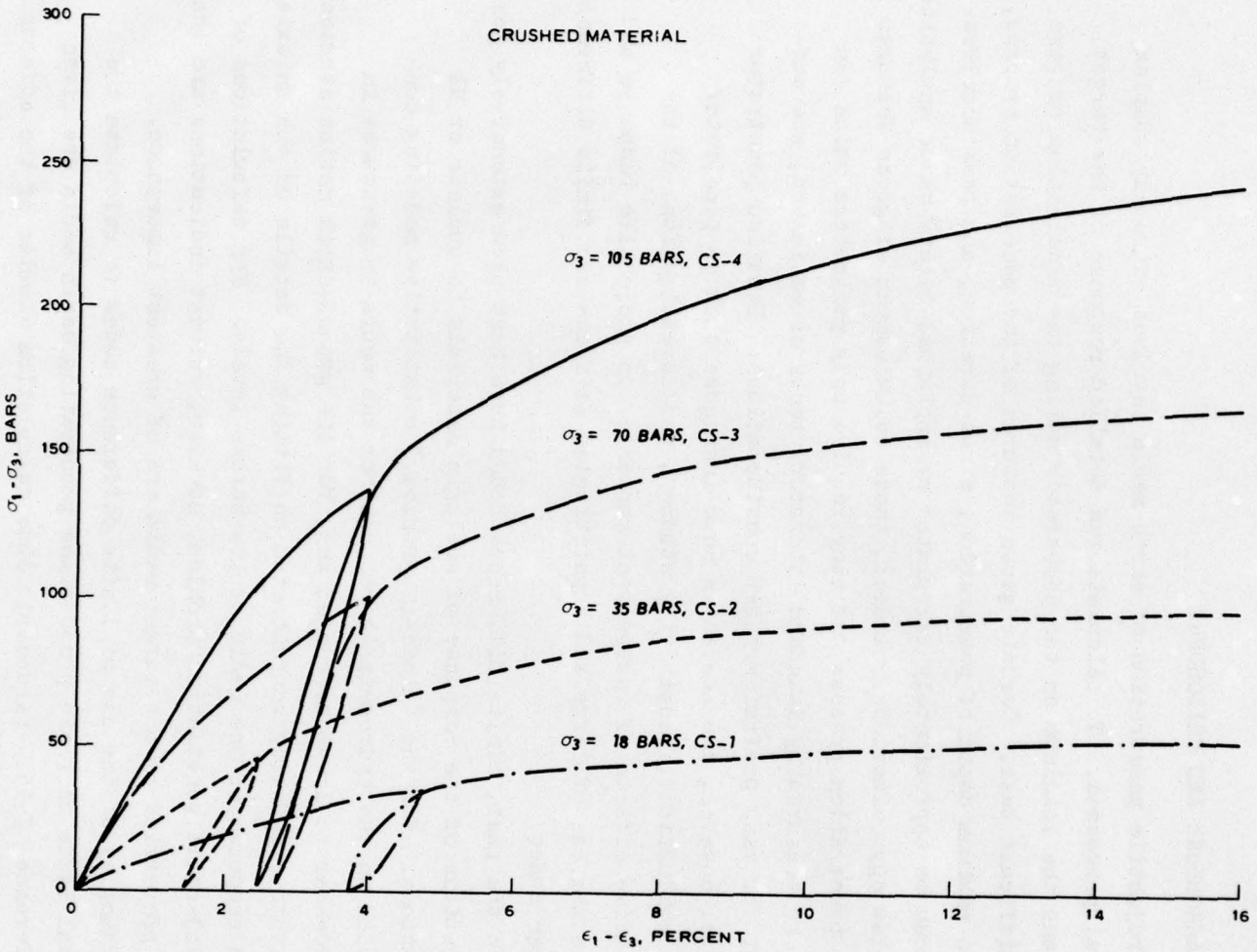

Figure 3.18. Deviator stress-strain response of crushed sandstone specimens during TX tests.

CHAPTER 4

CONSTITUTIVE PROPERTY ANALYSIS

4.1 BACKGROUND AND PHILOSOPHY

Projectile penetration of earth media involves extremely complex physical processes. To calculate the detailed response of the target media and the loadings on the penetrator during the penetration process is a difficult task. Certain gross features of the penetration process, such as maximum depth of penetration, event duration, and peak deceleration, can be approximately calculated by empirical relations or analytical force law approximations. Indeed, these calculations of gross features of the penetration process, if they require only parameters which can easily be measured by standard laboratory tests or estimated, are sufficient for many preliminary EPW considerations. Detailed penetrator loadings, however, are needed in some instances such as penetrator design evaluations, sensitivity studies, and investigations of the qualitative effects of independent variables on projectile response and require the use of large and sophisticated axisymmetric finite difference computer codes.

In the past, finite difference codes have been used extensively for calculations of the response of geologic materials to nuclear or HE detonations. For the "close-in problem," constitutive modeling concentrated on the hydrodynamic response of the media to pressures in the 100-kbar to low-Mbar range; and, for the ground-shock motion studies, constitutive modeling concentrated on fitting the details of the uniaxial strain response of the media at low stress levels. For calculations of the projectile penetration problem, however, current indications are that shear properties of the target media are of greatest importance.

Examples of the use of finite difference codes to calculate the external loads on rigid projectiles penetrating earth media are given in References 7-15. Parametric code calculation studies of the effects of constitutive property and material model variations on the maximum

external loads on a penetrator (impacting a rock not much different from that present at the San Ysidro site)[15] indicated:

(1) Penetration dynamics are sensitive to strength and frictional characteristics of the material next to the penetrator, i.e., the comminuted rock.

(2) For a given media type, a factor-of-two change in basic target properties leads to changes in penetrator deceleration of 5 to 50 percent.

(3) A factor-of-two change in bulk modulus produced negligible effects. Shear modulus variations were not investigated.

These conclusions appear to be qualitatively valid for soils also.[16,17]

Results of penetration code studies and event calculations show that the stress paths for typical target locations vary from states of pure shear to states of triaxial compression (TX).[8,12,15-17] For the majority of the time in the calculations, the stress states lie on the yield surface defined for the media. Thus, for the projectile penetration problem, it is of greatest importance to model the shear behavior of the target media, and the triaxial compression (TX) test is the most appropriate of the common laboratory material property tests for this purpose. It is also desirable to model in some manner the postfailure strength degradation of the target media. Therefore, the constitutive property recommendations to be presented in this chapter will depart from the format used in past WES constitutive property studies relative to ground motion problems and will be based primarily on TX and IC stress-strain data instead of UX stress-strain and stress path data. Indeed, the test program reported in the previous chapter was planned on this basis.

In the following paragraphs, the results of the WES and TT laboratory tests on intact sandstone will be analyzed, considering the results of the field geophysical survey and the laboratory wave velocity study on the large-diameter cores. Recommendations and guidelines will also be discussed for constitutive models to be used in calculational studies of the field penetration tests and the reverse ballistic tests.

4.2 RECOMMENDED CONSTITUTIVE PROPERTIES FOR INTACT DAKOTA SANDSTONE

4.2.1 Pressure-Volumetric Strain Behavior in Hydrostatic (Isotropic) Compression for Intact Specimens. As discussed in Section 3.2.5, the IC data presented in Figures 3.6 and 3.7 appear reasonable. Figure 4.1 is a recommended load-unload isotropic compression response curve for loading to 1 kbar. Since penetration calculations involve dynamic response, and also considering the possible bias of strain data discussed in Section 3.2.3, the recommended curve is chosen as the mean of the data in Figure 3.7. The error bars at the top of the curve in Figure 4.1 are based on the discussion in Section 3.2.3 and fall within the scatter of data indicated by Figures 3.6 and 3.7; these error bars indicate the degree of freedom which may be taken in numerically fitting this curve for calculation purposes. Figure 4.2 presents the recommended isotropic compression response load-unload curves for loading to 8 kbar. The behavior of the tangent bulk modulus (K)* in virgin loading is illustrated in Figure 4.3. Various limiting values of loading and unloading bulk moduli are indicated in Figures 4.1 and 4.2. Figure 4.2 was obtained by using the WES data to a pressure of 1 kbar and then smoothly connecting with the TT data at a pressure of 2 kbar. The details of the joining of the two sets of data or of arriving at the recommended curve in Figure 4.1 from the scatter bands defined in Figures 3.6 and 3.7 are not of major concern for finite difference penetration calculations since it has been demonstrated that a factor-of-two change in the bulk modulus of the target medium has only a 10 to 15 percent effect on the deceleration-time curve of the penetrator.[12]

4.2.2 Deviatoric Stress-Strain Behavior of Intact Specimens. With the exception of the anomalously large initial slope of the deviatoric stress-strain curve for test No. 4 of Figure 3.10 and the change from dilatation to compaction indicated in the mean normal pressure-volumetric

---

* Bulk modulus is used here to mean the slope of the pressure-engineering volumetric strain curve (Figures 4.1 and 4.2).

strain curve, again for test No. 4 of Figure 3.10, the data of Figures 3.8, 3.10, and 3.14 appear reasonable and consistent. The results of the TT and WES TX tests indicate an increasing initial shear modulus (G) with increasing confining pressure (the TT results indicate a softening in initial modulus for confining pressures greater than 1 kbar). Figure 4.4 compares the initial shear moduli from the WES static and dynamic tests and the TT static tests, and presents a recommended relation between initial shear modulus and confining pressure (which can be related to volumetric strain through the hydrostat). The deviatoric stress-strain response of the sandstone is linear (constant slope) initially for most of the tests, and the points on the curves indicating significant departure from linearity can be used to define an envelope in stress difference-mean normal pressure space marking the onset of nonlinear (inelastic) behavior, as in Figure 4.5. The slopes of the curves (shear moduli) approach zero as the failure stress is approached; Figure 4.6 is a plot of the deviatoric strain at maximum deviatoric stress versus confining pressure for the TT and WES TX tests, and the dashed line is a possible relation (σ_c can be related to volumetric strain through the hydrostat). Unfortunately, unloading deviatoric stress-strain data (hence, unloading shear moduli) from deviatoric stress states prior to the attainment of the maximum deviatoric stress are available from only three of the TT and WES TX tests; initial unloading shear modulus values for these three tests are plotted versus confining pressure in Figure 4.7.

4.2.3 Failure Data. Figure 4.8 is a summary plot of failure data derived from the WES TX compression tests and various tensile tests plotted in $\sqrt{3J_2'}$ versus mean normal stress space, where J_2' is the second invariant of the stress deviator tensor. The solid curve is the recommended failure relation for the intact sandstone. Error bars on the uppermost data point indicate the possible error associated with a TX test failure data point and also give some indication of the freedom which may be taken in weighing each data point when numerically approximating the recommended failure surface. Also shown are the failure

relation for comminuted sandstone (short-dashed line) and the relation defining the onset of inelastic behavior (dotted line) for the intact material. The results of the Brazilian tensile tests and the direct pull tensile tests allow a logical extension of the failure relation from the UC data toward the $\sqrt{3J_2'}$ axis. The hollow cylinder data point shown is not on the recommended failure curve although the simpler interpretation of the hollow cylinder test results is in substantial agreement with the recommended relation. Figure 4.9 combines TT and WES results to extend the recommended failure relation to higher stress levels. Again, the failure relation for comminuted sandstone is shown and joins the intact failure curve at a mean normal stress of 1.6 kbar. Also shown in Figure 4.9 is the stress path from a TT UX test (see Figure 7, Appendix D).

4.2.4 Volume Change During TX Compression Tests. An increase in volume during shear (in a TX compression test) relative to the material hydrostat is called dilatation. Figures 3.7 and 3.9 show evidence of both compaction and dilatation during the TX tests. Figure 4.10 compares the mean normal pressure-volumetric strain curves for the WES static TX tests with the recommended intact sandstone hydrostat. Dilatation is observed in all the test results, although there is little or no net volume change relative to the hydrostat in the two higher confining pressure tests due to compaction during the earlier phases of shear. Figure 4.11 is a plot of the net volume change relative to the hydrostat for the static and dynamic TX tests versus the confining pressure for each test. The net volume change relative to the hydrostat is seen to change from dilatation to compaction at a confining pressure of approximately 0.25 kbar.

4.2.5 Construction of Hypothetical Deviatoric Stress-Strain Curves. It is possible, using the suggested relations in Figures 4.4-4.8, to construct hypothetical deviatoric stress-strain curves for the intact sandstone. In Figure 4.12, deviatoric stress-strain curves are constructed for hypothetical TX tests with confining pressures corresponding to the TX tests in Figure 3.8. The procedure is as follows:

(1) Use Figure 4.4 to select the appropriate initial loading shear modulus G_0 for the test confining pressure.

(2) Use a TX loading stress path in Figure 4.5 to determine the deviatoric stress at which the deviatoric stress-strain curve departs from linearity, and draw a line with slope G_0 to this stress to determine points A in Figure 4.12.

(3) Use the dashed line in Figure 4.6 and the recommended failure surface for the intact material in Figure 4.8 to determine the deviatoric strain and deviatoric stress, respectively, at failure and, hence, determine points B in Figure 4.12.

(4) Using the lines AC and BC as guides, join points A and B with smooth curves in such a manner that the slopes are continuous at points A and the slopes approach zero at points B.

Figure 4.13 compares three of the hypothetical curves from Figure 4.12 with the experimental test results from Figure 3.8. The error bars at the ends of the experimental curves were determined using the considerations of Section 3.2.3. The hypothetical curves are seen to qualitatively reproduce all significant features of the stress-strain curves and are considered quantitatively acceptable considering possible errors in individual test results and data scatter when considering WES static and dynamic test results and TT static test results as a composite data set.

4.3 COMPARISON OF ELASTIC MODULI CALCULATED FROM FIELD AND LABORATORY VELOCITY MEASUREMENTS WITH DETERMINATIONS FROM LABORATORY MECHANICAL PROPERTY TESTS

4.3.1 Field and Laboratory Velocity Measurements. Comparison of Figures 2.4-2.7 and Figure 3.3 reveals a discrepancy between the field seismic P- and S-wave velocities and the laboratory ultrasonic P- and S-wave velocities. The magnitude of the discrepancy is larger than can be attributed to in situ rock quality[18] or differences in water content, particularly for the upper 3 to 4 m of the site. However, there is substantial agreement between the data in Table 3.3 for P-wave velocity measurements on the large-diameter core and the field seismic (P-wave

velocities) results. Table 4.1 summarizes the wave velocity measurements relevant to the upper metre of the site. It is clear that more extensive and better controlled testing would be necessary to conclusively determine the causes of the discrepancy between the laboratory ultrasonic velocities and the velocities determined from the in situ seismic and large-diameter core measurements. Whether the discrepancy is due to differences in water content, to the type of source (impulsive or vibratory), to the source frequency, or to some combination of these factors, it is felt that the in situ seismic and large-diameter core measurements of velocity are more appropriate for describing the bulk behavior of the sandstone. In fact, the slight difference between the large-core P-wave velocity and the in situ P-wave velocity is about the difference to be expected due to the in situ rock quality.

4.3.2 Elastic Moduli Determination. The equations relating the bulk and shear moduli to the compressional and shear wave velocities are well known and not repeated here. The appropriate moduli from laboratory mechanical property tests for comparison are the initial slope of the isotropic compression curve and one-half the initial slope of the deviatoric stress-strain curve (at low confining pressure). Table 4.2 summarizes the elastic moduli determined by the various methods. The initial moduli from the laboratory test results agree quite well with the moduli calculated from the large-core velocities. Moduli calculated from the laboratory ultrasonic velocities are considerably larger than the laboratory initial moduli. The shear modulus determined from the in situ seismic shear wave velocity is somewhat smaller than the laboratory shear modulus. Also included in Table 4.2 is a column for constrained modulus ($M = K + 4/3\ G$); the first four values of constrained modulus were calculated from the K and G values while the last two values are the measured initial slopes of two TT UX stress-strain curves. The constrained modulus values derived from the large-core velocities and WES mechanical

property tests are in good agreement with the first of the TT UX constrained modulus values. Initial slopes of the WES UX stress-strain curves are anomalously low (see footnote in Section 3.2.7).

4.4 POST-FAILURE BEHAVIOR

Information regarding the post-failure behavior of the sandstone comes from three sources: (1) stress-strain data from WES dynamic TX tests subsequent to attaining the peak deviator stress, (2) unloading stress-strain data from some of the TT static strain-controlled TX tests subsequent to the peak deviatoric stress, and (3) WES and TT tests on comminuted sandstone. The TT TX data can be used to obtain unloading shear moduli for unloading from the failure surface for intact material. Some idea of the rate of loss of strength as a function of the amount of strain greater than the strain at the peak strength can be obtained from the WES dynamic TX test results. The dynamic TX deviatoric stress-strain plots appear to define a "residual" strength state for those tests with some confining pressure (see Figure 4.6), although the true significance of this state is not understood due to the nature of the test. Results of the WES and TT tests on comminuted sandstone can be used to define or at least provide guidelines for defining mechanical behavior of the rock in a completely fractured condition, although the initial grain size distribution and density are admittedly somewhat arbitrary and the sequence of events in the crushing and testing operation certainly do not duplicate the in situ case during penetration events. It is significant, however, that the "residual" stress states discussed previously for tests on intact specimens lie close to the crushed failure envelope (see Figure 4.6).

4.5 RELEVANCE OF RECOMMENDED CONSTITUTIVE PROPERTIES FOR THE IN SITU SANDSTONE AND LARGE-DIAMETER SANDSTONE CORES

It is always necessary to interpret or extrapolate the results of laboratory tests on earth materials to apply to the in situ condition when it is desired to perform analytical studies of full-scale field

events (projectile penetration, high explosive tests, etc.). Two questions always arise: (1) is the limited region sampled representative of the whole, and (2) has the process of removal of the sample from the ground and its preparation for testing significantly altered its engineering properties? Many times the interpretation process which deals with these questions may be as simple as just accepting the laboratory test results in an unaltered form and, indeed, this induces little error in the case of some soils and in some massive rock formations provided sampling is done carefully. A common procedure is to adjust the initial slopes of laboratory stress-strain curves to correspond to moduli determined from in situ seismic velocities, and more complicated adjustments are sometimes attempted to account for in situ water content, rock quality, tectonic stresses, etc. Consistent with this, as was stated in Section 4.1, it is desired to interpret the recommendations of Section 4.2 for application to calculational studies of reverse ballistic tests into the large-diameter sandstone cores and full-scale in situ penetration tests.

4.5.1 Constitutive Properties for Large-Diameter Sandstone Cores. The large cores were free from any visible fractures or other discontinuities. Results of limited size effect studies indicate no appreciable strength decrease with test specimen size increase (Figure 3.12). Moduli calculated from compressive and shear wave velocity measurements on the large core are almost identical with moduli determined from initial slopes of laboratory stress-strain curves. Furthermore, if tectonic stresses were present in situ, they should have been relieved to roughly the same degree in the laboratory test specimens and in the large-diameter cores. On the basis of these considerations, it is recommended that the constitutive properties presented in Section 4.2 be used without adjustments for calculational studies of the Avco reverse ballistic tests. Table 4.3 summarizes selected physical properties for the large-diameter sandstone cores.

4.5.2 Constitutive Properties for the In Situ Condition. The sandstone at the San Ysidro, New Mexico, site is massive, and the rock quality is quite high, approaching RQD = 100 percent for the upper metre at the site. Moduli determined from in situ seismic velocities indicate a bulk modulus identical with the initial slope of the recommended isotropic compression curve (Figure 4.1) but a shear modulus which is about one-half the laboratory-determined initial shear modulus (see Table 4.2). Thus, more caution needs to be exercised in using the recommended properties of Section 4.2 for calculations of the in situ penetration tests. For calculations of the early-time response of the penetrator, it is recommended that the only adjustment that should be made is to the slope of the deviatoric stress-strain curves. One possibility is to shift the initial shear modulus versus confining pressure curve (Figure 4.4) downward such that G = 6 kbar for σ_c = 0, and then, using the relation defined in Figure 4.5 to determine the stress at the onset of nonlinear behavior, vary the shear modulus in a manner consistent with the behavior shown in Figures 3.8, 3.10, and 3.14 to a peak deviatoric stress defined by the recommended failure relation for intact sandstone of Figures 4.6 and 4.7. For calculational schemes that extend to depths greater than 3 m, it should be noted that the in situ seismic velocity profiles indicate considerable increases in both the shear and bulk moduli below 3 m, the composition properties change with depth (Figures 3.1 and 3.2), and the rock quality shows a significant decrease with depth. The recommendations of Section 4.2 do not apply to these deeper materials. Since there are no calculation studies presently planned which involve these materials, only a limited study of the deeper materials was conducted.

TABLE 4.1 SUMMARY OF WAVE VELOCITY MEASUREMENTS RELEVANT TO THE UPPER METRE OF THE SAN YSIDRO SITE

Identification	Technique			Velocities m/sec
	Method	Source	Receiver	
In situ	Seismic refraction	Hammer	Geophone (14 Hz)	V_{PF} = 1000 ± 100
	Crosshole	Vibrator (100 Hz)	Geophone (8 Hz)	V_{SF} = 550 ± 50
	Downhole	Hammer	Geophone (8 Hz)	
NX core specimens	Ultrasonic laboratory measurement (resonant)	Piezocrystal (1 MHz)	Piezocrystal (1 MHz)	V_{PL} = 2200 ± 100
				V_{SL} = 1400 ± 100
Large-diameter core specimen	Various laboratory techniques			
	Transit time	Hammer	Accelerometer (10 kHz)	V_{PL} = 1150 ± 50
	Soniscope	Vibrator (20 kHz)	(20 kHz)	V_{PL} ≃ 1050

TABLE 4.2 ELASTIC MODULI

Derived From	Bulk Modulus K kbar	Shear Modulus G kbar	Constrained Modulus M kbar
Ultrasonic velocities	45	40	98
Large-core velocities	14*	10*	27
In situ seismic velocities	12	6	20
WES laboratory mechanical property tests ($\sigma_3 = 0$)	12	11	27
TT UX tests			25 45

* Calculated using $\frac{V_{SL}}{V_{PL}} = 0.6$

TABLE 4.3 SELECTED PHYSICAL PROPERTIES FOR LARGE-DIAMETER SANDSTONE CORES

Dry density (γ_d)	2.02 ± 0.02 g/cm^3
Specific gravity of solids (G_s)	2.68 ± 0.02
Water content (w) (assumed air dry)	0.5 ± 0.5%
Volume of voids (V_V)	25 ± 1%
Volume of air (V_A)	24 ± 1%
Compression wave velocity (V_{PL})	1150 ± 50 m/sec
Shear wave velocity (V_{SL})	690 ± 50 m/sec
Unconfined compressive strength	0.23 ± 0.07 kbar
Unconfined tensile strength	0.007 ± 0.002 kbar
Shear modulus (G) (from V_{PL} and V_{SL})	10 kbar
Bulk modulus (K) (from V_{PL} and V_{SL})	14 kbar

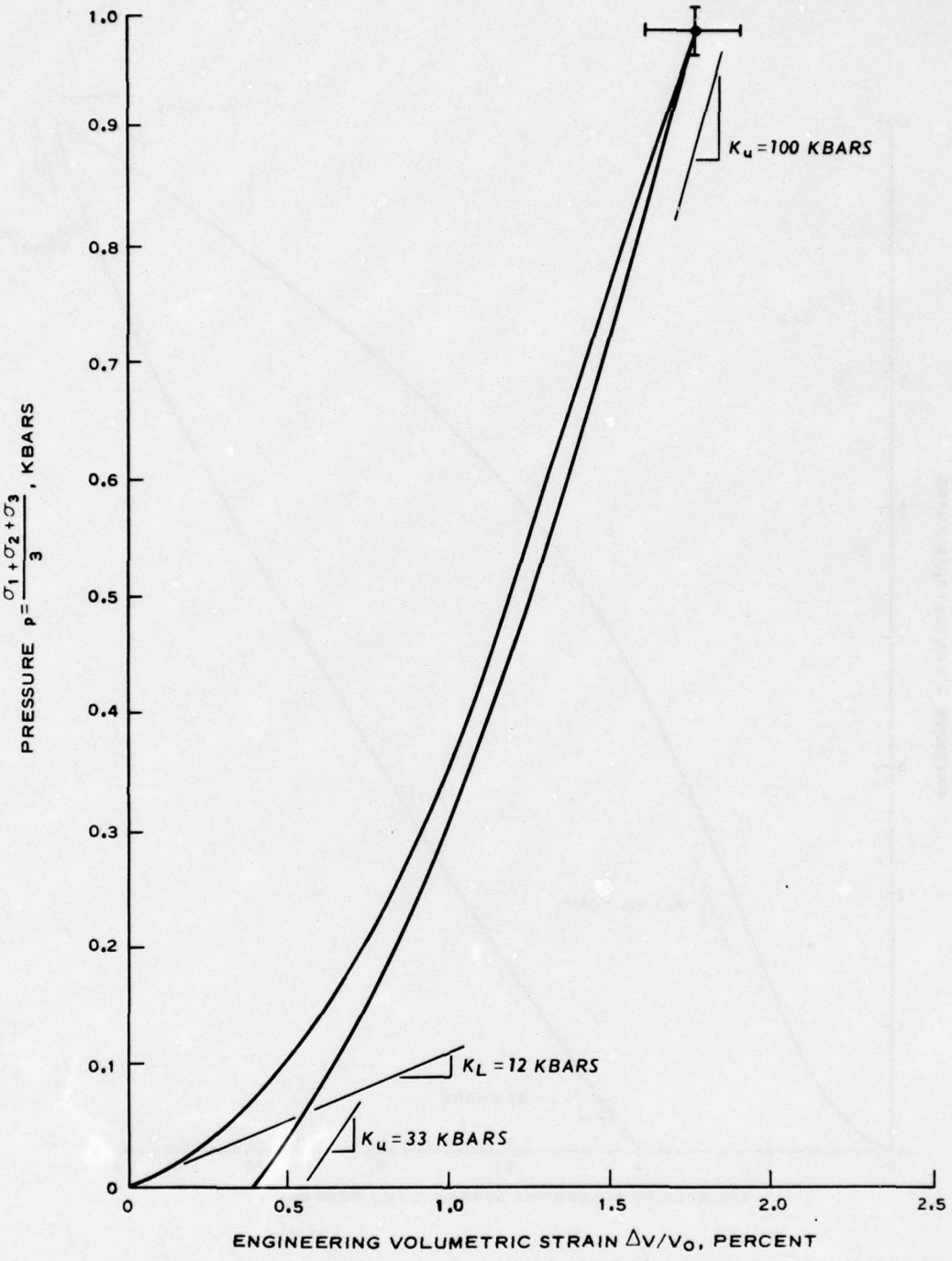

Figure 4.1. Recommended load-unload hydrostat for intact sandstone for stress levels up to 1 kbar.

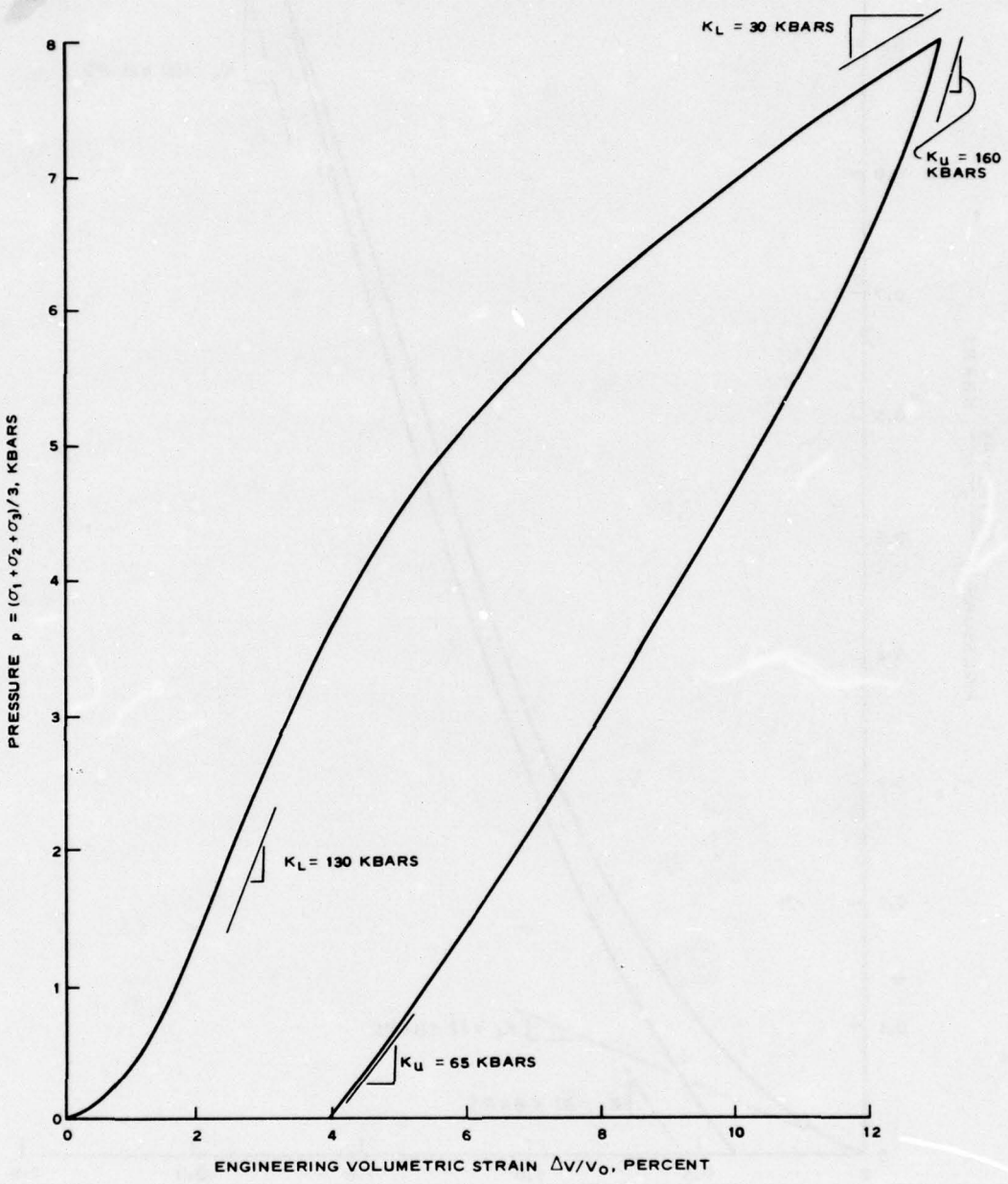

Figure 4.2. Recommended load-unload hydrostat for intact sandstone for stress levels up to 8 kbar.

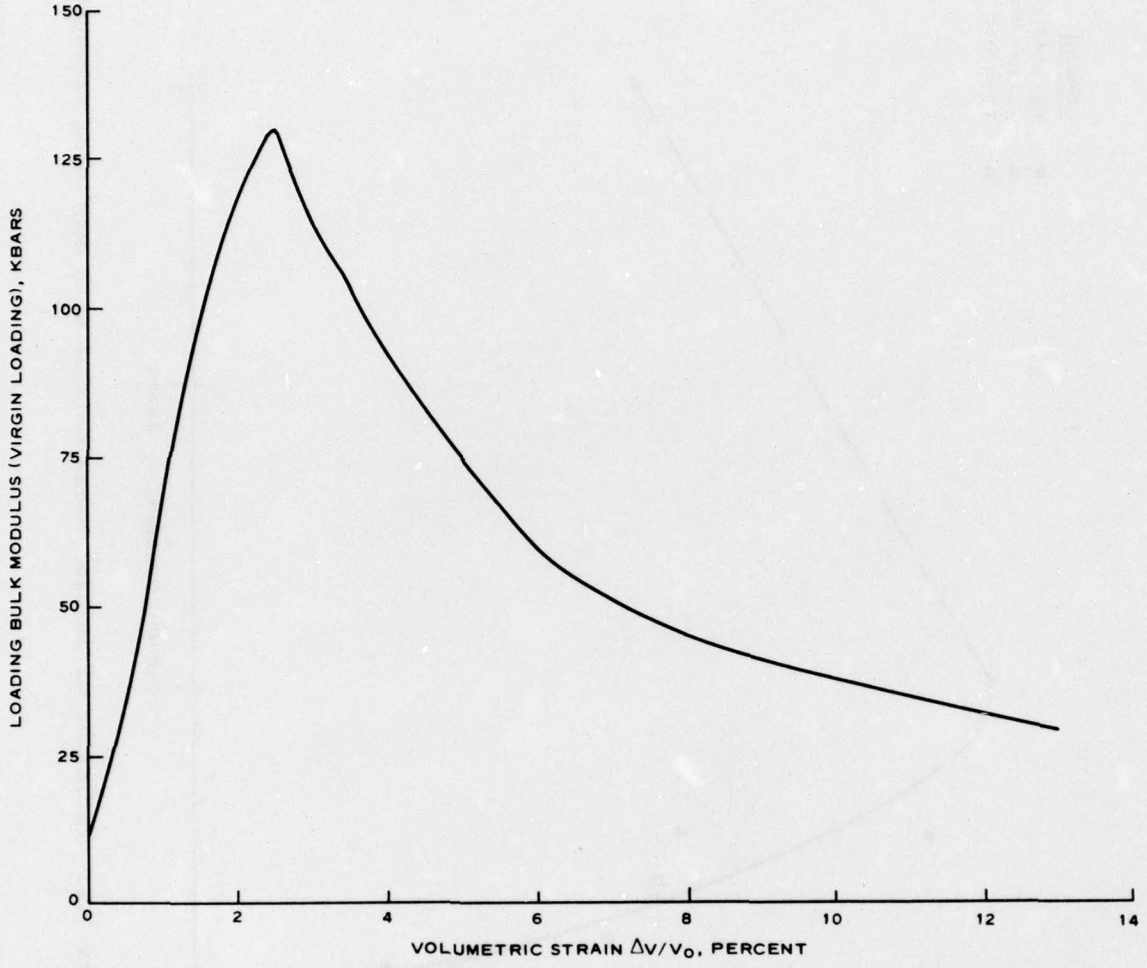

Figure 4.3. Variation of virgin-loading bulk modulus with volumetric strain.

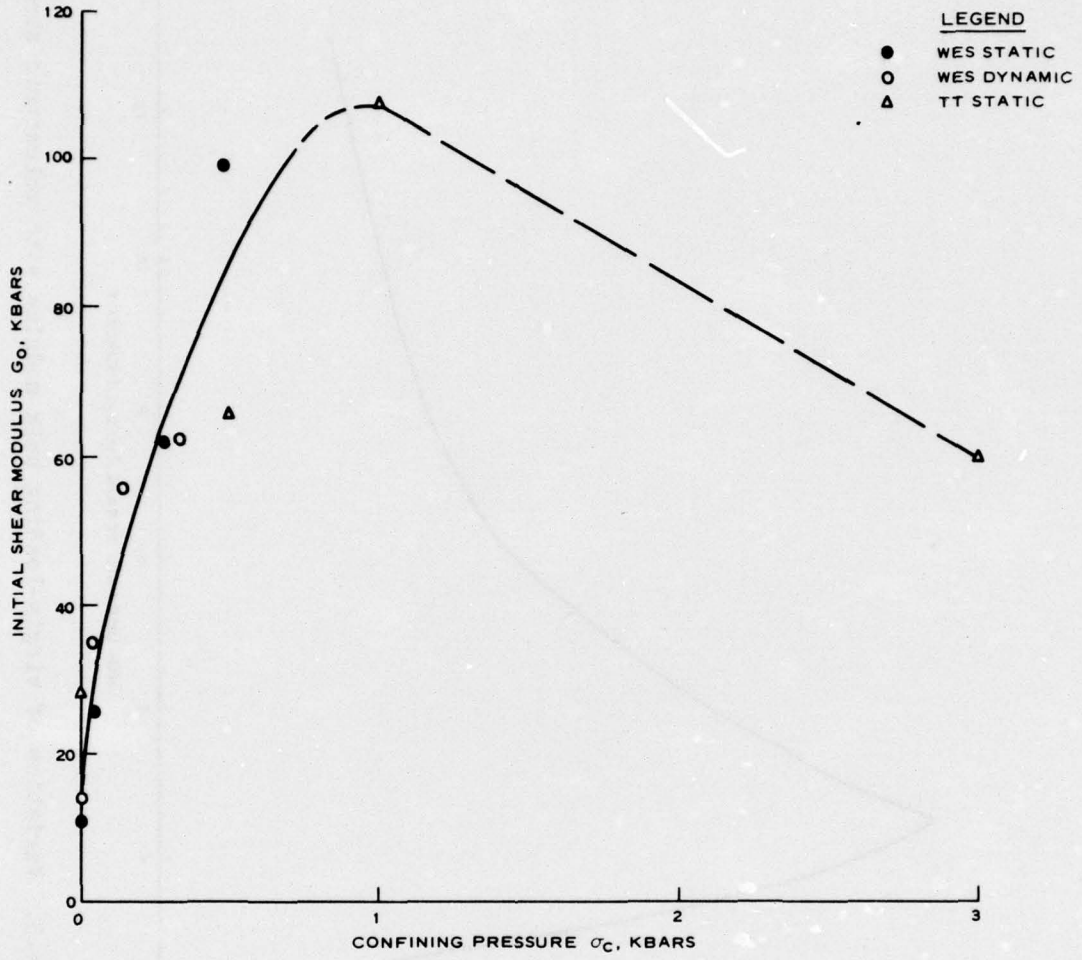

Figure 4.4. Variation of initial shear modulus with confining pressure.

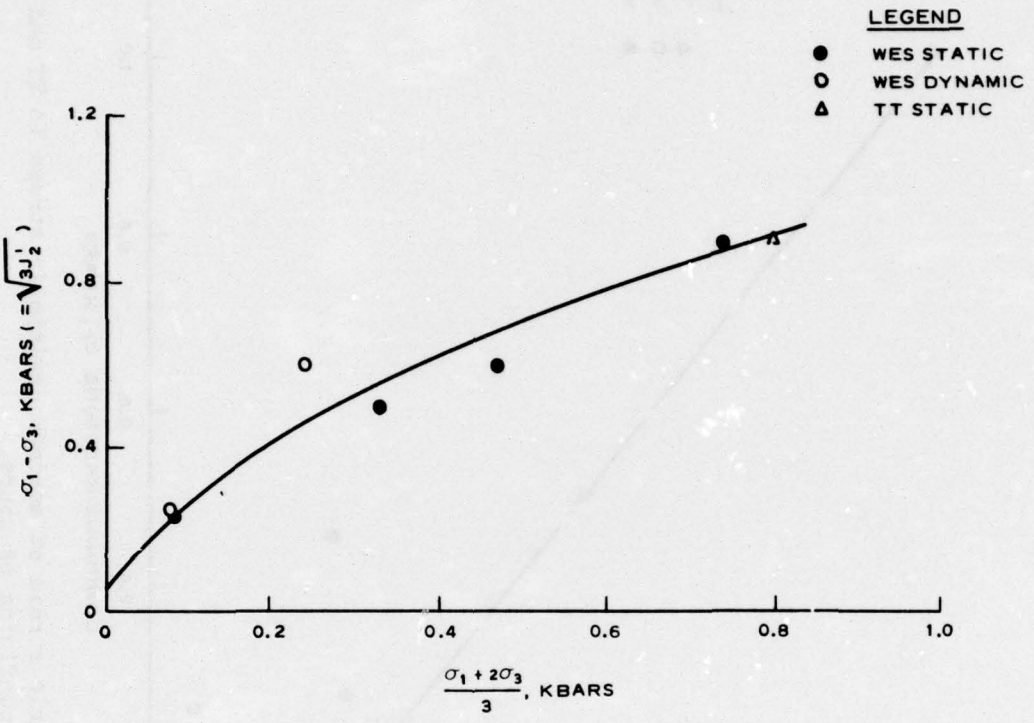

Figure 4.5. Envelope defining onset of inelastic (nonlinear) deviatoric stress-strain behavior in TX tests ($\sigma_3 = \sigma_c$).

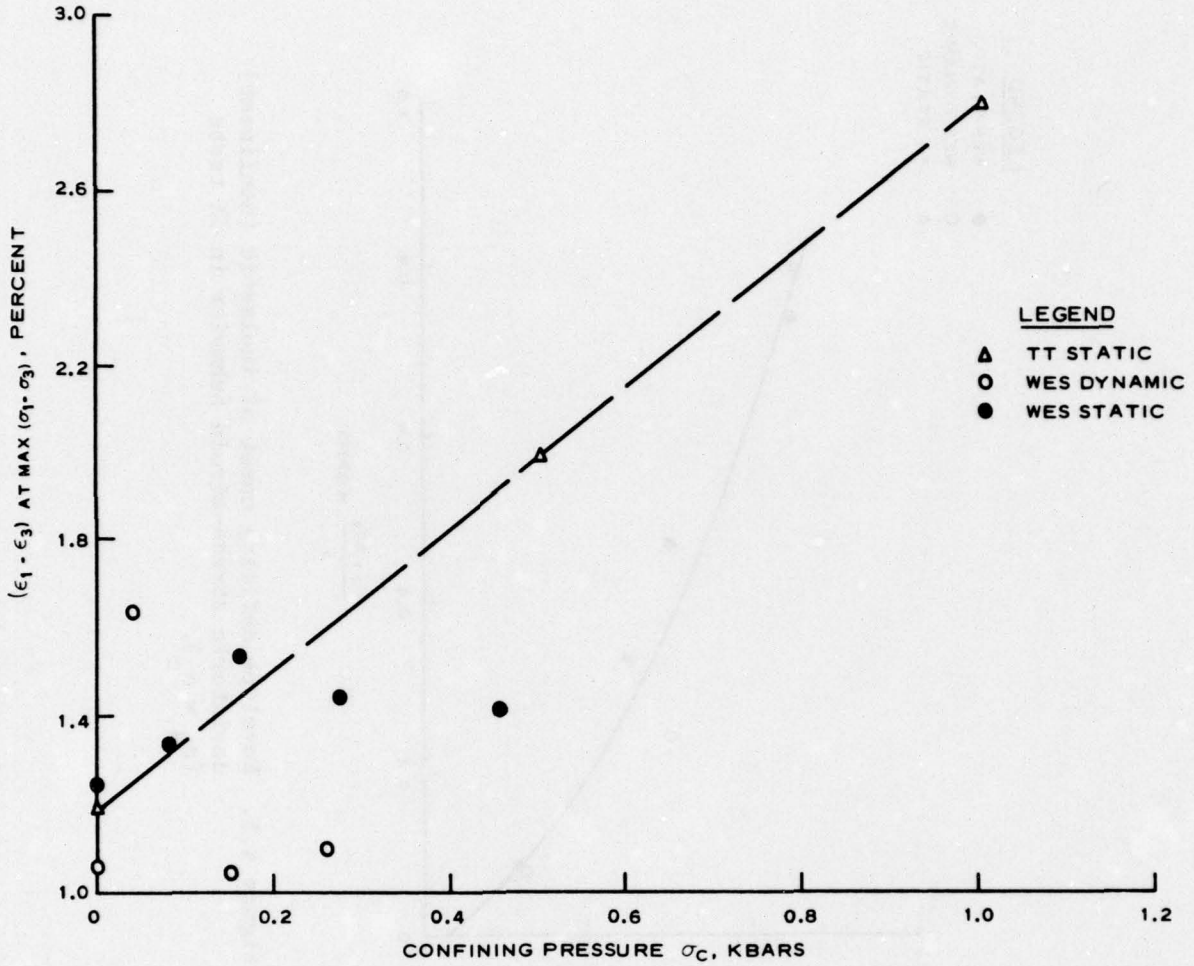

Figure 4.6. Deviatoric strain at maximum deviatoric stress in TT and WES TX tests versus confining pressure.

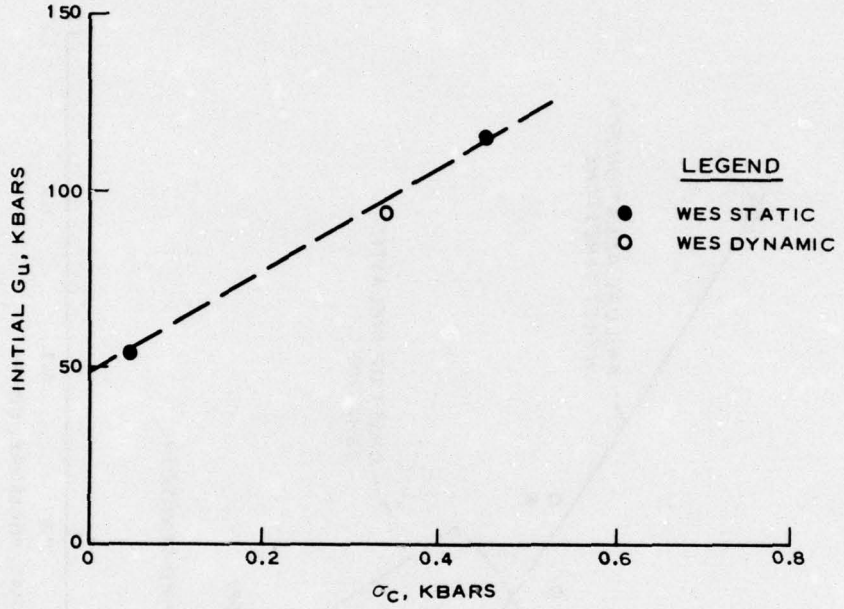

Figure 4.7. Initial unloading shear modulus (G_u) versus confining pressure (σ_c) for intact Dakota sandstone.

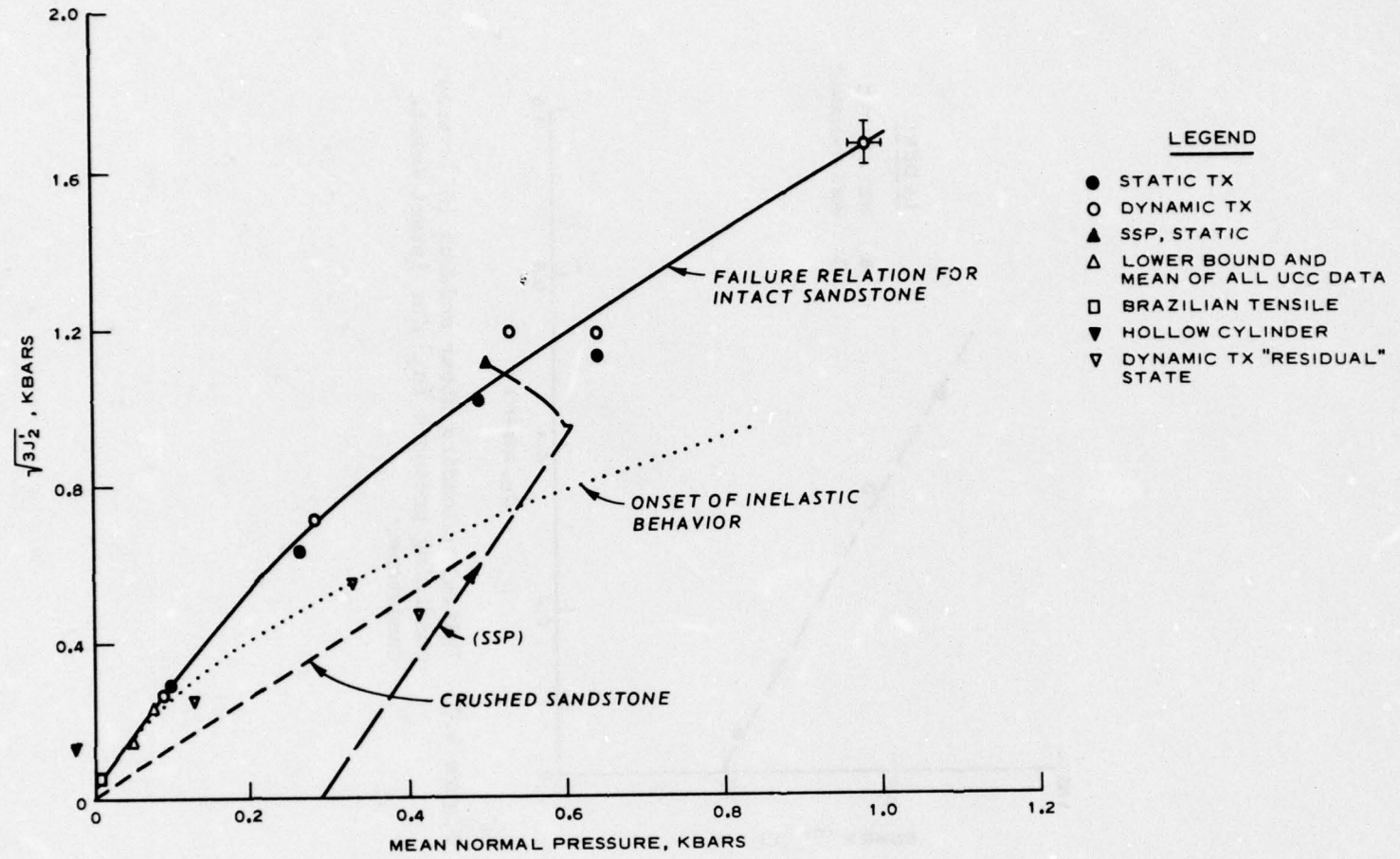

Figure 4.8. Failure data and recommended failure relation, Dakota sandstone, San Ysidro, N. Mex.

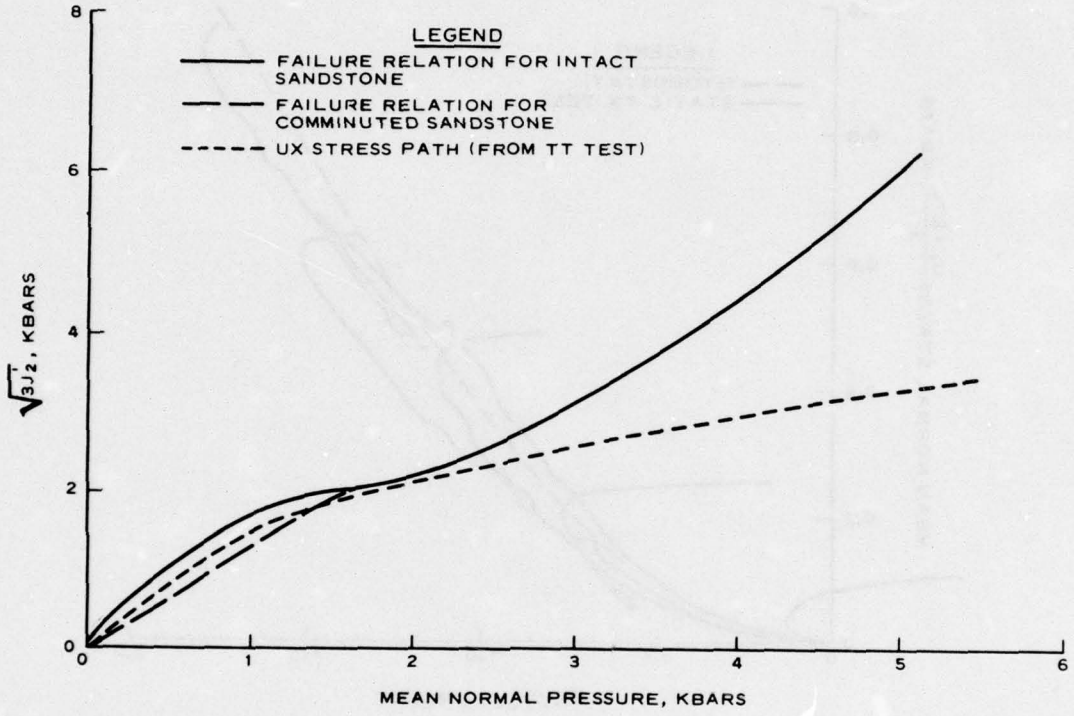

Figure 4.9. Recommended failure relation for intact sandstone.

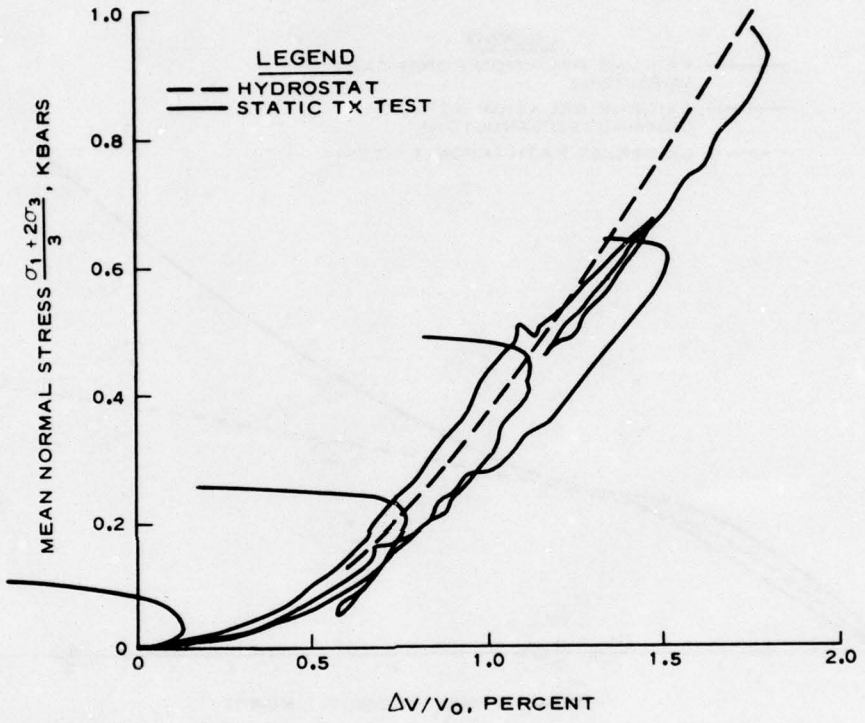

Figure 4.10. Mean normal stress versus volumetric strain behavior during shear.

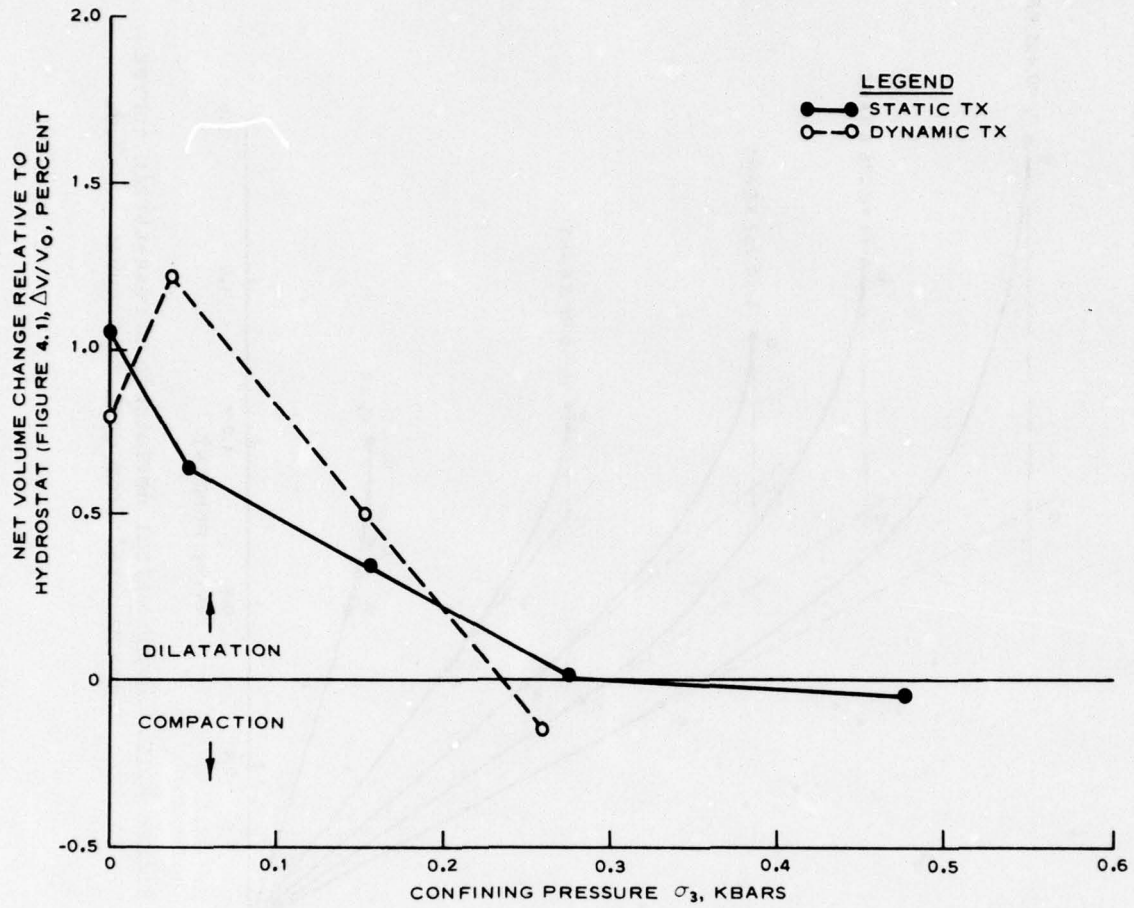

Figure 4.11. Amount of dilatation relative to hydrostat.

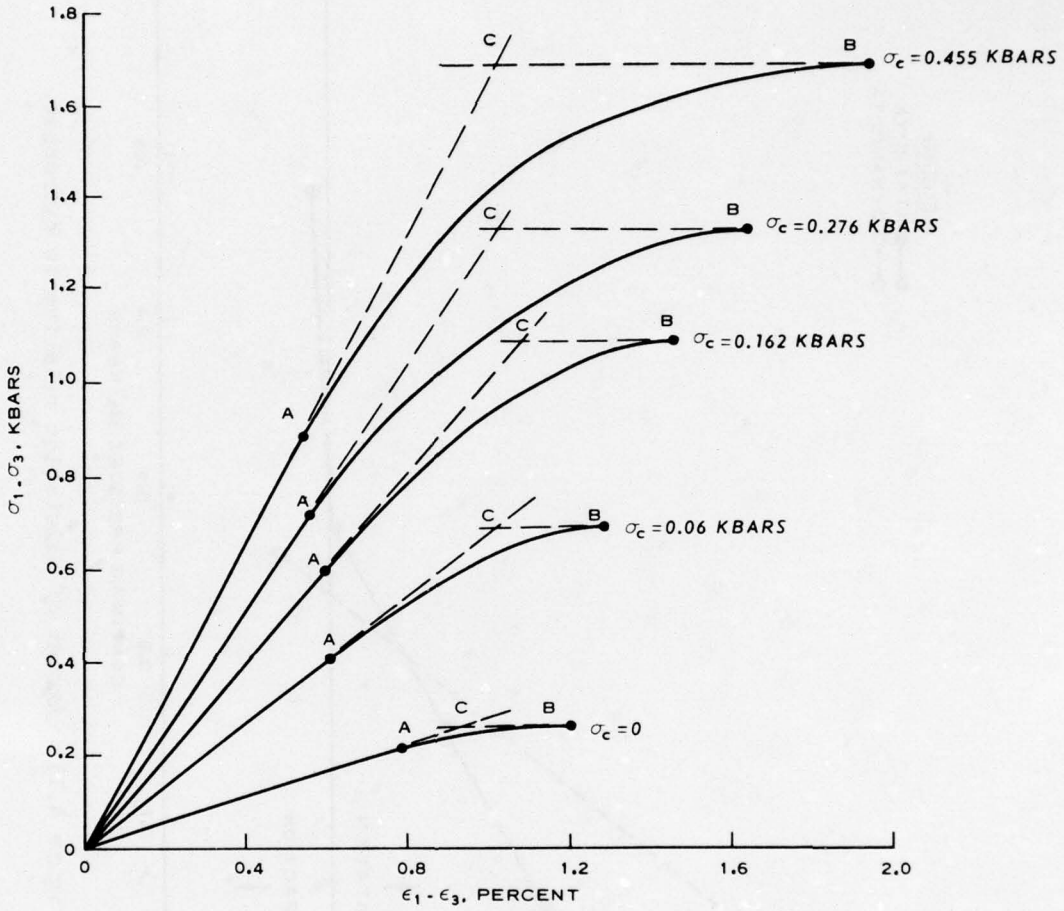

Figure 4.12. Hypothetical deviatoric stress-strain curves constructed from data in Figures 4.4-4.8.

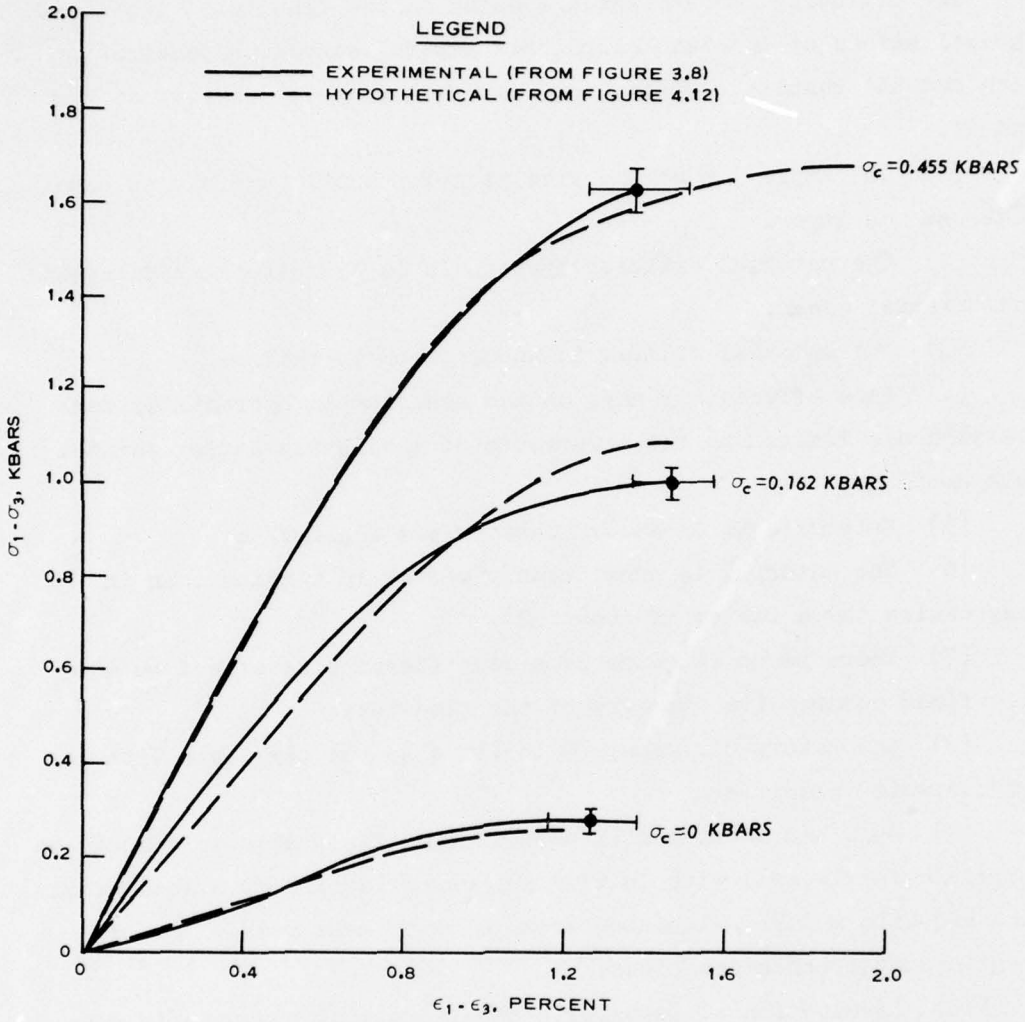

Figure 4.13. Comparison of selected hypothetical TX curves from Figure 4.12 with experimental TX curves from Figure 3.8.

CHAPTER 5

CONCLUSIONS AND RECOMMENDATIONS

The following conclusions are based on the results of the field investigations at the San Ysidro, New Mexico, sandstone penetration site and the results of laboratory material property testing at WES and TT.

(1) The upper 3 m of the site is sufficiently uniform to consider as one layer.

(2) The material exhibits hysteresis in hydrostatic compression and triaxial shear.

(3) The material dilates in shear prior to failure.

(4) Rate effects, if any, on the behavior in hydrostatic compression are limited to the occurrence of a slightly larger initial bulk modulus.

(5) Rate effects on shear behavior are negligible.

(6) The material is considerably weaker in tension than in compression (by a factor of about 30).

(7) There is no evidence of a significant size effect on the unconfined compressive strength of the sandstone.

(8) Laboratory ultrasonic velocities do not correlate with in situ seismic velocities.

(9) Bulk and shear moduli deduced from field seismic velocities correlate fairly well with initial slopes of laboratory stress-strain data and with moduli calculated from velocity measurements on the large-diameter sandstone cores.

(10) Examination of deviatoric strains during hydrostatic compression of small test specimens and the comparison of crosshole and downhole field seismic velocities give no evidence of significant anisotropy.

(11) The question of laboratory versus in situ properties is not a problem for the reverse ballistic test calculation application.

With regard to construction of constitutive models of the mechanical behavior of the sandstone for calculations of the Avco reverse ballistic tests and the SLA in situ penetration tests, the following recommendations are presented:

(1) Model the upper 3 m of the site as one homogeneous, isotropic layer.

(2) Use the laboratory test results unmodified in developing constitutive models for the reverse ballistic test calculations.

(3) The ideal constitutive model for this problem should:

a. Be mathematically rigorous (i.e., satisfy stability and uniqueness).

b. Be rate independent.

c. Exhibit hysteresis over a load-unload cycle in shear and in hydrostatic compression.

d. Dilate in shear.

e. Have limited tensile strength and shear strength which is a function of stress level.

f. Provide, as a minimum, for post-failure strength degradation to the residual strength of crushed sandstone.

REFERENCES

1. D. U. Deere, A. J. Hendron, F. D. Patton, and E. J. Cording, "Design of Surface and Near-Surface Construction in Rock," Eighth Symposium on Rock Mechanics, University of Minnesota, 1966.

2. J. Q. Ehrgott and R. C. Sloan, "Development of a Dynamic High-Pressure Triaxial Device," Technical Report S-71-15, Nov 1971, U. S. Army Engineer Waterways Experiment Station, CE, Vicksburg, MS.

3. L. Schindler, "Design and Evaluation of a Device for Determining the One-Dimensional Compression Characteristics of Soils Subjected to Impulse-Type Loads," Technical Report S-68-9, Nov 1968, U. S. Army Engineer Waterways Experiment Station, CE, Vicksburg, MS.

4. J. G. Jackson, Jr., "Uniaxial Strain Testing of Soils for Blast Oriented Problems," Miscellaneous Paper S-68-17, Sep 1968, U. S. Army Engineer Waterways Experiment Station, CE, Vicksburg, MS.

5. E. A. Day, "Rock/Steel Dynamic Friction Measurements--Addition to the Rotary Viscometer," Progress Report to DNA on Contract No. DNA 001-75-C-0183, Report No. SSS-R-75-2599, Mar 1975.

6. E. S. Gaffney, "Friction Tests on Sandstone and Grout," Bimonthly Progress Report on DNA Contract No. DNA 001-75-C-0183, Report No. SSS-R-76-2881, Mar 1976.

7. D. L. Orphal, W. F. Borden, and J. E. Reaugh, "A Computation of a DNA Earth Penetration Experiment at the Watching Hill Site, DRES, Canada," Technical Report No. DNA 3685F, Oct 1975, Physics International Co., San Leandro, CA.

8. M. H. Wagner, K. N. Kreyenhagen, and W. S. Goerke, "Numerical Analysis of DNA Earth Penetration Experiment at DRES," Technical Report No. DNA 3537F, Oct 1974, California Research and Technology, Inc., Woodland Hills, CA.

9. M. H. Wagner, K. N. Kreyenhagen, and W. S. Goerke, "Numerical Analysis of Projectile Impact and Deep Penetration into Earth Media," Contract Report S-75-4, Aug 1975, U. S. Army Engineer Waterways Experiment Station, CE, Vicksburg, MS.

10. R. K. Byers, A. J. Chabai, and R. T. Walsh, "Predictions of Projectile Penetration Phenomena and Comparison with Experiments in a Soil Medium," Technical Report No. SAND-75-0174, Sandia Laboratories, Albuquerque, NM.

11. R. L. Bjork, "Calculations of Earth Penetrators Impacting Soils," Technical Report PT-4-75-0013, Sep 1975, Pacifica Technology, Inc., Del Mar, CA.

12. M. H. Wagner, "Finite Difference Code Solutions of Penetration into Rock," A Presentation at the DNA Earth Penetration Technology Review, 29-30 Oct 1975, California Research and Technology, Inc., Woodland Hills, CA.

13. Y. M. Ito, K. N. Kreyenhagen, G. E. Eggum, and W. S. Goerke, "Analysis of Dynamic Stresses within a Terminal Delivery Vehicle During Penetration of a Hard Earth Target," Contract Report S-75-1, Feb 1975, U. S. Army Engineer Waterways Experiment Station, CE, Vicksburg, MS.

14. M. H. Wagner, "Parametric Study of the Effects of Target Properties, Projectile Design and Impact Conditions on Penetration Processes," 30 Oct 1975, A Presentation at the DNA Penetration Technology Review, California Research and Technology, Inc., Woodland Hills, CA.

15. K. N. Kreyenhagen, Letter to MAJ Todd Stong, DNA, dated 3 Jul 1975, subject: Results of TTR Tuff Calculation, California Research and Technology, Inc., Woodland Hills, CA.

16. P. F. Hadala, "Laboratory Support Studies for all Pretest Predictions of Rock Penetration Tests in TTR Welded Tuff," Oct 1975, A Presentation at the DNA Penetration Technology Review, U. S. Army Engineer Waterways Experiment Station, CE, Vicksburg, MS.

17. P. F. Hadala, Letter to Mr. K. N. Kreyenhagen, dated 16 Dec 1974, U. S. Army Engineer Waterways Experiment Station, CE, Vicksburg, MS.

18. D. U. Deere, A. H. Merritt, and R. F. Coon, "Engineering Classification of In Situ Rock," Technical Report No. AFWL-TR-67-144, Jan 1969, Air Force Weapons Laboratory.

APPENDIX A

IN SITU SEISMIC SURVEY

SANDSTONE PENETRATION SITE, SAN YSIDRO, NEW MEXICO

A.1 INTRODUCTION

An in situ seismic survey was conducted at the proposed Defense Nuclear Agency (DNA) sandstone penetration site near San Ysidro, New Mexico, during the period 19-23 September 1975. The purpose of the survey was to provide in situ seismic information relative to the site material(s). More specifically, compression- and shear-wave (P- and S-wave) velocities and depths to interfaces were to be determined from the ground surface to a depth of about 20 feet using surface refraction seismic, crosshole seismic, and downhole seismic techniques. The survey was planned by Mr. D. K. Butler, Physicist, Soil Dynamics Division, WES, and was conducted by Messrs. E. Gomez, D. H. Douglas, and J. R. Curro, Jr., of the Earthquake Engineering and Vibrations Division, WES. This appendix was prepared by Mr. Curro.

A.2 EQUIPMENT AND TEST PROCEDURES

A.2.1 Surface Refraction Seismic Tests. The surface refraction seismic tests were conducted using a battery-operated 24-channel seismograph and camera. The camera produced a permanent record on oscillograph paper by transforming a signal, in the form of electrical impulses, into a light beam response which was then recorded on the paper. Resolution time with this recording unit was about 0.5 msec. Response of the soil was monitored by vertical velocity-type geophones. A 16-pound hammer provided the seismic energy source. Twenty-four geophones were used to detect the signal produced by the energy source. These geophones were placed in a straight line at 5-foot intervals along the surface of the ground. A metal plate, placed on the ground surface near the first geophone at one end of the line, was struck with the hammer, and a recording of the compression-wave arrival detected by each geophone

was obtained, the first geophone having recorded zero time. The plate was then moved to the opposite end of the line and again struck with the hammer, and another recording was obtained. When this procedure had been completed, two seismic traverses (forward and reverse) resulted. The above procedure was supplemented by using fewer geophones and closer interval spacing on each traverse to obtain more detailed information relative to the near-surface materials.

Data obtained from refraction seismic tests consist basically of the time required for a compression wave to travel from the seismic source (hammer) to points of detection (geophones). Data are plotted in graphic form as travel time from the seismic source to each geophone versus the respective distances of the geophones from the source. Velocities and depths to interfaces are calculated using procedures commonly found in seismology texts.[A.1]

A.2.2 Downhole Test. The downhole test was conducted with the same seismograph as used in the surface refraction seismic tests but only four channels of the data were recorded. Geophones consisted of one triaxial array of transducers housed in a unit having an integral extendable spring and one vertical velocity-type geophone. The downhole test was performed by placing the triaxial geophone in a borehole at a known depth with the vertical geophone placed 5 feet from the mouth of the borehole on the ground surface. The metal plate, positioned near the vertical geophone, was struck with the hammer with the resulting seismic signal being recorded from the triaxial geophone and zero time being recorded by the vertical geophone. The triaxial geophone was then moved to the next desired test evaluation in the borehole and the seismic signal again recorded. The above procedure was repeated until all desired depth locations in the borehole had been tested. For the downhole test in this survey, testing was done at 5-foot increments from the ground surface to a depth of 20 feet. Data obtained from a downhole test consist basically of the time required for particular wave types (P- and S-waves for this

test) to travel from a seismic source on the ground surface to a point of detection in a borehole. Data are plotted as travel time from the seismic source to the geophone versus the slant distance of the geophone from the source. Average vertical P- and S-wave velocities are then computed from the inverse slope of lines drawn through the plotted points.

A.2.3 Crosshole Tests. Crosshole tests were conducted using a portable single-channel enhancement seismograph and associated instrumentation as shown and described in Reference A.2. With this complement of instrumentation, seismic wave arrival times can be determined with an accuracy of 0.5 msec. A strip chart recorder was used in conjunction with the enhancement unit to provide a permanent record of the data. Both the unit and recorder are battery-operated. Two geophones were used in the crosshole tests with each being a triaxial array of transducers housed as a unit. The crosshole tests were performed using existing boreholes at the site which had been drilled in the sandstone and, therefore, did not necessitate plastic casing to prevent caving. Borehole orientation surveys to establish the vertical alignment of the holes were not conducted.

The crosshole test procedure consists of placing a triaxial geophone at a known elevation in a borehole, which acts as a seismic source when used with the complement of instrumentation. In another borehole, a second triaxial geophone is placed at the same elevation as the seismic source, which acts as a receiver for the transmitted seismic signal. When the P- and S-wave data had been obtained at the first test elevation, both geophones were moved either up or down the boreholes to the next desired test depth and the P- and S-wave data recorded. This procedure was repeated until all desired elevations had been tested. The geophones were then moved to other boreholes at the site and the above procedure repeated.

Data obtained from a crosshole test are the times required for P- and S-waves to propagate from a source in a borehole to a point of

detection in a different borehole. These times are then divided into the straight-line distance between source and receiver geophones to yield apparent velocities. If a nearby higher velocity layer exists, the wave will refract and travel along that layer, thus traveling a faster path than the direct distance path. In such instances, calculations based on Snell's law of refraction must be used to determine true velocities by accounting for zones of high velocity contrast. Due to the nature and number of calculations involved in a typical application of the crosshole technique to a layered site, a computer program for crosshole seismic interpretation was used for reducing the data.[A.3] This program uses Snell's law of refraction to develop a plausible true velocity interpretation from the apparent velocity profile as determined from the field data.

A.3 TEST RESULTS

A.3.1 Surface Refraction Seismic Tests. Four surface refraction seismic traverses (two lines) were run at the site. These traverses, designated S-1 through S-4, were located and oriented as shown in the test layout, Figure A.1.

The P-wave arrival time versus distance plots for traverses S-1 through S-4 are shown in Figures A.2 and A.3 as are computed velocities and depths to interfaces. These data were used to construct P-wave velocity profiles for the subsurface materials. These profiles are presented in Figures A.4 and A.5. Two velocity zones were indicated from the data. The near-surface zone ranged from 3325 to 3415 fps and varied in thickness from 10 to 13 feet. The underlying zone ranged from 5160 to 5345 fps and extended to an undetermined depth.

A.3.2 Downhole Test. The results of the downhole test which was conducted in boring NX-3 (Figure A.1) are shown in Figure A.6. Two velocity zones were indicated from the downhole test data. The near-surface zone exhibited average P- and S-wave velocities of 3725 and 1665 fps, respectively. The second zone yielded velocities of

6295 fps (P-wave) and 2850 fps (S-wave). The depth to the interface between the two zones is questionable because of the slant distance parameter involved but should average about 7.5 feet.

A.3.3 Crosshole Tests. Two crosshole tests were conducted at the site; one test used borings NX-1 and NX-3 and the other used borings NX-2 and U-1. The orientation and location of the tests are shown in Figure A.1.

The seismic source and geophone placements used in the conduct of the crosshole tests from borings NX-1 and NX-3 and from borings NX-2 and U-1 are shown in Figures A.7 and A.8, respectively. P-wave velocities determined from the crosshole tests are presented alongside the geophone positions. In a like manner, seismic source and geophone locations used in the crosshole tests are again presented in Figures A.9 and A.10 but S-wave velocities determined from the tests are included beside the geophone position.

A.4 DATA INTERPRETATION

The P-wave velocity results from the crosshole, surface refraction seismic, and downhole tests were analyzed and an interpretation made which produced two velocity zones at the site as shown in Figures A.11 and A.12. The near-surface zone ranged from 3325 to 3415 fps and extended to a depth of about 12 feet. The underlying zone had a velocity range from 5160 to 5345 fps and extended to an undetermined depth.

The S-wave velocity results from the crosshole and downhole tests were contoured into velocity zones which are shown in Figures A.13 and A.14. Three zones were interpreted from the crosshole and downhole data obtained from borings NX-1 and NX-3 as shown in Figure A.13. The near-surface zone had a velocity of 1665 fps and extended to a depth of about 6 feet where a 2825-fps zone was encountered. This zone was noted to a depth of about 15 feet. The third velocity zone, 3390 fps, extended to an undetermined depth. The data from borings NX-2 and U-1 were contoured into two velocity zones as shown in Figure A.14. The near-surface

zone with a velocity of 1665 fps was evident to a depth of about 6 feet. The second zone, 2790 fps, extended from 6 to 10 feet (limit of testing) in depth. It should be noted that borings NX-2 and U-1 were only 10 feet deep; therefore, the third velocity zone at 15 feet could not have been detected. The velocities and interface depths for zones 1 and 2 from borings NX-1 and NX-3 correlate very well with those from NX-2 and U-1.

REFERENCES

A.1. Heiland, C. A. "Geophysical Exploration," Hafner Publishing Company, Inc., New York, NY, 1968.

A.2. Ballard, R. F., Jr., "A Method for Crosshole Seismic Testing," Shock and Vibration Problems in Geotechnical Engineering, Meeting Preprint 2536, American Society of Civil Engineers National Convention, 2-7 Nov 1975.

A.3. Skoglund, G. R., "Procedures for Crosshole Seismic Investigations," (in preparation), U. S. Army Engineer Waterways Experiment Station, CE, Vicksburg, MS.

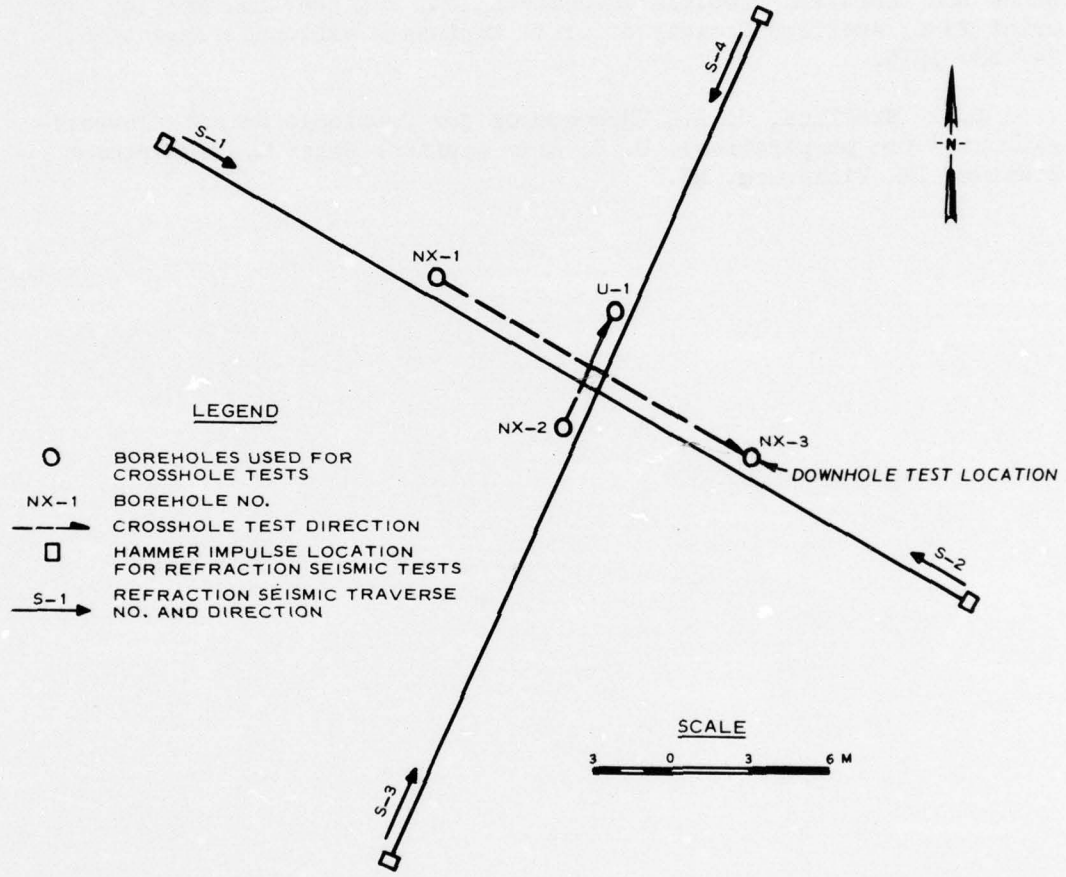

Figure A.1. Plan view showing crosshole, downhole, and surface refraction seismic test layouts.

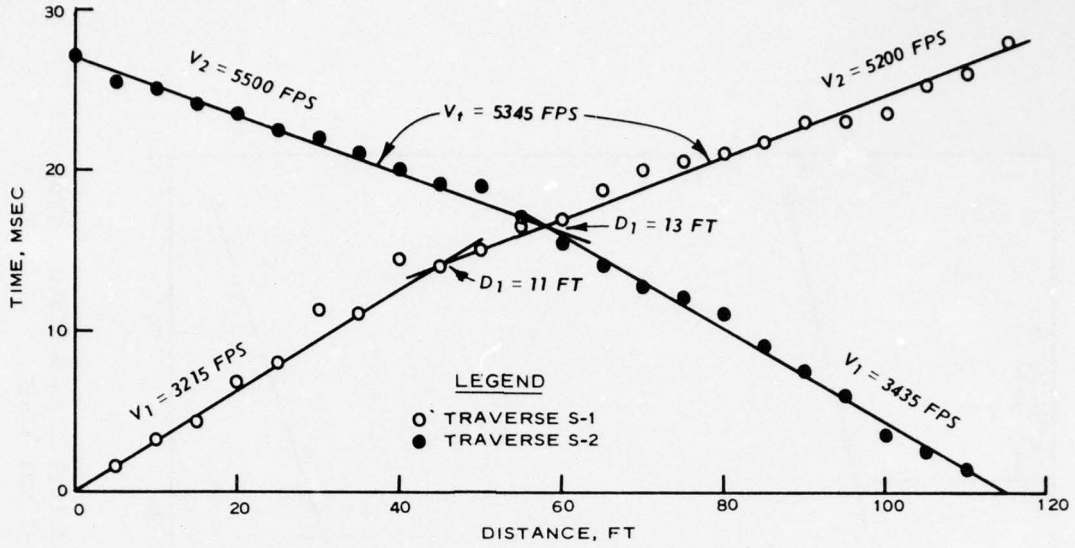

Figure A.2. P-wave arrival time versus distance from surface refraction seismic test conducted across borings NX-1 and NX-3.

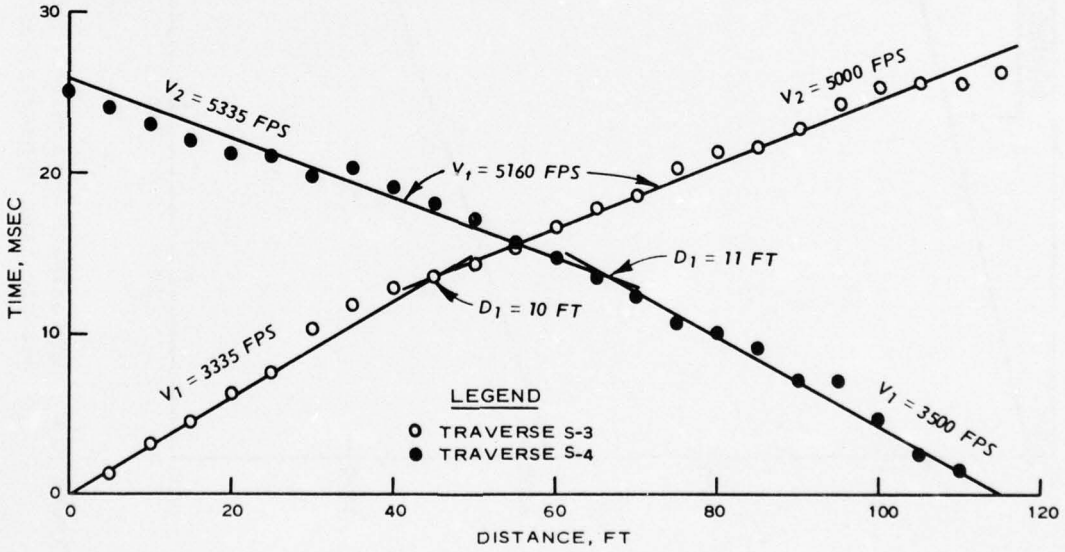

Figure A.3. P-wave arrival time versus distance from surface refraction seismic test conducted across borings NX-2 and U-1.

AD-A040 056 TERRA TEK INC SALT LAKE CITY UTAH F/G 8/7
CONSTITUTIVE PROPERTY INVESTIGATIONS IN SUPPORT OF FULL-SCALE P--ETC(U)
APR 77 D K BUTLER, R R NIELSEN, R K DROPEK DNA001-75-C-0177
WES-TR-S-77-3 NL

UNCLASSIFIED

2 OF 2
AD
A040056

END

DATE
FILMED
6-77

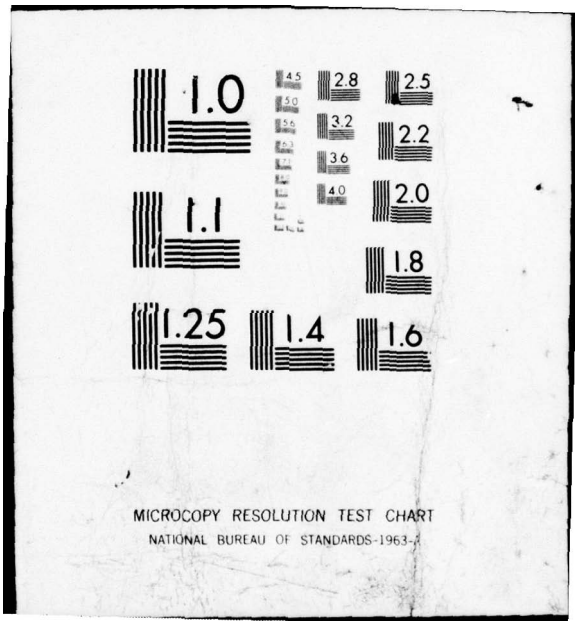
1.0
1.1
1.25
1.4
1.6
1.8
2.0
2.2
2.5
2.8
3.2
3.6
4.0
4.5
5.0
5.6
MICROCOPY RESOLUTION TEST CHART
NATIONAL BUREAU OF STANDARDS-1963-A

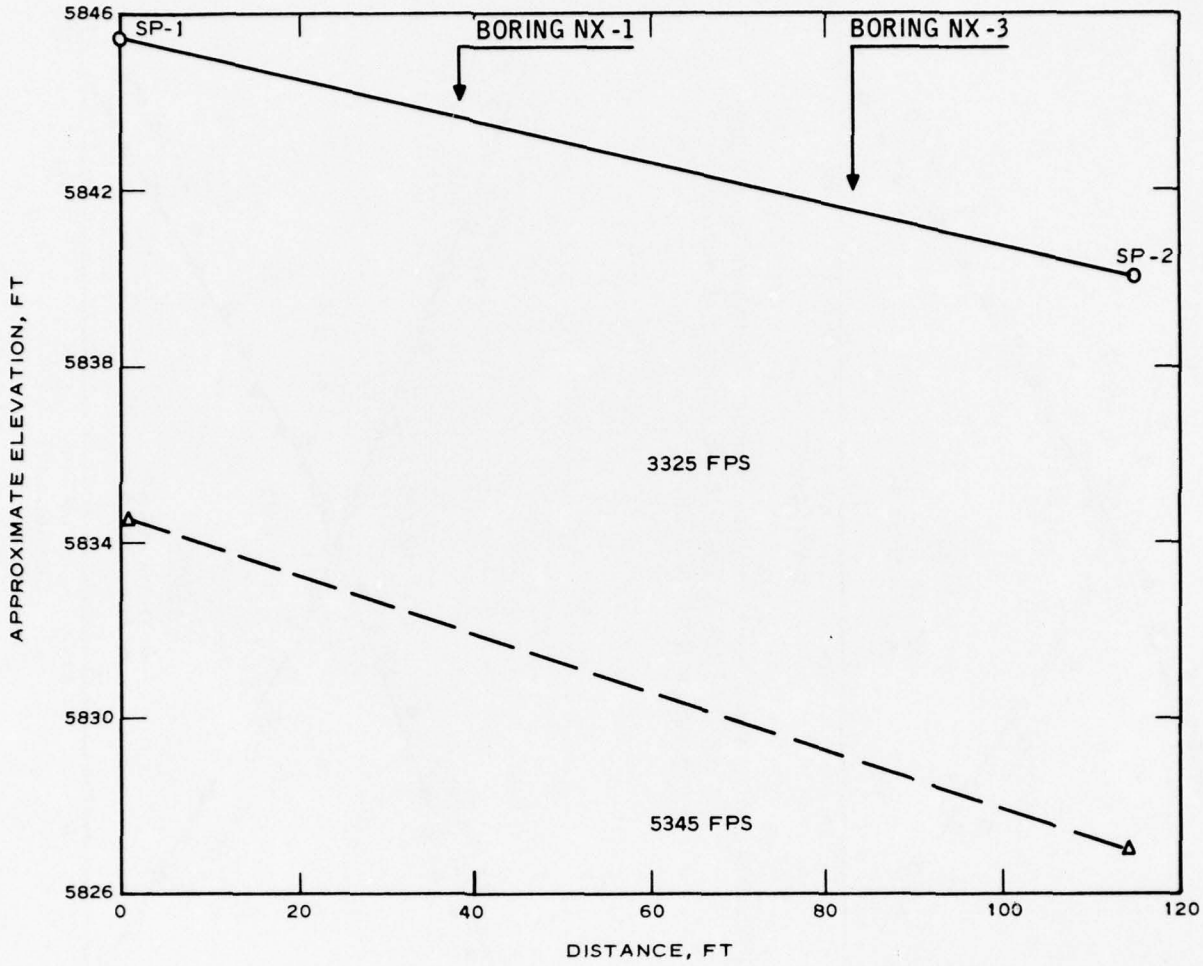

Figure A.4. Approximate P-wave velocity profile determined from surface refraction seismic test conducted across borings NX-1 and NX-3.

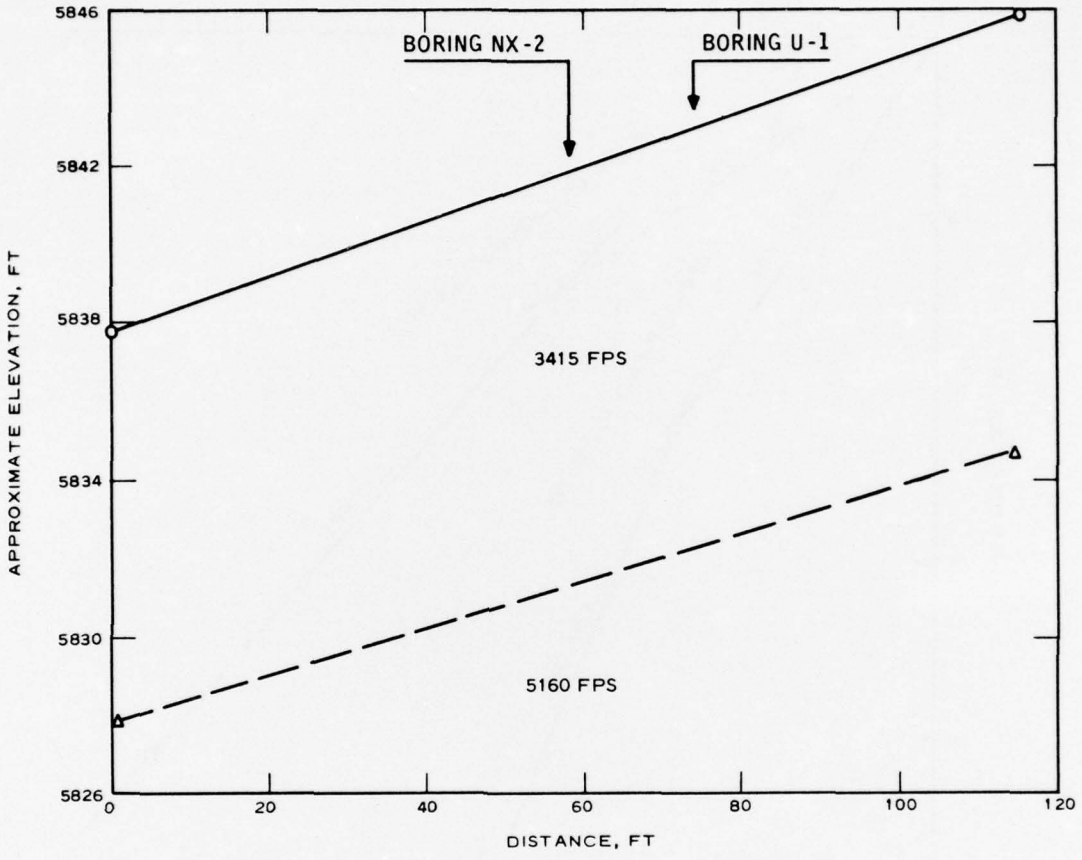

Figure A.5. Approximate P-wave velocity profile from surface refraction seismic test conducted across borings NX-2 and U-1.

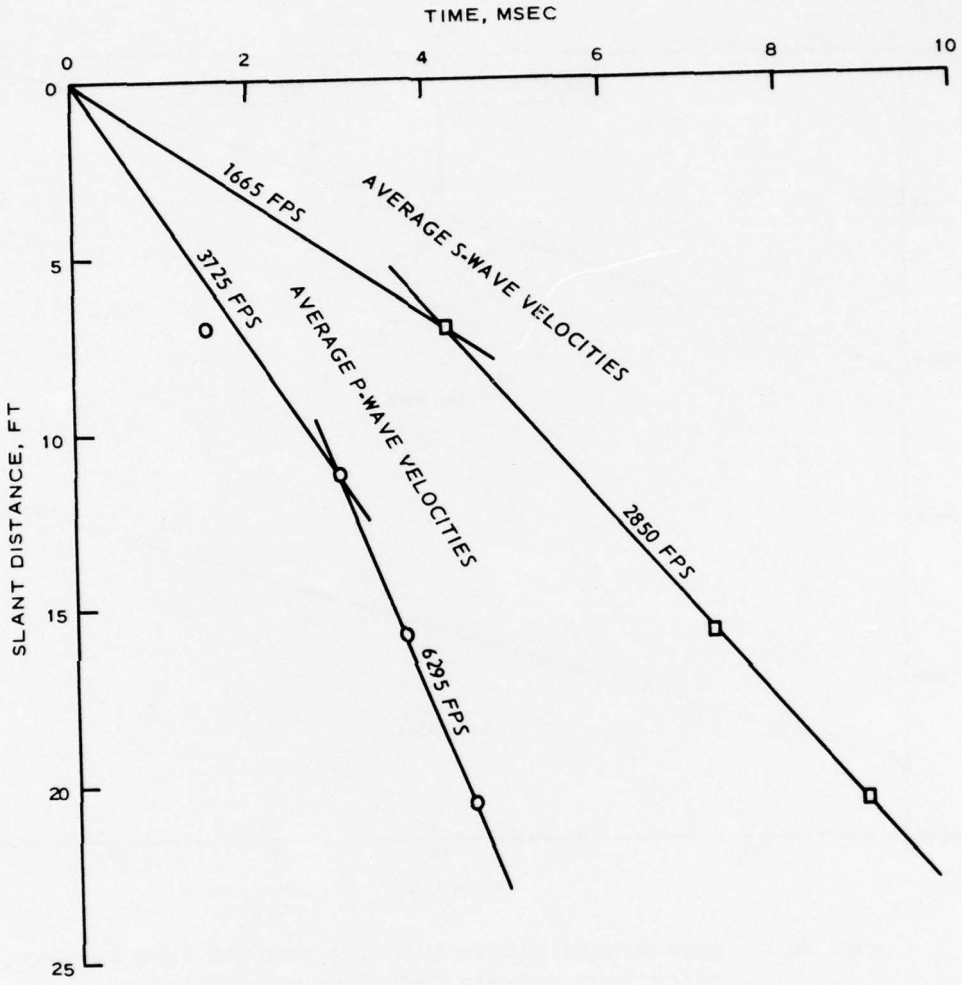

Figure A.6. P- and S-wave arrival times versus slant distance from downhole test conducted in boring NX-3.

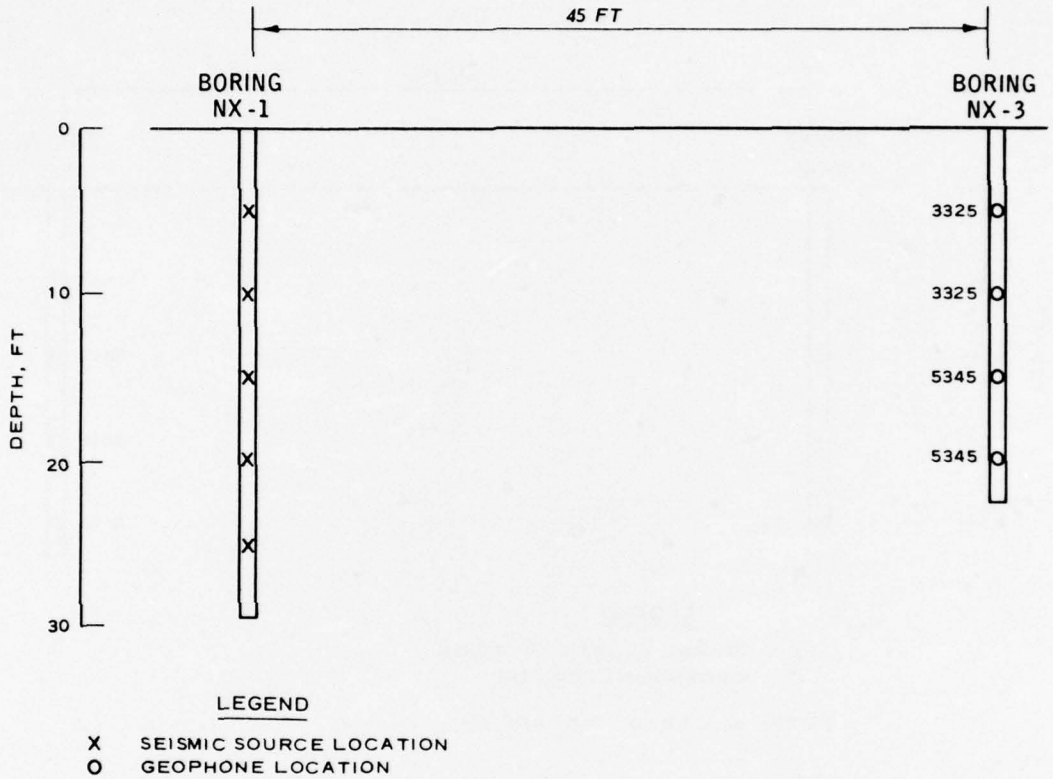

Figure A.7. Seismic source and geophone placements used in conduct of crosshole tests and corresponding true P-wave velocities determined from borings NX-1 and NX-3.

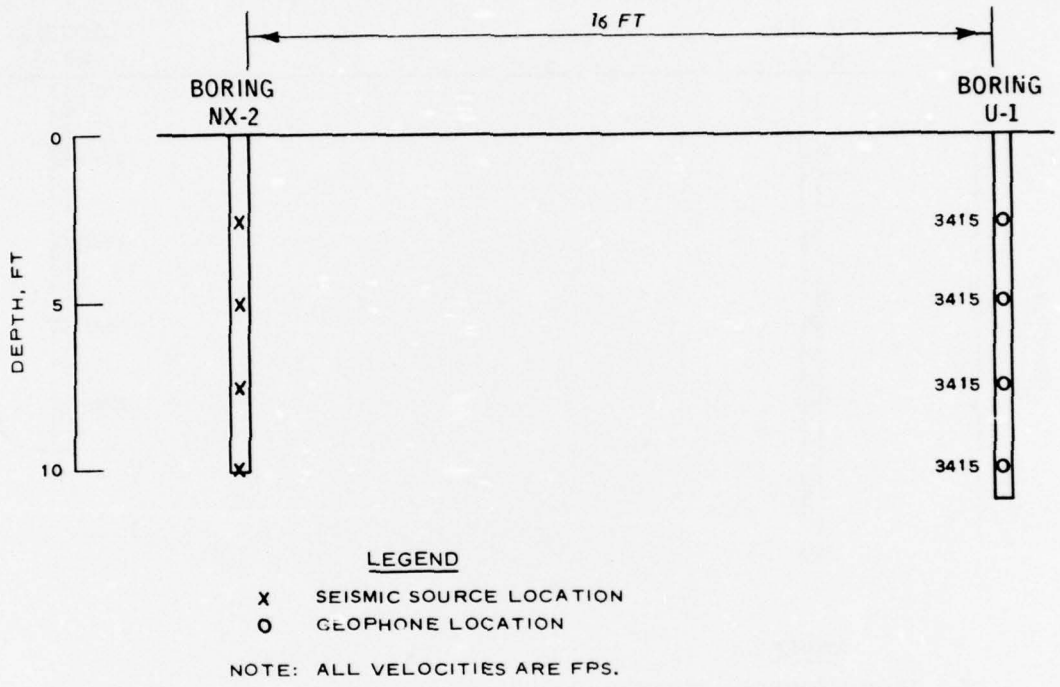

Figure A.8. Seismic source and geophone placements used in conduct of crosshole tests and corresponding true P-wave velocities determined from borings NX-2 and U-1.

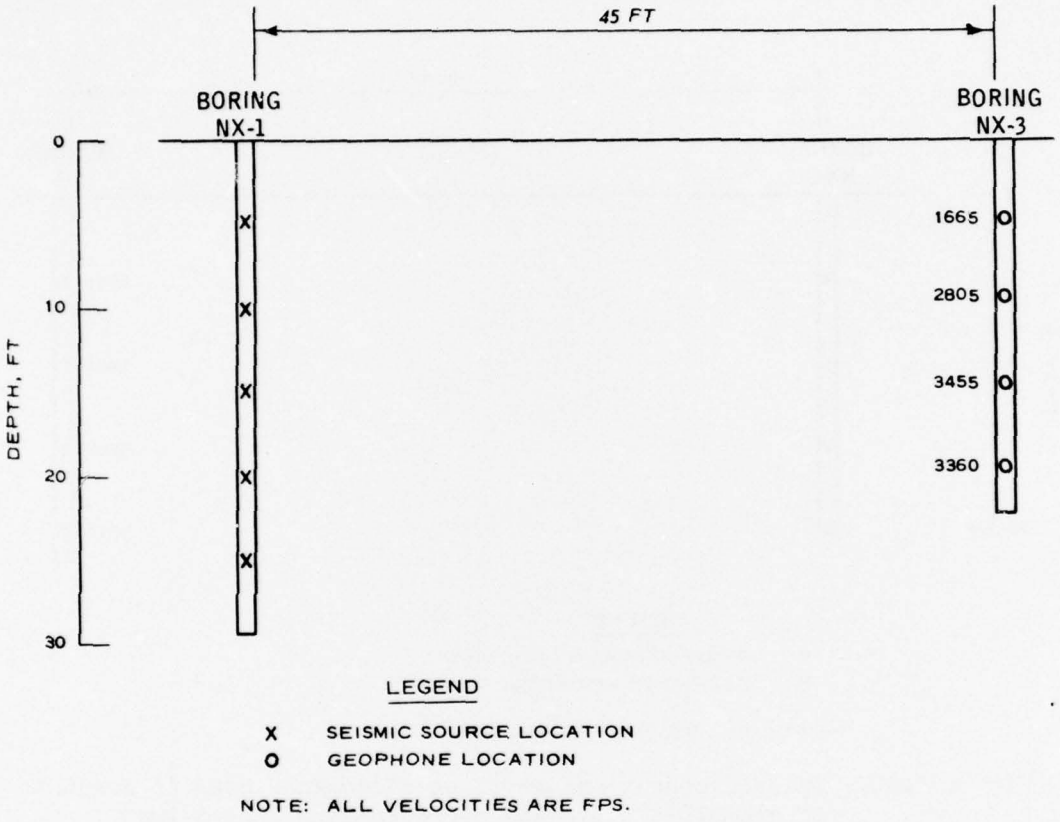

Figure A.9. Seismic source and geophone placements used in conduct of crosshole tests and corresponding true S-wave velocities determined from borings NX-1 and NX-3.

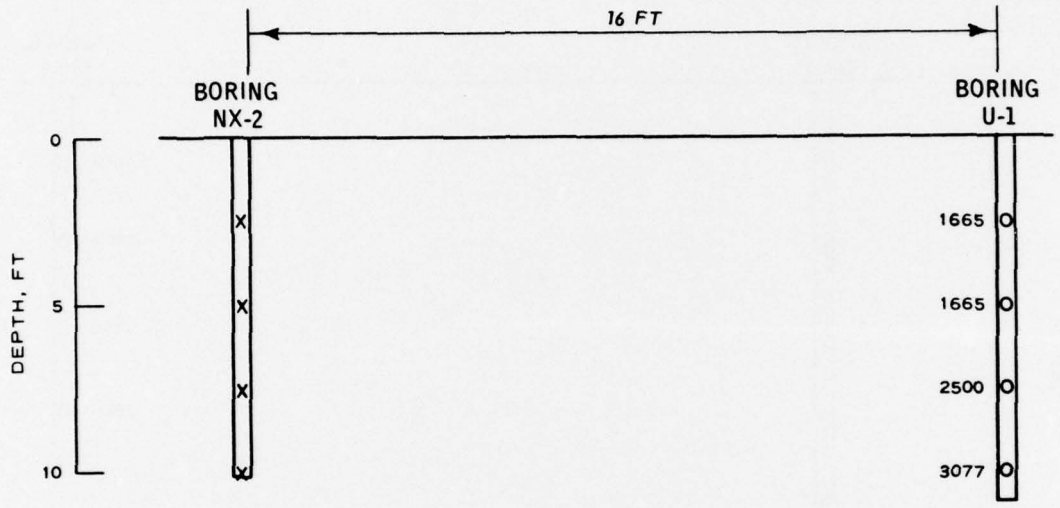

Figure A.10. Seismic source and geophone placements used in conduct of crosshole tests and corresponding true S-wave velocities determined from borings NX-2 and U-1.

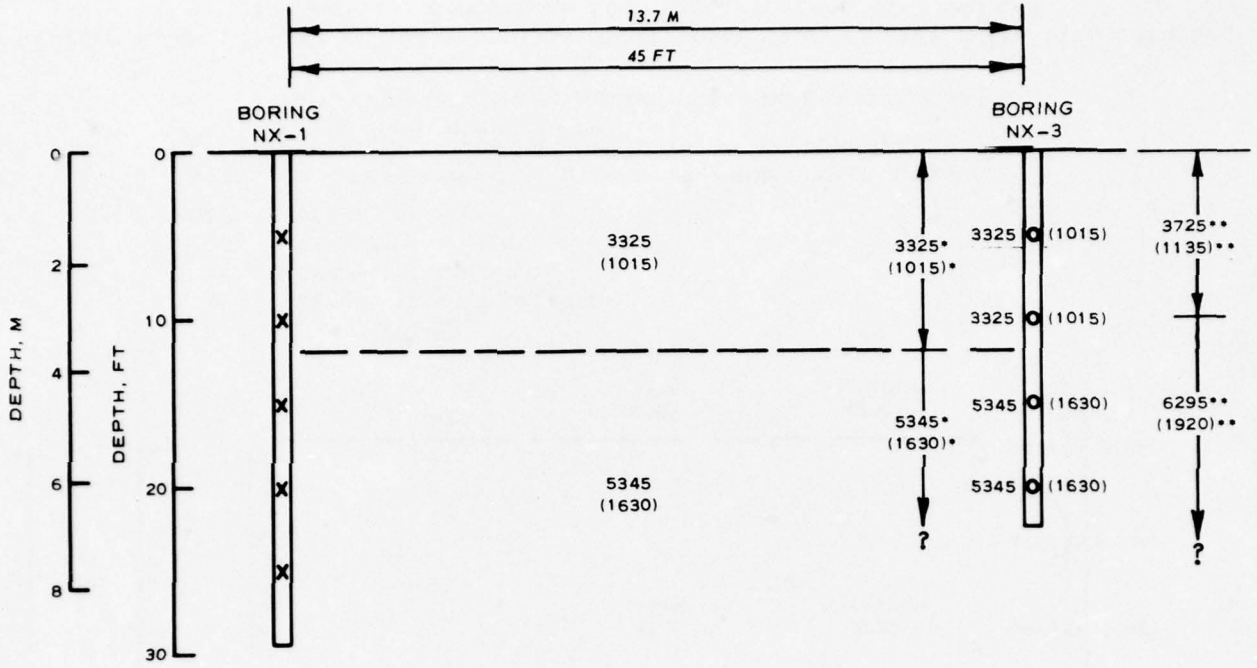

LEGEND

X	SEISMIC SOURCE LOCATION
O	GEOPHONE LOCATION
(1015)	VELOCITY IN M/SEC
3325	VELOCITY IN FPS

NOTE: NO ASTERISK DENOTES VELOCITIES FROM CROSSHOLE DATA.
ONE ASTERISK DENOTES VELOCITIES FROM SURFACE REFRACTION SEISMIC DATA.
TWO ASTERISKS DENOTE VELOCITIES FROM DOWNHOLE DATA.

Figure A.11. P-wave velocity profile interpreted from surface refraction seismic, crosshole, and downhole test data, borings NX-1 and NX-3.

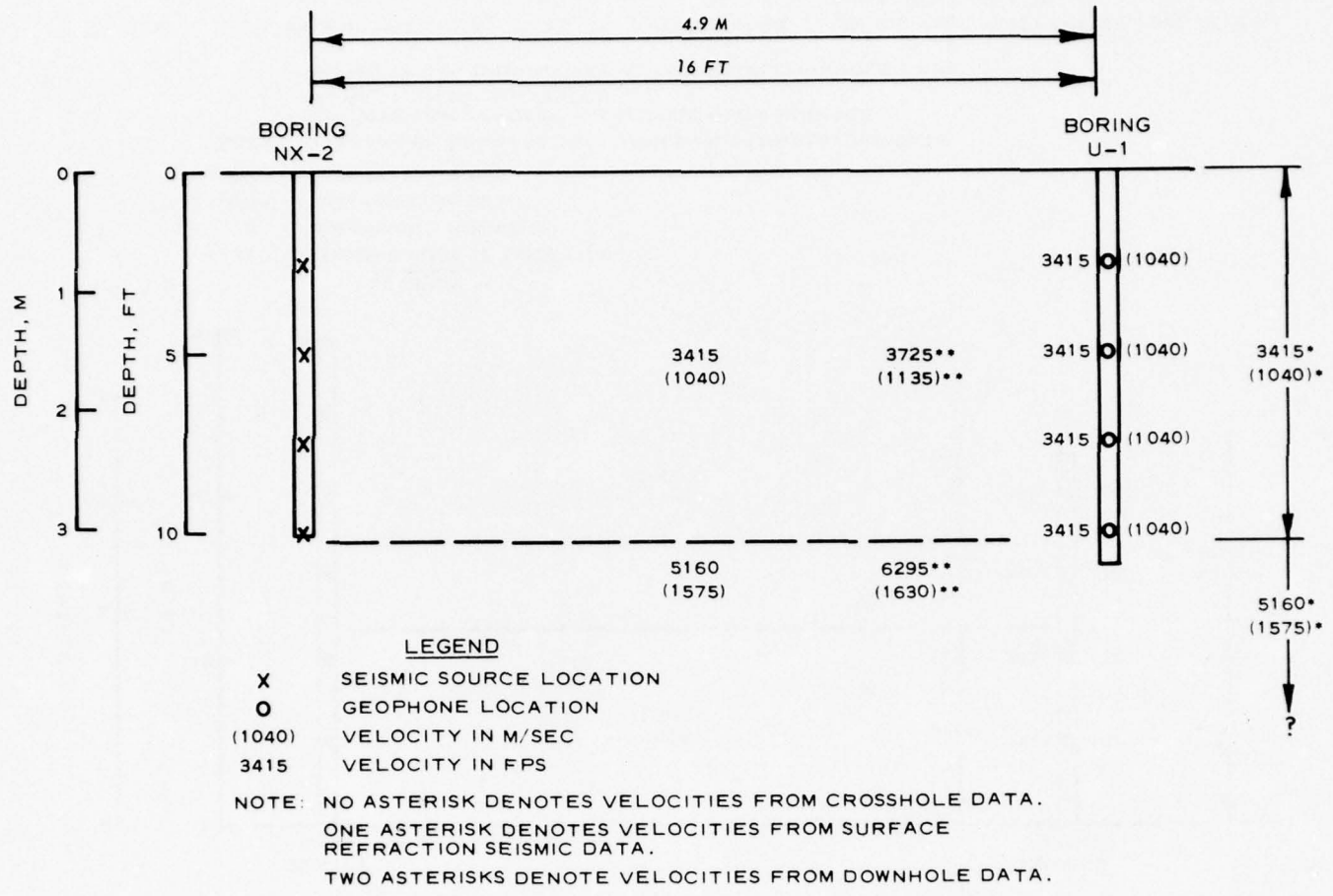

Figure A.12. P-wave velocity profile interpreted from surface refraction seismic, crosshole, and downhole test data, borings NX-2 and U-1.

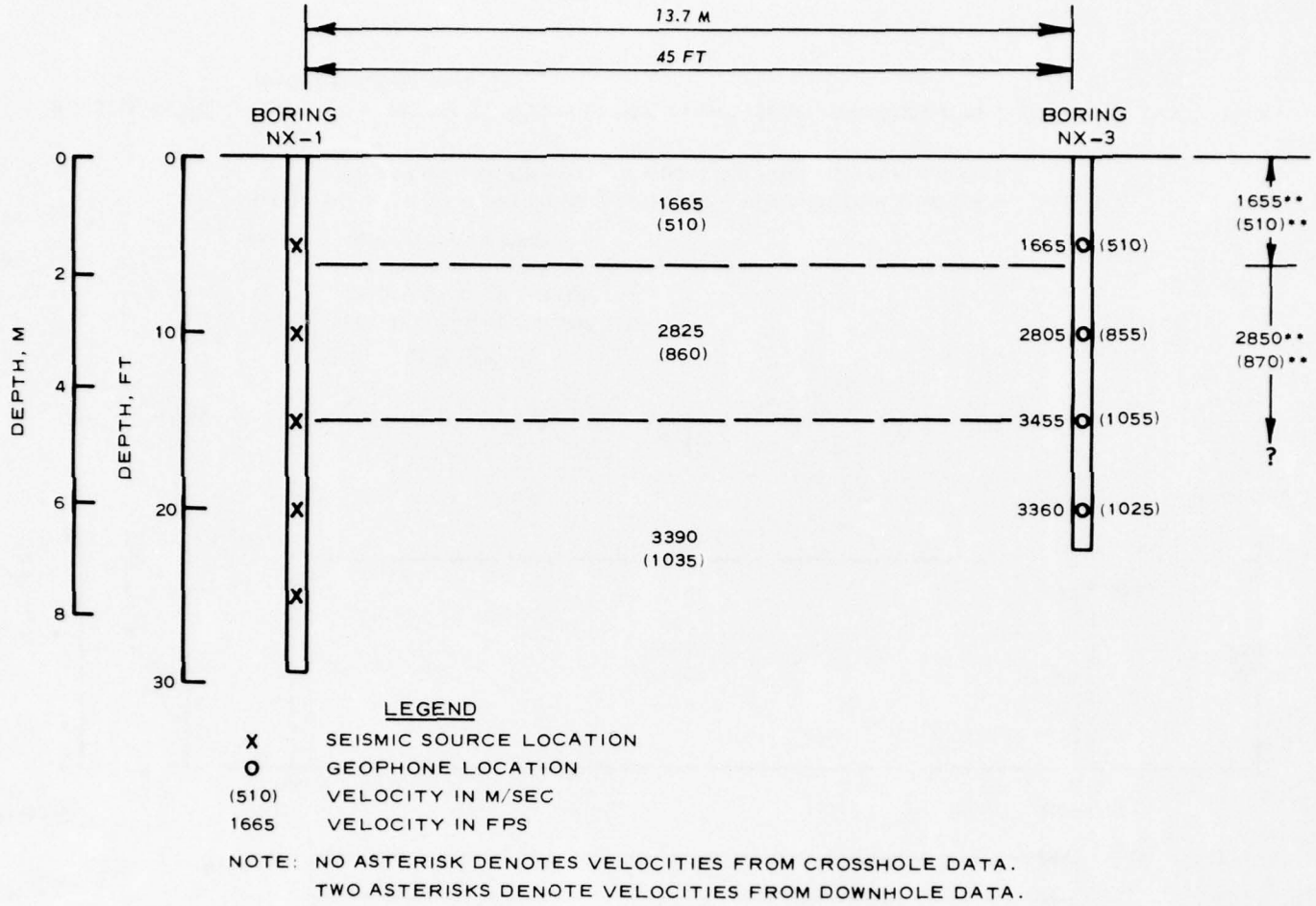

Figure A.13. S-wave velocity profile interpreted from crosshole and downhole test data, borings NX-1 and XN-3.

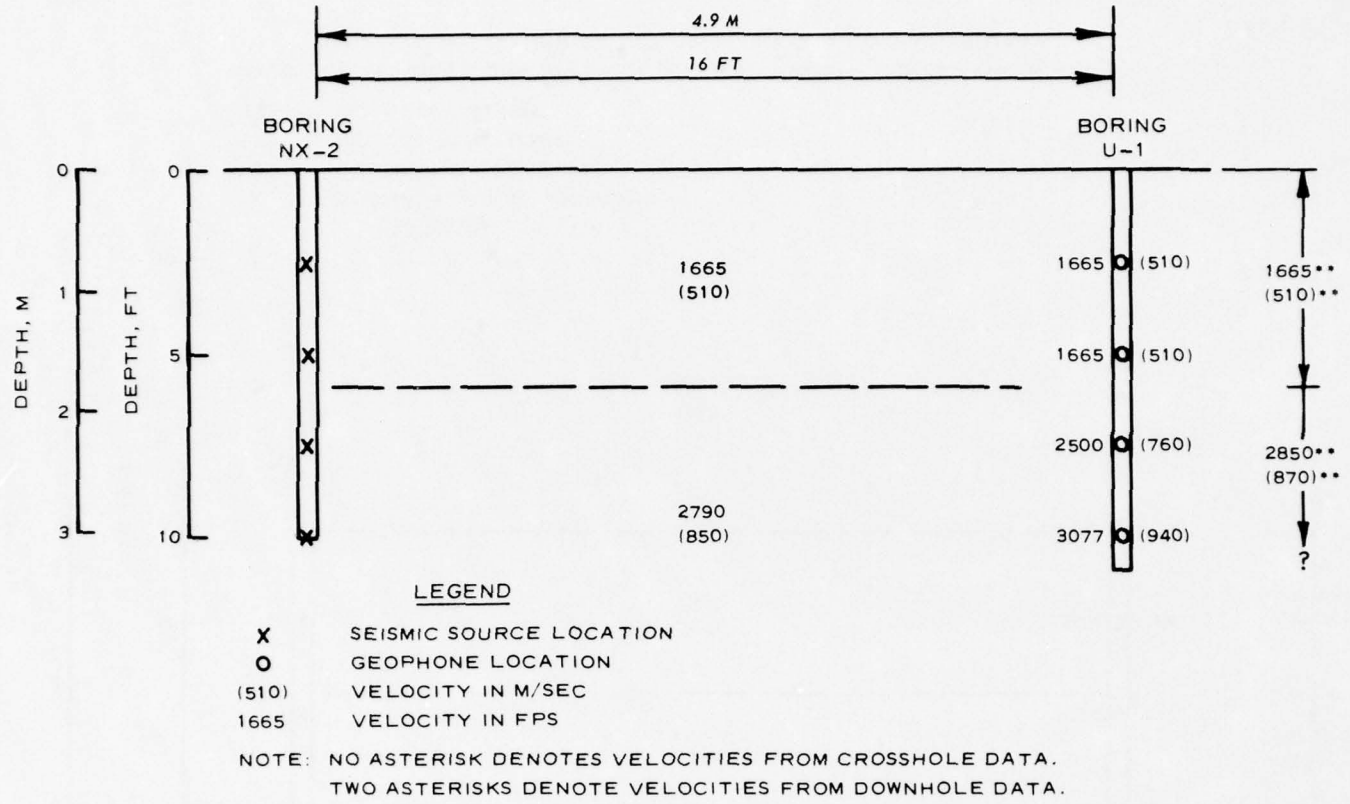

Figure A.14. S-wave velocity profile interpreted from crosshole and downhole test data, borings NX-2 and U-1.

APPENDIX B

DYNAMIC TEST DATA PLATES

Data plates for the dynamic uniaxial strain, dynamic isotropic compression, and dynamic triaxial compression tests conducted in the WES laboratory testing program are presented in the following order:

Test Type	Plate Number
Dynamic uniaxial strain	B.1
Dynamic isotropic compression	B.2-B.4
Dynamic triaxial compression	B.5-B.9

For the isotropic compression tests and triaxial compression tests, the first sheet of each plate for each test presents the time histories of pressure, deviator load, and axial and radial strains; the second sheet of each plate presents stress-strain plots.

PROJECT DNA PENETRATION
LOCATION SAN YSIDRO, NEW MEX

BORING NO. U1 DEPTH .762 METERS
DATE OF TEST 6-6-75

SPECIMEN DATA AT ZERO LIVE VERTICAL STRESS

SPECIMEN HEIGHT	6.360	CM	SPECIFIC GRAVITY	2.68	
SPECIMEN DIAMETER	12.700	CM	SATURATION	23.1	%
WET DENSITY	2.049	G/CC	VOLUME AIR	19.8	%
DRY DENSITY	1.909	G/CC	VOLUME WATER	6.0	%
WATER CONTENT	3.00	%	VOLUME SOLIDS	74.2	%

CLASSIFICATION:
TEST REMARKS:

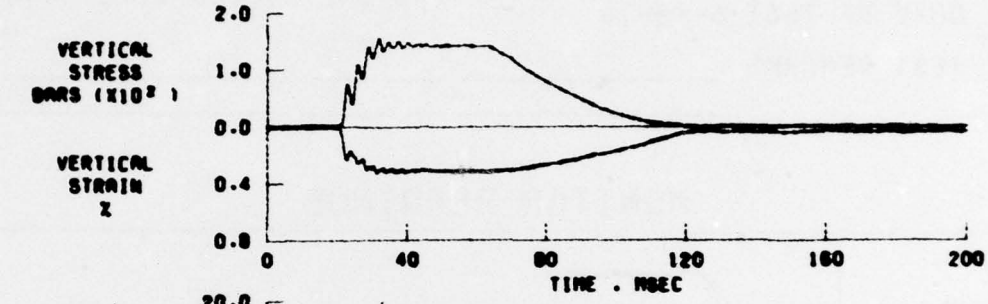

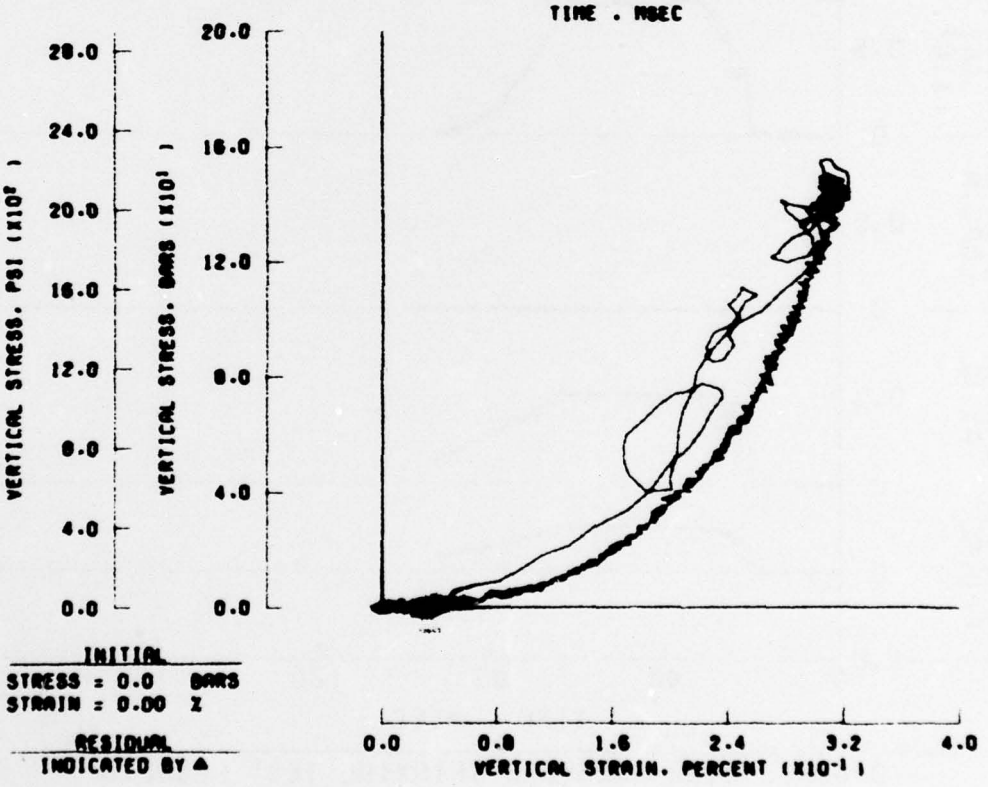

UNIAXIAL STRAIN TEST RESULTS
DYNAMIC TEST NO. DNA PEN. DUX/U1/2.5C

PLATE B.1

PROJECT DNA PENETRATION
LOCATION SAN YSIDRO, NEW MEX

BORING NO. NX2
DEPTH .M 2.44

TEST NO. DNA DIC NX2-8.0

SPECIMEN HEIGHT H.CM	12.233	SPECIFIC GRAVITY G	2.68
SPECIMEN DIAMETER D.CM	5.471	SATURATION S.%	25.7
WET DENSITY .G/CC	2.103	VOID RATIO E	0.312
WATER CONTENT W.%	3.0	VOLUME AIR Va.%	17.7
DRY DENSITY .G/CC	2.042	VOLUME WATER Vw.%	6.1
		VOLUME SOLIDS Vs.%	76.2

DATE OF TEST 6-10-75

TEST REMARKS _____

MONITOR READINGS

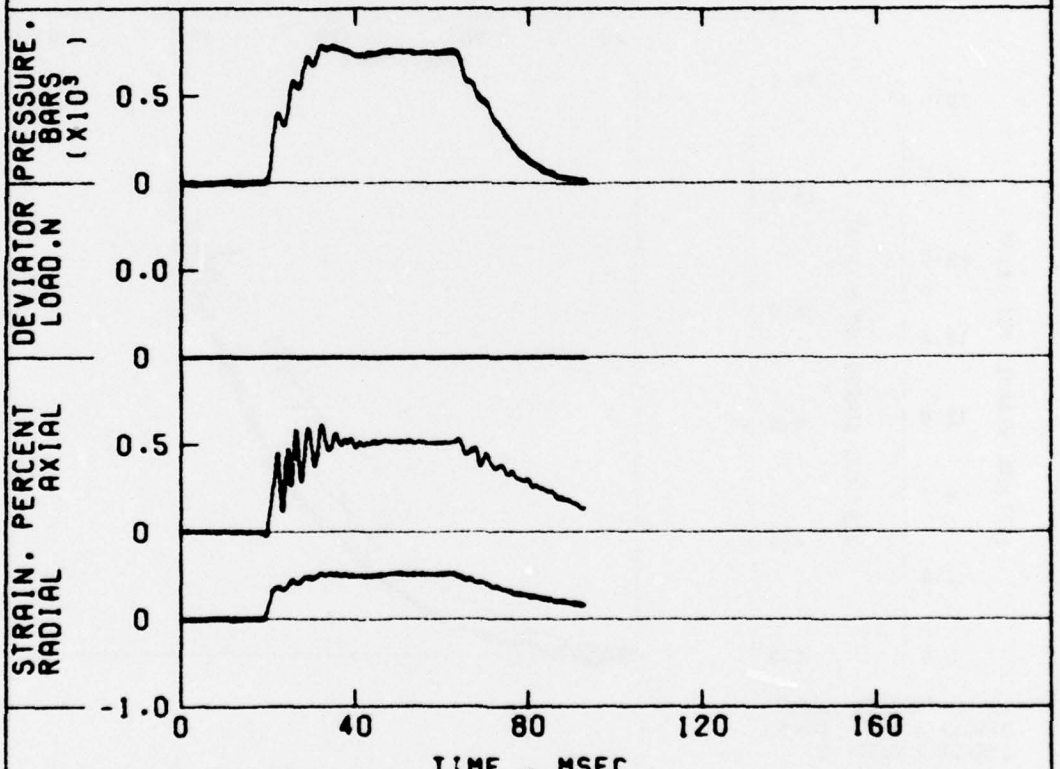

DYNAMIC HIGH-PRESSURE TRIAXIAL TEST RESULTS

TEST NUMBER DNA DIC NX2-8.0

PLATE B.2
(SHEET 1 OF 2)

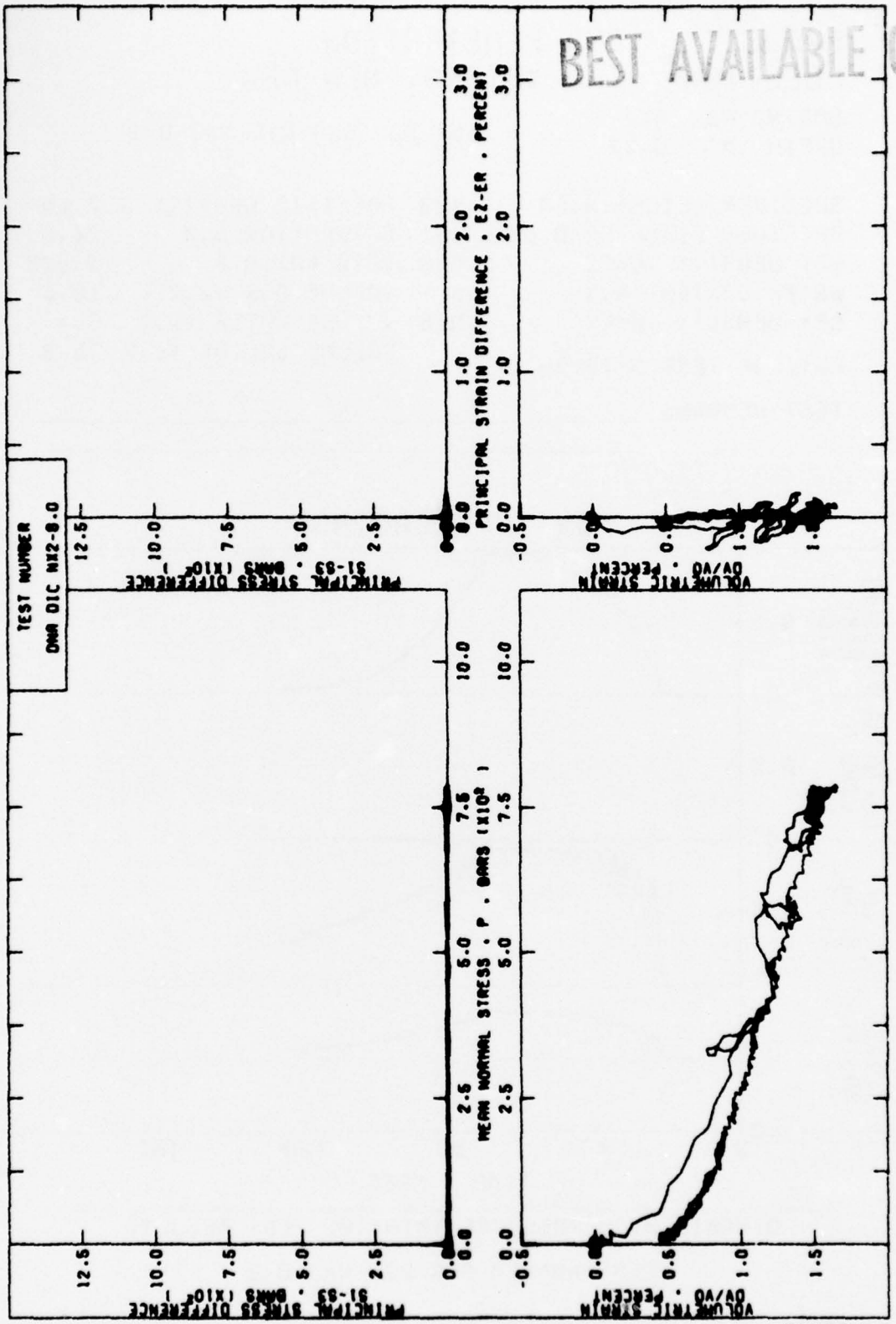

PLATE B.2
(SHEET 2 OF 2)

PROJECT DNA PENETRATION
LOCATION SAN YSIDRO, NEW MEX

BORING NO. NX2
DEPTH .M 0.27

TEST NO. DNA DIC-NX2-0.9

SPECIMEN HEIGHT H.CM	7.483	SPECIFIC GRAVITY G	2.68
SPECIMEN DIAMETER D.CM	5.461	SATURATION S.%	24.5
WET DENSITY .G/CC	2.078	VOID RATIO E	0.328
WATER CONTENT W.%	3.0	VOLUME AIR Va.%	18.6
DRY DENSITY .G/CC	2.018	VOLUME WATER Vw.%	6.1
		VOLUME SOLIDS Vs.%	75.3

DATE OF TEST 5-16-75

TEST REMARKS _____

MONITOR READINGS

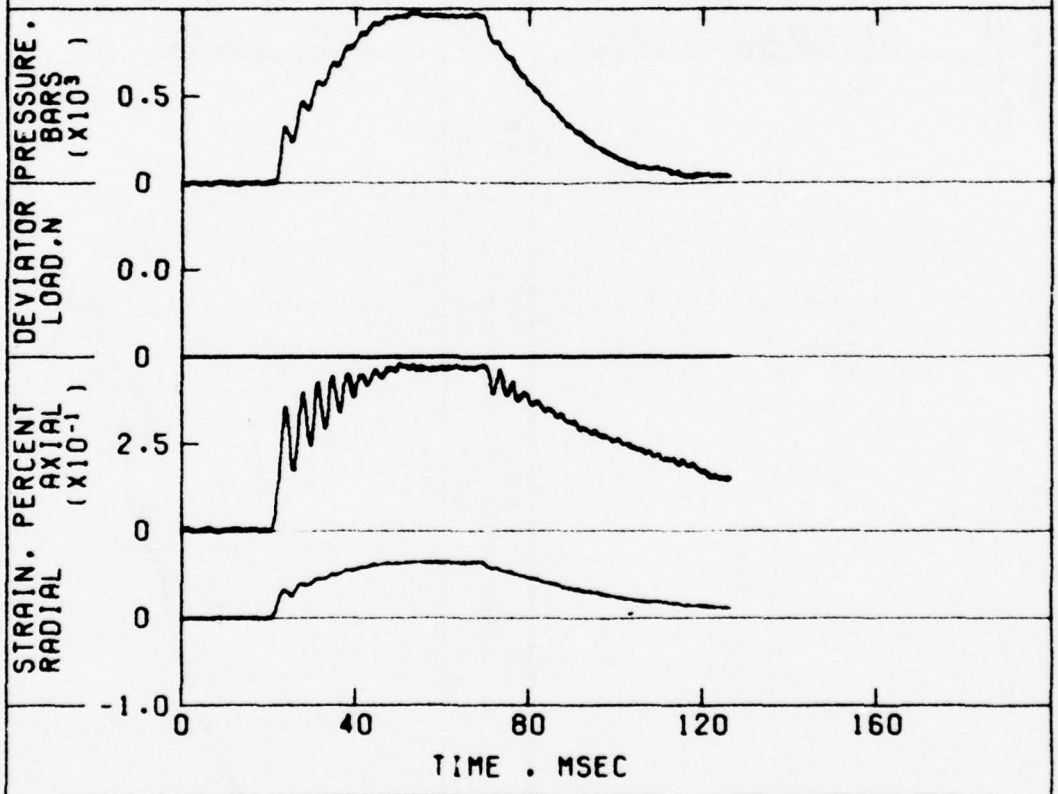

DYNAMIC HIGH-PRESSURE TRIAXIAL TEST RESULTS

TEST NUMBER DNA DIC-NX2-0.9

PLATE B.3
(SHEET 1 OF 2)

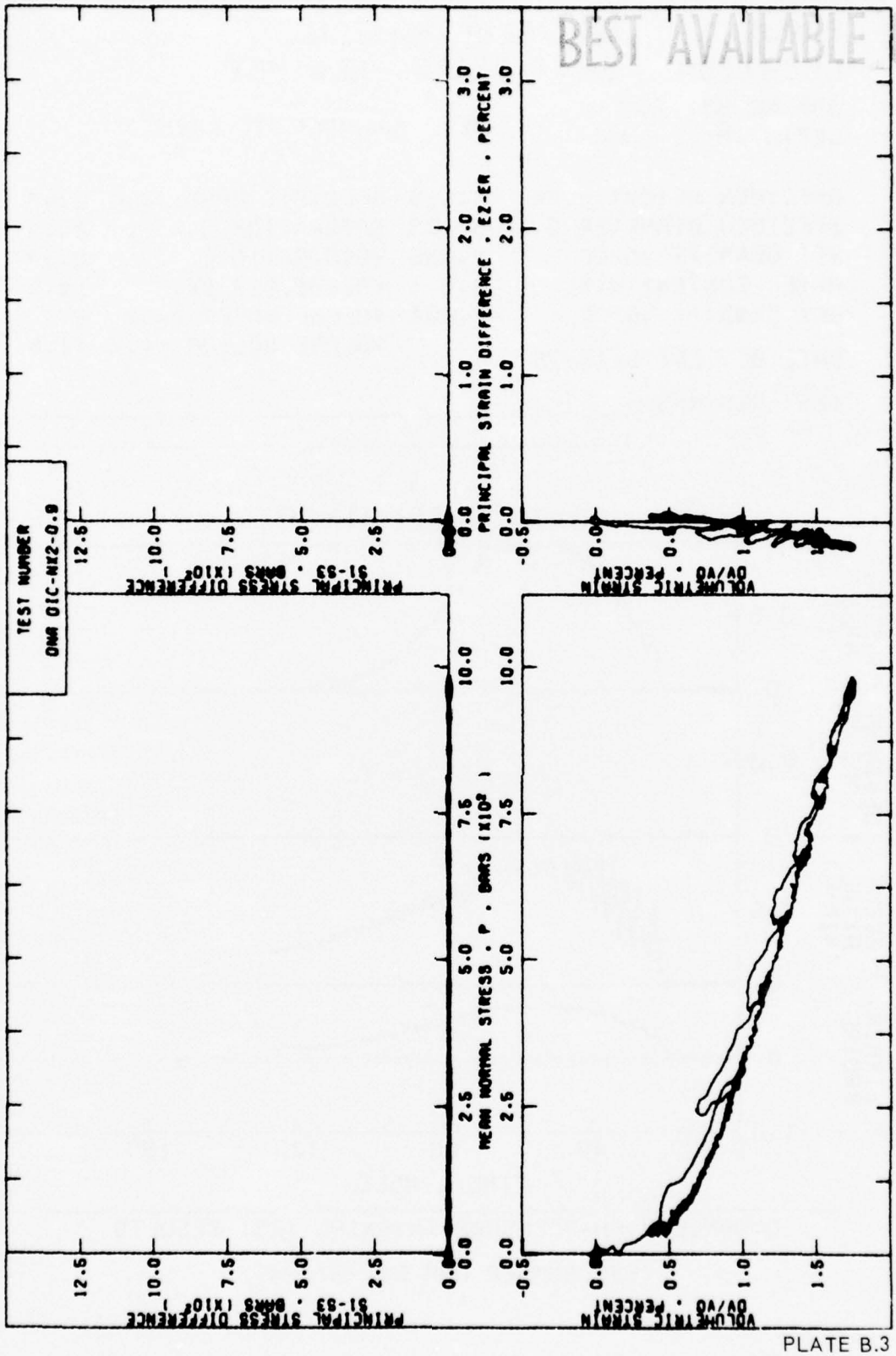

PLATE B.3
(SHEET 2 OF 2)

PROJECT DNA PENETRATION
LOCATION SAN YSIDRO. NEW MEX

BORING NO. NX2
DEPTH .M 1.43

TEST NO. DNA DIC-NX2-4.7

SPECIMEN HEIGHT H.CM	7.658	SPECIFIC GRAVITY G	2.68
SPECIMEN DIAMETER D.CM	5.453	SATURATION S.%	23.9
WET DENSITY .G/CC	2.065	VOID RATIO E	0.337
WATER CONTENT W.%	3.0	VOLUME AIR Va.%	19.2
DRY DENSITY .G/CC	2.004	VOLUME WATER Vw.%	6.0
		VOLUME SOLIDS Vs.%	74.8

DATE OF TEST 5-16-75

TEST REMARKS _____

MONITOR READINGS

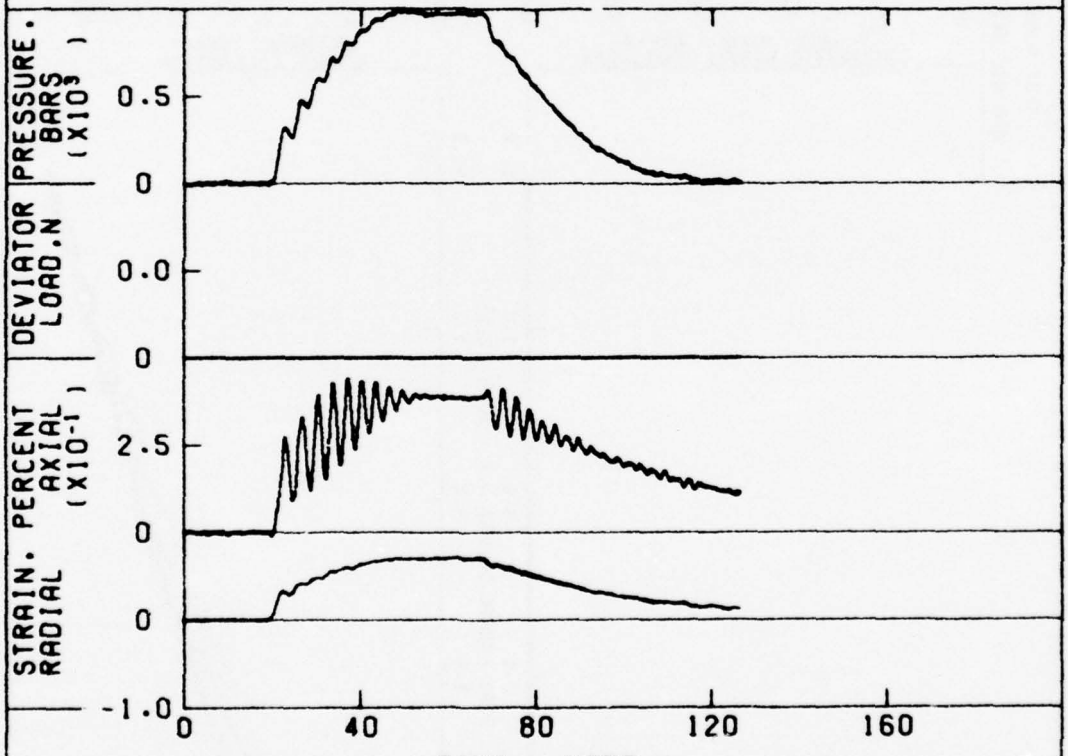

DYNAMIC HIGH-PRESSURE TRIAXIAL TEST RESULTS

TEST NUMBER DNA DIC-NX2-4.7

PLATE B.4
(SHEET 1 OF 2)

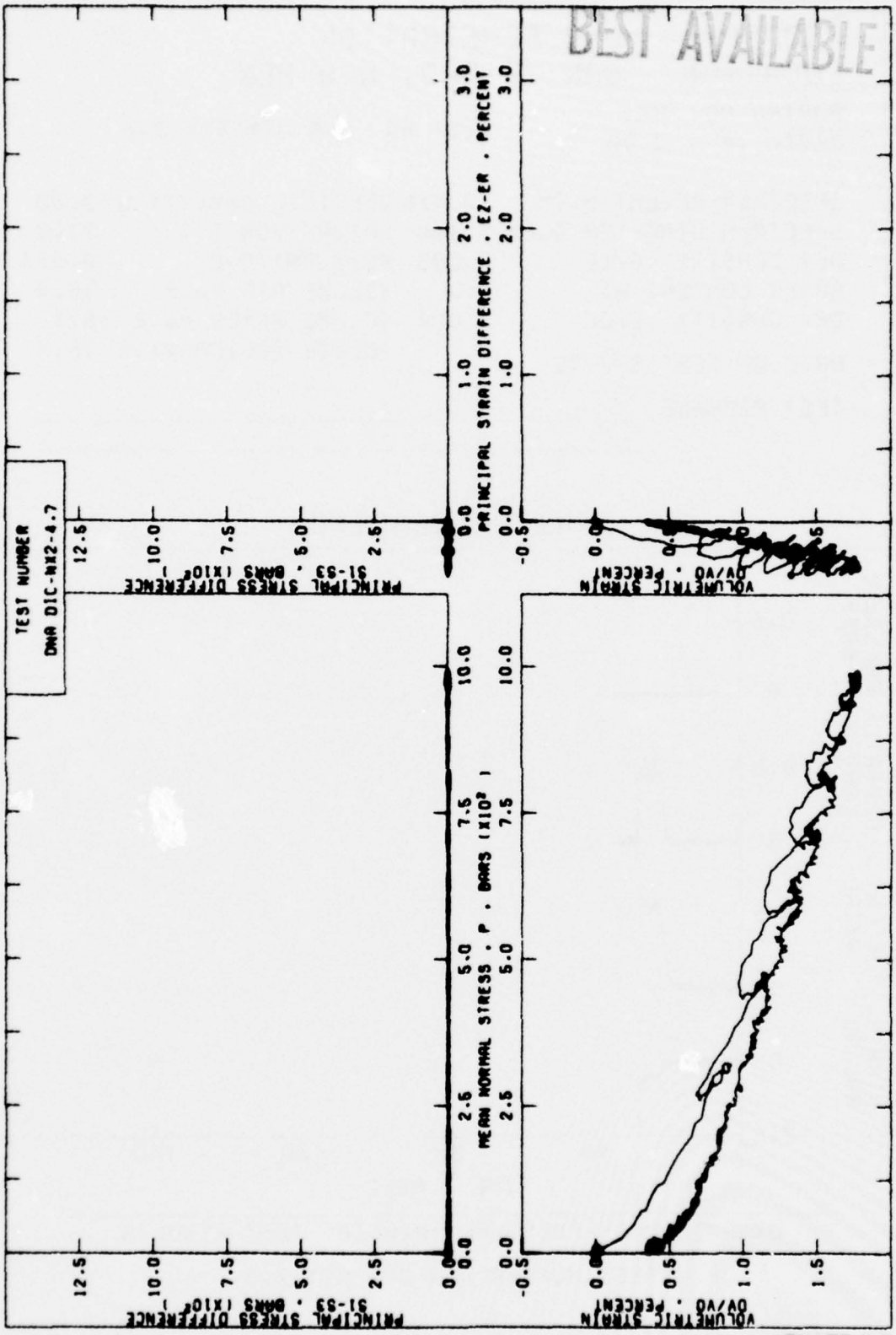

PLATE B.4
(SHEET 2 OF 2)

PROJECT DNA PENETRATION
LOCATION SAN YSIDRO, NEW MEX

BORING NO. NX1
DEPTH .M 0.70

TEST NO. DNA DTX-NX1-2.3

SPECIMEN HEIGHT H.CM	12.416	SPECIFIC GRAVITY G	2.68
SPECIMEN DIAMETER D.CM	5.466	SATURATION S.%	24.8
WET DENSITY .G/CC	2.085	VOID RATIO E	0.324
WATER CONTENT W.%	3.0	VOLUME AIR Va.%	18.4
DRY DENSITY .G/CC	2.024	VOLUME WATER Vw.%	6.1
		VOLUME SOLIDS Vs.%	75.5

DATE OF TEST 6-2-75

TEST REMARKS _____

MONITOR READINGS

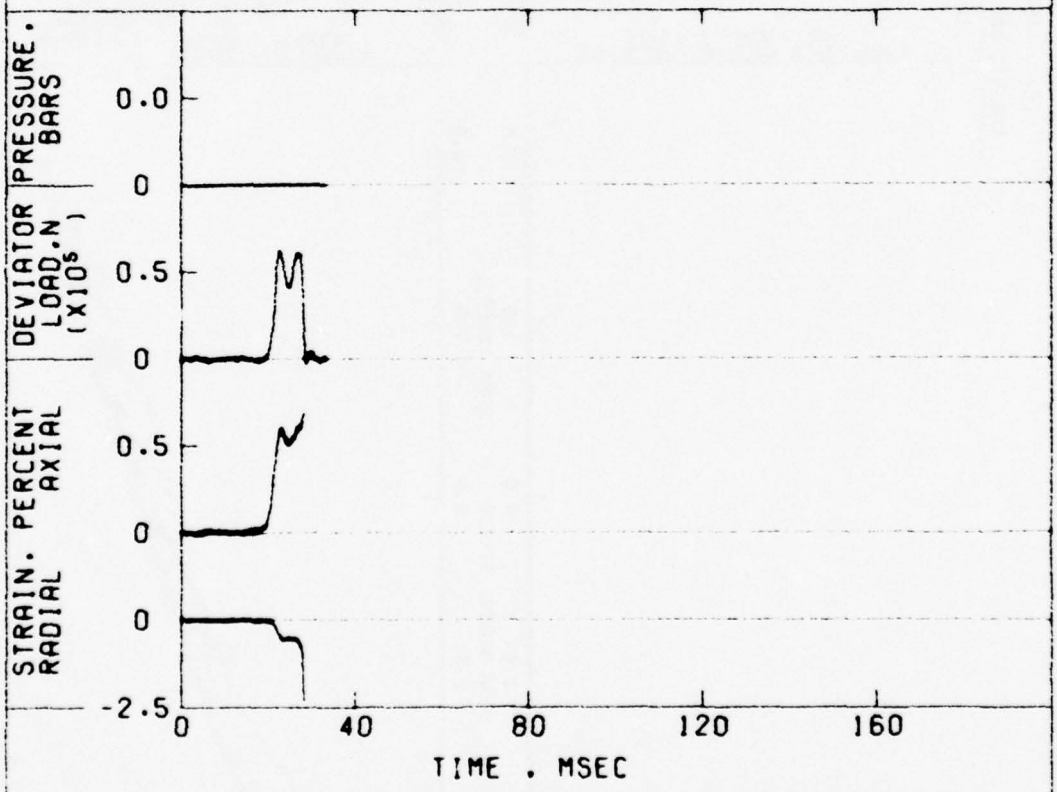

DYNAMIC HIGH-PRESSURE TRIAXIAL TEST RESULTS

TEST NUMBER DNA DTX-NX1-2.3

PLATE B.5
(SHEET 1 OF 2)

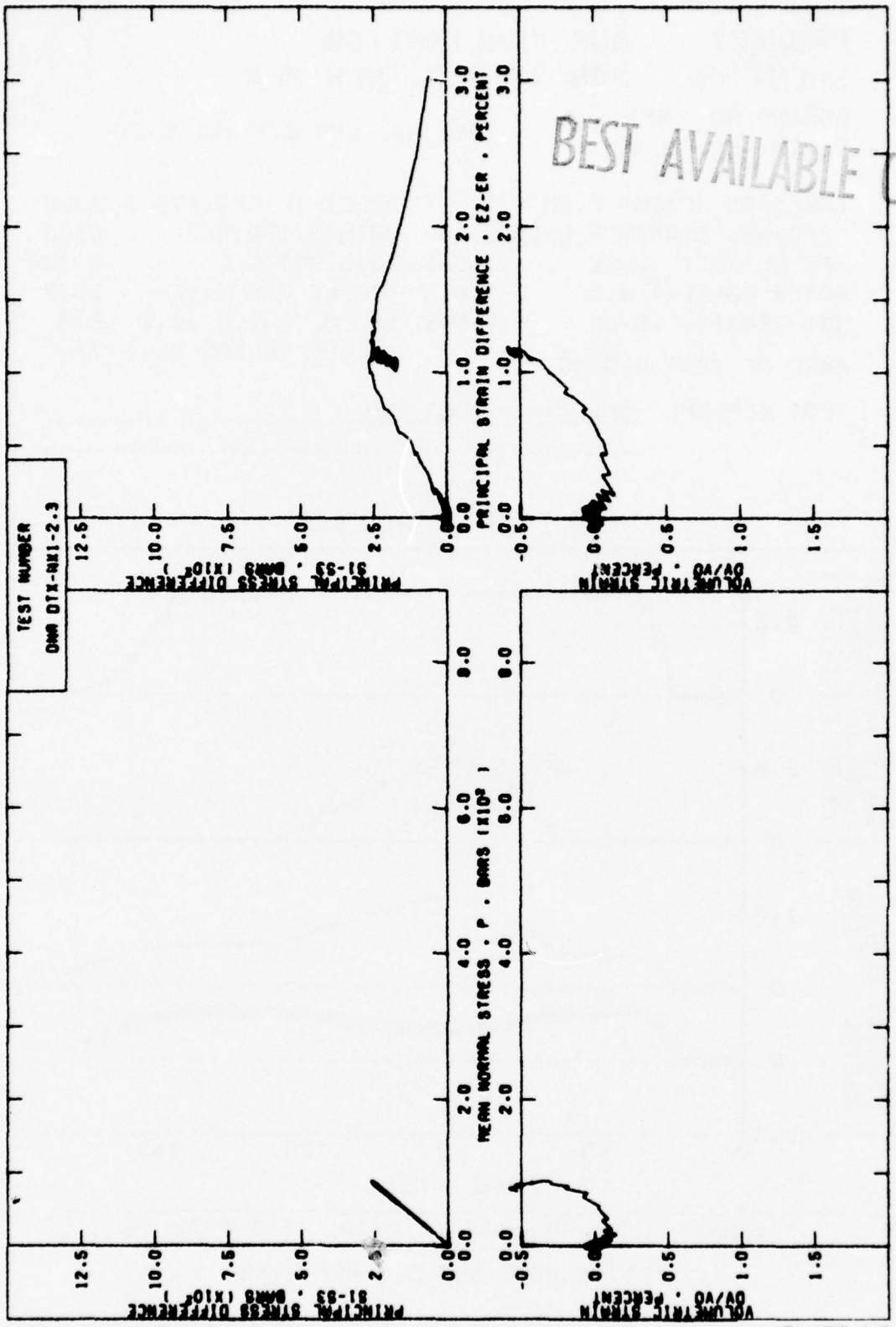

PLATE B.5
(SHEET 2 OF 2)

PROJECT DNA PENETRATION
LOCATION SAN YSIDRO, NEW MEX

BORING NO. NX1
DEPTH .M 2.93

TEST NO. DNA DTX-NX1-9.6A

SPECIMEN HEIGHT H.CM	12.713	SPECIFIC GRAVITY G	2.68
SPECIMEN DIAMETER D.CM	5.469	SATURATION S.%	23.8
WET DENSITY .G/CC	2.063	VOID RATIO E	0.338
WATER CONTENT W.%	3.0	VOLUME AIR Va.%	19.2
DRY DENSITY .G/CC	2.003	VOLUME WATER Vw.%	6.0
		VOLUME SOLIDS Vs.%	74.8

DATE OF TEST 6-9-75

TEST REMARKS SPECIMEN DID NOT FAIL

MONITOR READINGS

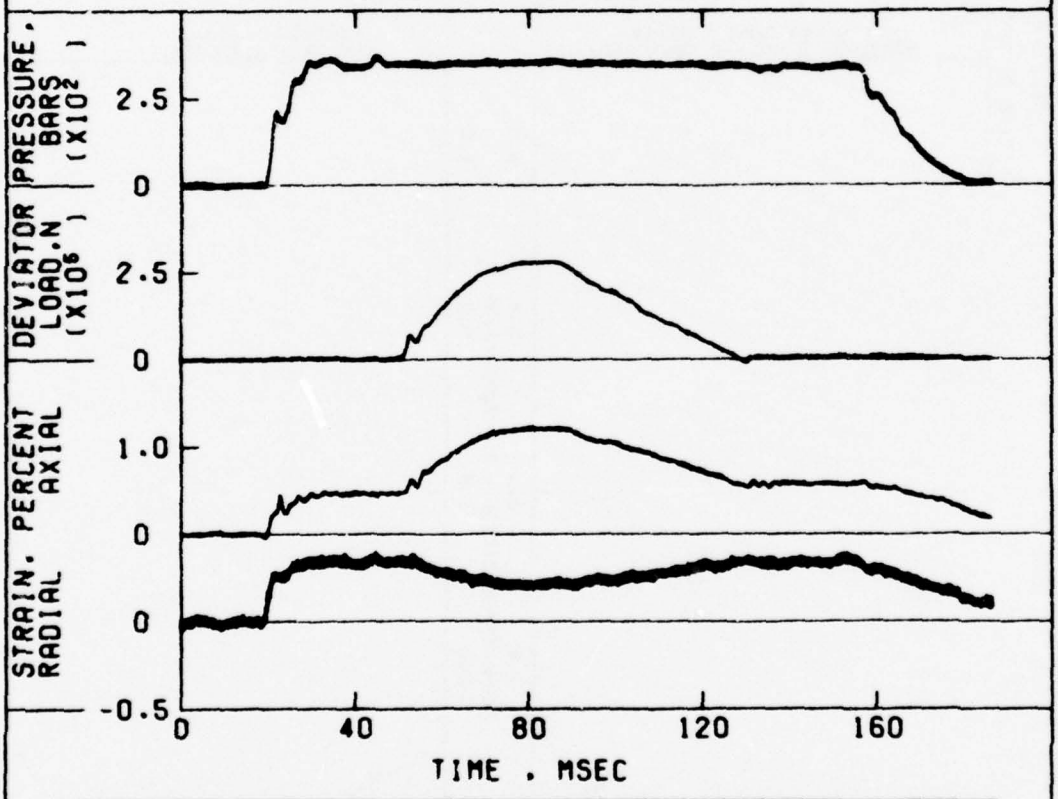

DYNAMIC HIGH-PRESSURE TRIAXIAL TEST RESULTS

TEST NUMBER DNA DTX-NX1-9.6A

PLATE B.6
(SHEET 1 OF 2)

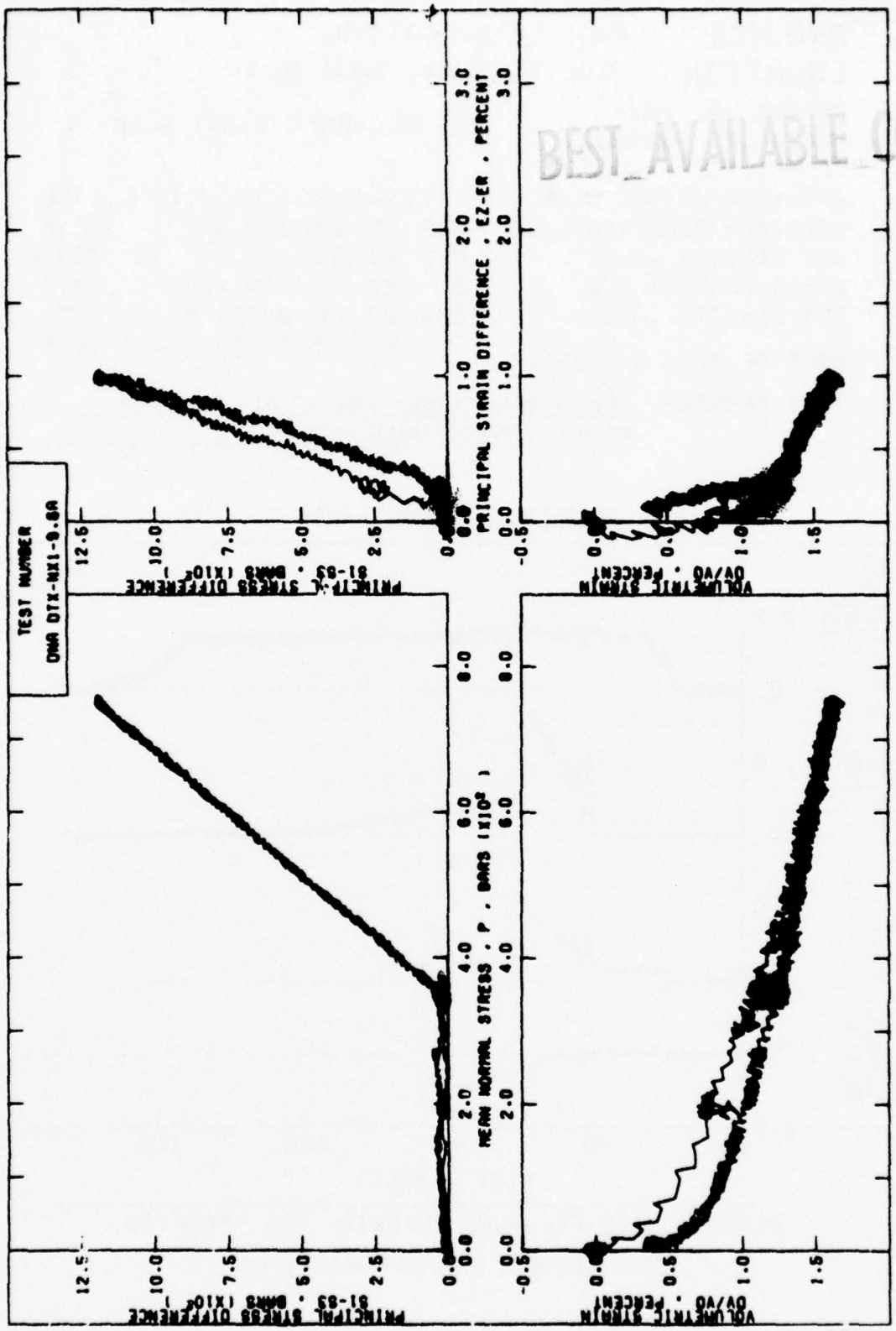

PLATE B.6
(SHEET 2 OF 2)

PROJECT DNA PENETRATION
LOCATION SAN YSIDRO. NEW MEX

BORING NO. NX1
DEPTH .M 2.93

TEST NO. DNA DTX-NX1-9.6B

SPECIMEN HEIGHT H.CM	12.713	SPECIFIC GRAVITY G	2.68
SPECIMEN DIAMETER D.CM	5.469	SATURATION S.%	23.8
WET DENSITY .G/CC	2.063	VOID RATIO E	0.338
WATER CONTENT W.%	3.0	VOLUME AIR Va.%	19.2
DRY DENSITY .G/CC	2.003	VOLUME WATER Vw.%	6.0
		VOLUME SOLIDS Vs.%	74.8

DATE OF TEST 6-9-75

TEST REMARKS RETEST OF SPECIMEN USED IN DTX-NX1-9.6A AT A LOWER CONFINING PRESSURE.

MONITOR READINGS

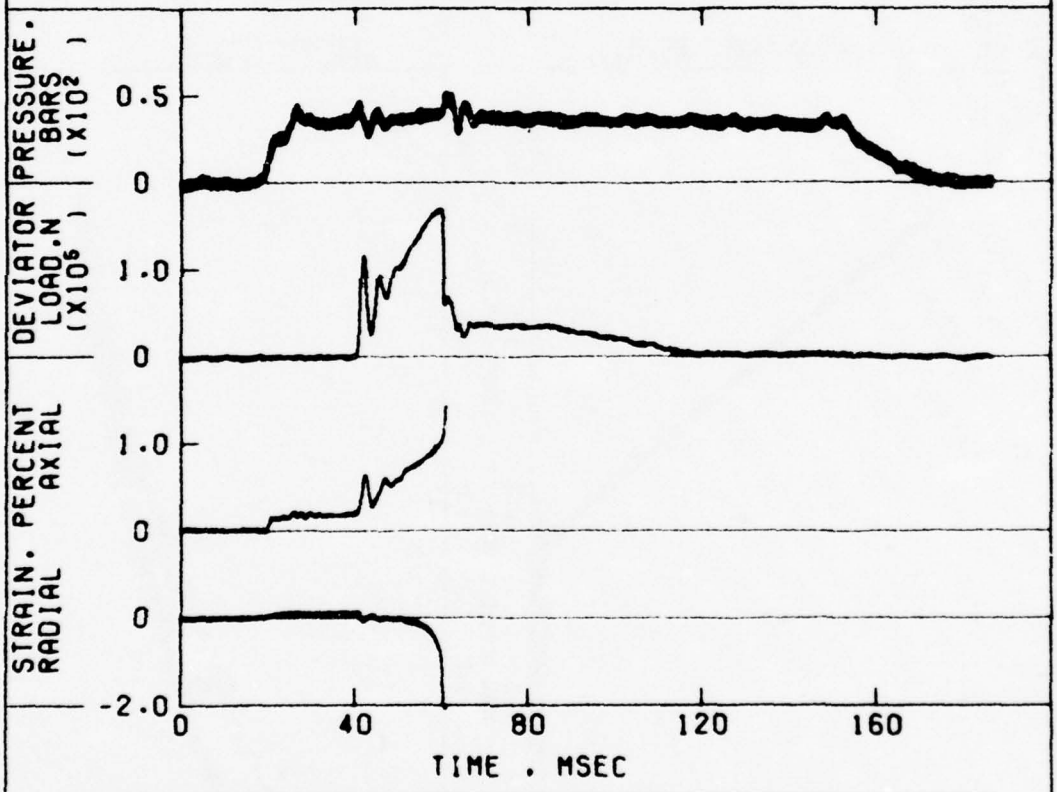

DYNAMIC HIGH-PRESSURE TRIAXIAL TEST RESULTS

TEST NUMBER DNA DTX-NX1-9.6B

PLATE B.7
(SHEET 1 OF 2)

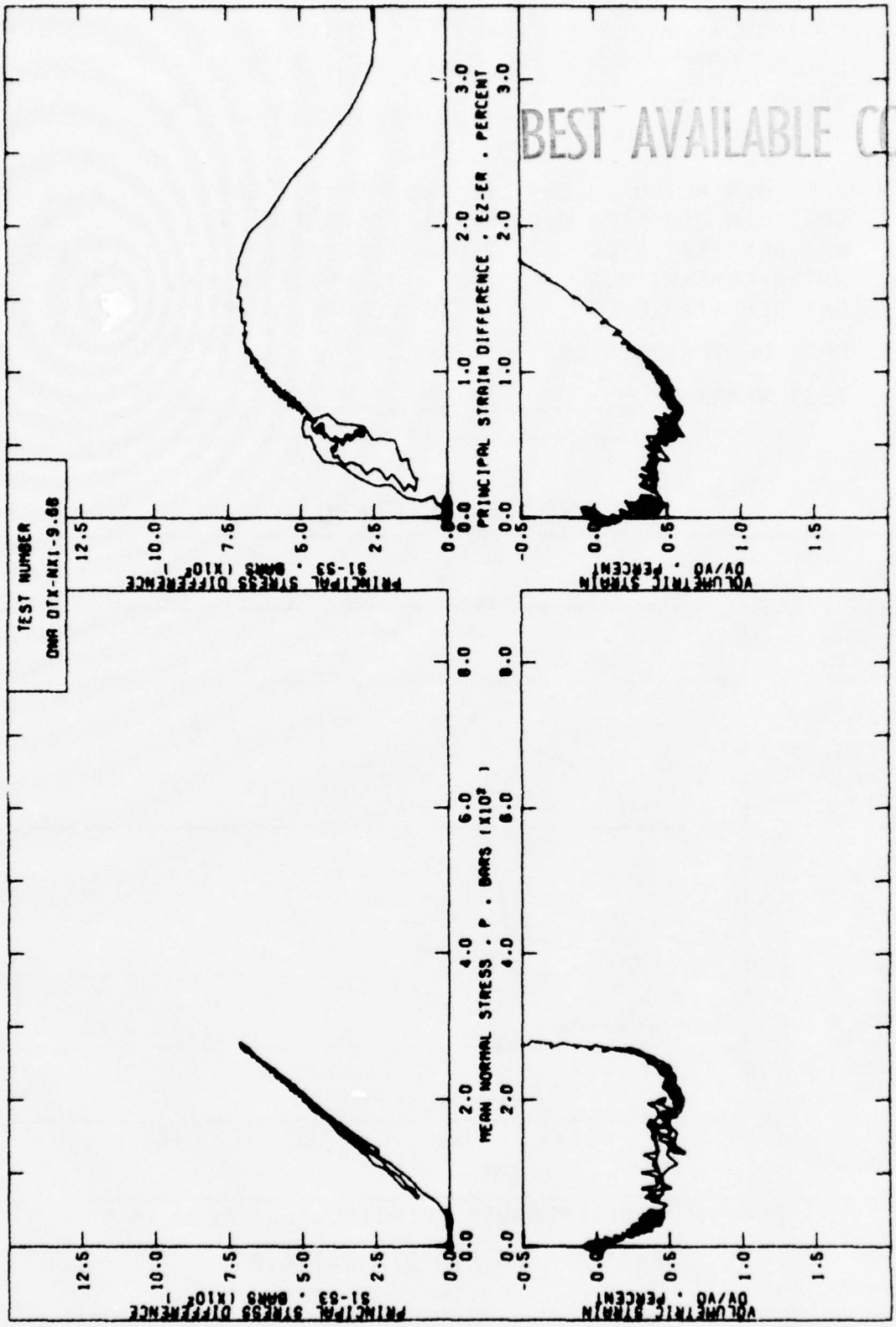

PLATE B.7
(SHEET 2 OF 2)

PROJECT DNA PENETRATION
LOCATION SAN YSIDRO, NEW MEX

BORING NO. NX1
DEPTH .M 2.44

TEST NO. DNA DTX-NX1-8.0

SPECIMEN HEIGHT H.CM	12.725	SPECIFIC GRAVITY G	2.68
SPECIMEN DIAMETER D.CM	5.456	SATURATION S.%	22.4
WET DENSITY .G/CC	2.032	VOID RATIO E	0.359
WATER CONTENT W.%	3.0	VOLUME AIR Va.%	20.5
DRY DENSITY .G/CC	1.973	VOLUME WATER Vw.%	5.9
		VOLUME SOLIDS Vs.%	73.6

DATE OF TEST 6-2-75

TEST REMARKS _____

MONITOR READINGS

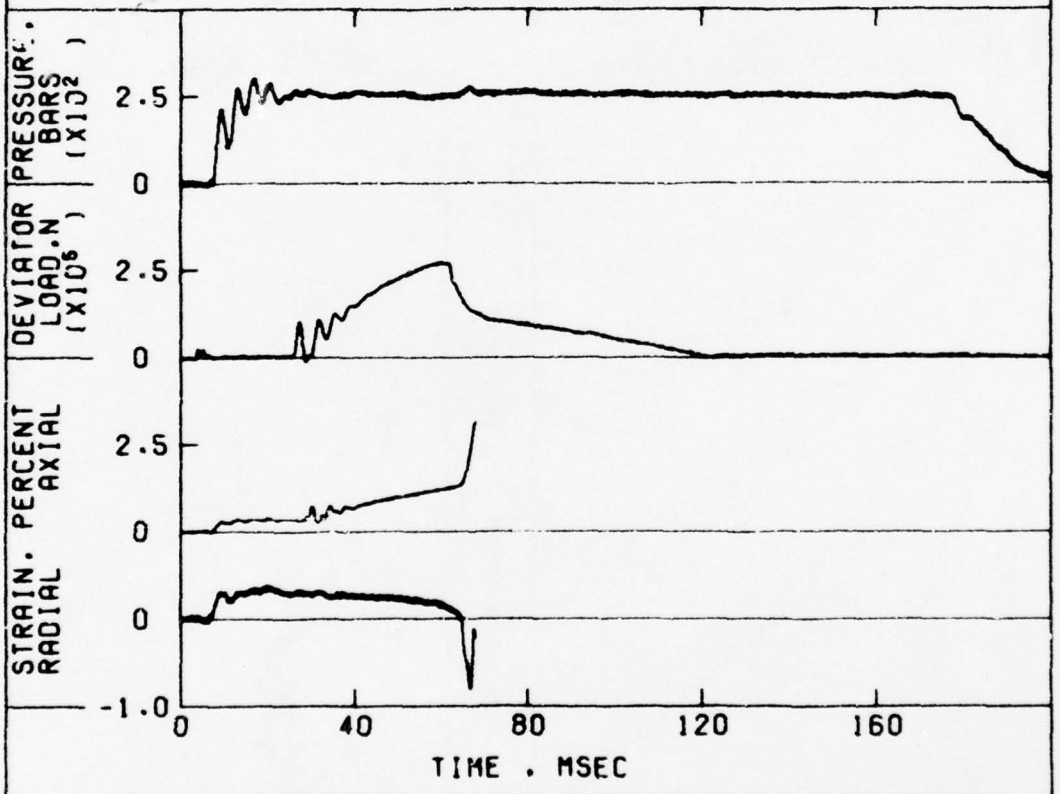

DYNAMIC HIGH-PRESSURE TRIAXIAL TEST RESULTS

TEST NUMBER DNA DTX-NX1-8.0

PLATE B.8
(SHEET 1 OF 2)

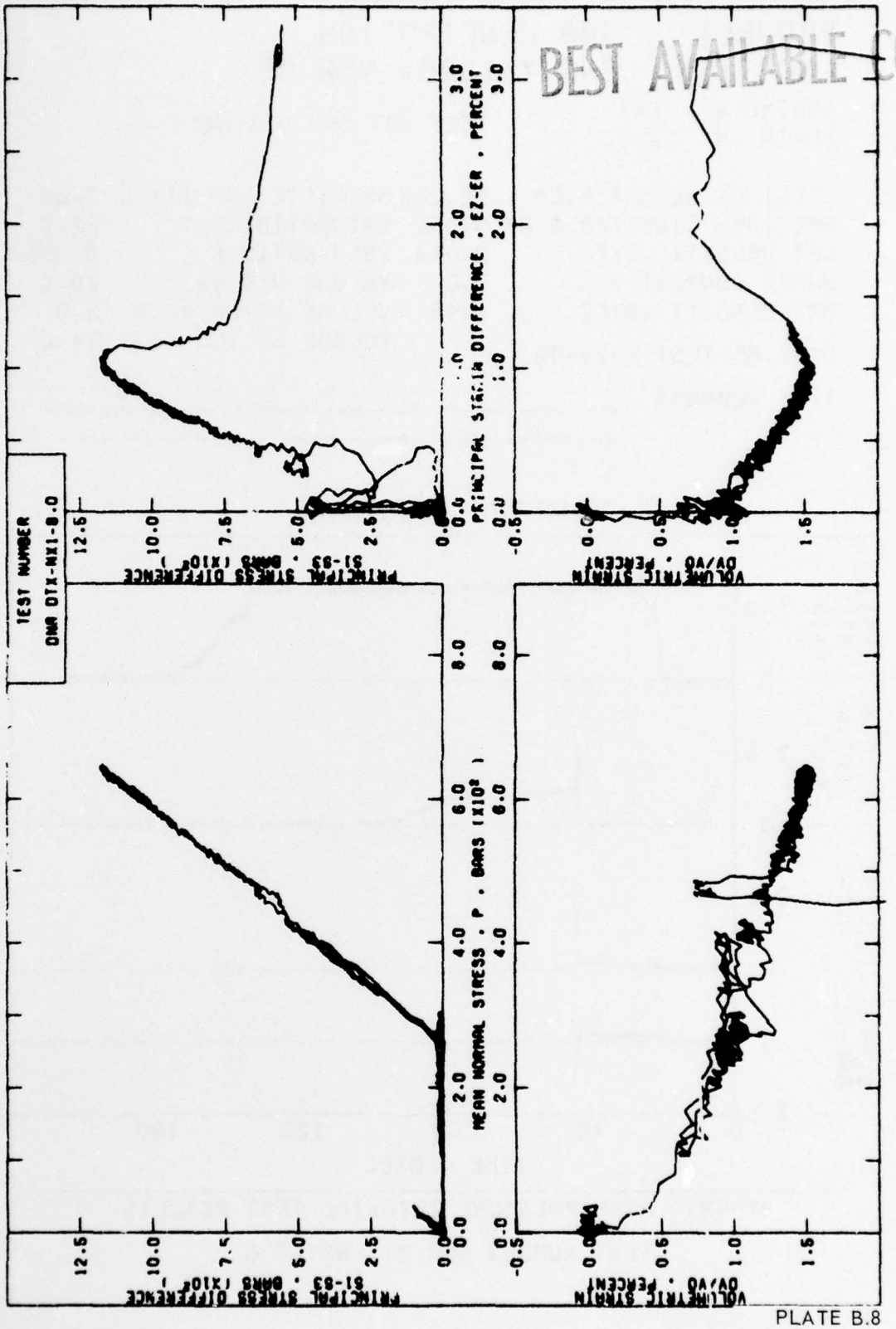

PLATE B.8
(SHEET 2 OF 2)

PROJECT DNA PENETRATION
LOCATION SAN YSIDRO, NEW MEX

BORING NO. NX1
DEPTH .M 2.32

TEST NO. DNA DTX-NX1-7.6

SPECIMEN HEIGHT H.CM	12.266	SPECIFIC GRAVITY G	2.68
SPECIMEN DIAMETER D.CM	5.466	SATURATION S.%	22.9
WET DENSITY .G/CC	2.044	VOID RATIO E	0.351
WATER CONTENT W.%	3.0	VOLUME AIR Va.%	20.0
DRY DENSITY .G/CC	1.984	VOLUME WATER Vw.%	6.0
		VOLUME SOLIDS Vs.%	74.0

DATE OF TEST 5-29-75

TEST REMARKS _____

MONITOR READINGS

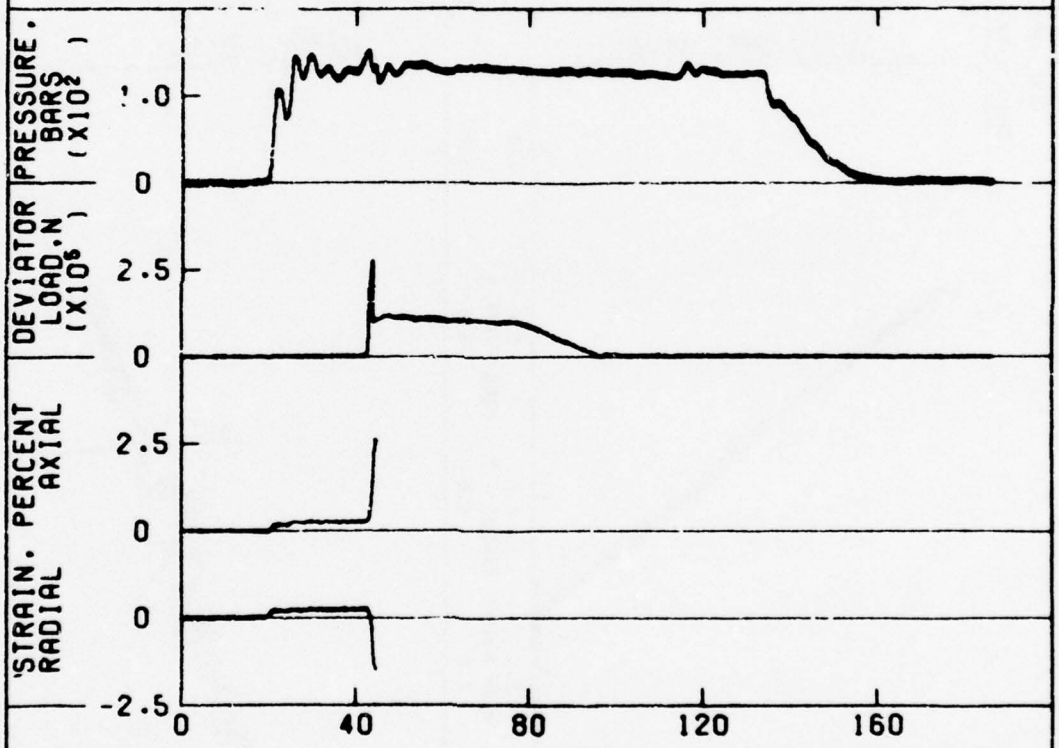

DYNAMIC HIGH-PRESSURE TRIAXIAL TEST RESULTS

TEST NUMBER DNA DTX-NX1-7.6

PLATE B.9
(SHEET 1 OF 2)

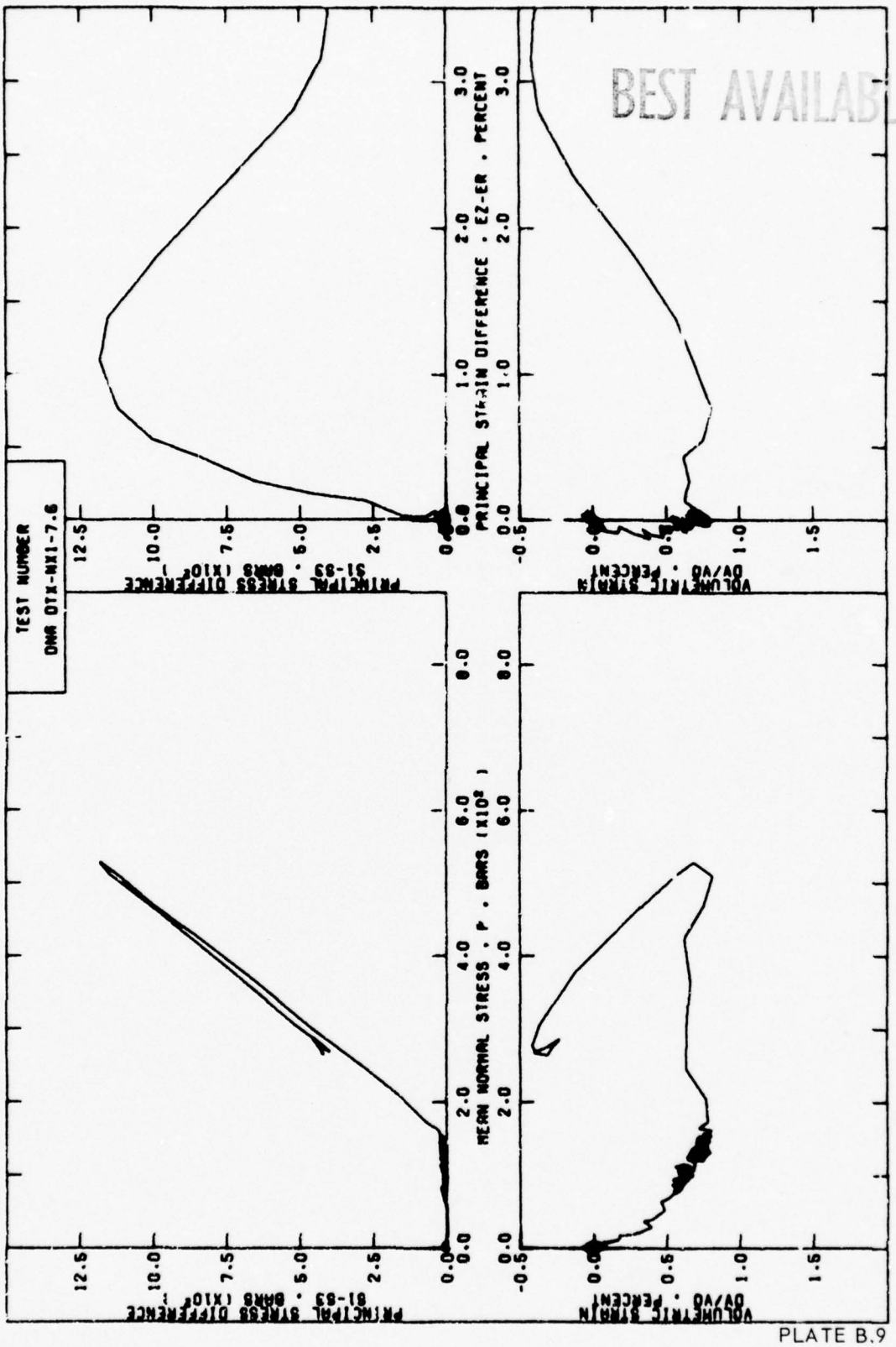

PLATE B.9
(SHEET 2 OF 2)

APPENDIX C

COMPRESSION WAVE VELOCITY MEASUREMENTS ON LARGE-DIAMETER CORES

Results of compression wave velocity measurements on two large-diameter sandstone cores from the proposed penetration site near San Ysidro, New Mexico, are tabulated below. The velocities were computed from transit time measurements on the two cores. Two types of impulsive sources (hammers) were used and two types of signal detectors were used (10-kHz accelerometer and 1-MHz piezocrystal).

Test No.	Axial v_{pL} m/sec	Radial v_{pL} m/sec	Remarks
			Core No. 1
1	1170	-	Hammer source and 10-kHz accelerometer receiver
2	1210	-	Hammer source and 10-kHz accelerometer receiver
3	1210	-	Hammer source and 10-kHz accelerometer receiver
4	1170	-	Hammer source and 10-kHz accelerometer receiver
5	1170	-	Hammer source and 10-kHz accelerometer receiver
6	1150	-	Hammer source and 10-kHz accelerometer receiver
			Core No. 2
1	1150	-	Hammer and accelerometer
2	1090	-	Hammer and accelerometer
3	1150	-	Hammer and accelerometer
4	1130	-	Hammer and accelerometer
5	1110	-	Hammer and accelerometer
6	1130	-	Hammer and accelerometer
7	1350	-	Schmidt hammer and piezocrystal receiver (1-MHz)
8	1380	-	Schmidt hammer and piezocrystal receiver (1-MHz)
9	1290	-	Schmidt hammer and piezocrystal receiver (1-MHz)
10	1290	-	Schmidt hammer and piezocrystal receiver (1-MHz)
11	1320	-	Schmidt hammer and piezocrystal receiver (1-MHz)
12	1090	-	Hammer and piezocrystal receiver
13	1110	-	Hammer and accelerometer
14	1000	-	Hammer and accelerometer
15	1000	-	Hammer and accelerometer
16	-	1060	Hammer and accelerometer
17	-	1000	Hammer and accelerometer
18	-	1100	Hammer and accelerometer
19	-	1210	Hammer and accelerometer

APPENDIX D

RESULTS OF THE TERRA TEK LABORATORY TESTING PROGRAM

This appendix contains a report submitted to the Defense Nuclear Agency by Terra Tek, Inc., Salt Lake City, Utah. The report presents the results of a laboratory testing program on Dakota sandstone from the proposed San Ysidro, New Mexico, penetration site and is reproduced here by permission.

SOME PROPERTIES OF SANDSTONE

FROM THE PENETRATOR TEST SITE, SAN YSIDRO, NEW MEXICO

by

R. R. Nielsen
R. K. Dropek
S. W. Butters

Submitted to

Headquarters
Defense Nuclear Agency
Washington, D.C. 20305

Attn: Major T. Stong

Submitted by

Terra Tek, Inc.
University Research Park
420 Wakara Way
Salt Lake City, Utah 84108

TR 75-60
November 1975

ABSTRACT

Tests were performed on samples of Dakota sandstone taken from the penetrator test site near San Ysidro, New Mexico. The sandstone was tested to determine its response to triaxial compression loading, hydrostatic compression loading, uniaxial strain loading and triaxial extension loading. The results showed this material to be generally typical of other sandstones although some results (such as the triaxial failure envelope) are somewhat unique and peculiar to this material.

Two triaxial compression tests were performed on crushed sandstone samples from which gradation curves were obtained showing grain size distributions before and after testing. These tests showed the crushed material strength at pressure to be little changed from the intact sandstone.

The Terra Tek effort was funded through Defense Nuclear Agency, contract number DNA001-75-C-0177, with Major Todd Stong as Contracting Officer Representative. Previous work for this program on welded tuff was reported in Terra Tek report number TR 75-9.[1] The TTI program was an effort in conjunction with Waterways Experiment Station to completely characterize the sandstone.

TABLE OF CONTENTS

INTRODUCTION

One aspect of the Defense Nuclear Agency earth penetrator program is the prediction of the penetrator performance. This prediction is possible through calculations which utilize material models based on the physical and mechanical properties of the target media. The target media in this case is Dakota Sandstone found near San Ysidro, New Mexico. The Terra Tek effort was to supply selected mechanical properties data and along with laboratory and field data from Waterways Experiment Station (WES), present the necessary material properties.

The proposed test program on the sandstone was as follows:

1. Triaxial compression tests at confining pressures of 0, 1/2, 1 4 and 10 kilobars.
2. Hydrostatic compression tests to 10 kilobars.
3. Uniaxial strain tests to 10 kilobars.
4. Extension tests at confining pressures of 1 and 2 kilobars.

These tests were all performed on conventional, intact samples with testing techniques similar to those previously reported.[2]

As a result of recent descriptions of the condition of the material surrounding the penetrator after the event, additional tests were conducted on pre-crushed samples supplied by WES personnel.[3] Those tests were:

1. Triaxial compression tests at 1.0 and 3.2 kilobars confining pressure.
2. Hydrostatic compression tests to 4 kilobars to determine grain size distributions before and after loading.

TEST RESULTS

The stress-strain response during the shearing phase of the triaxial compression and extension tests is shown in Figures 1 and 2, respectively. The "failure envelopes" (defined as the maximum stress the sample would support at a given confining pressure) for these tests are shown in Figure 3. A higher pressure (8 kilobars) triaxial compression test was performed, but because of the unreasonably low failure strength, this data is not included on the "failure envelope." The low failure is thought to have been caused by an unrepresentative sample. Figure 3 also shows the failure strengths of the crushed samples.

The hydrostatic compression response of the intact sandstone is shown in Figure 4 up to a confining pressure of 8 kilobars.

The uniaxial strain tests (1-D) on intact sandstone is shown in Figure 5. Both a 4 kilobar 1-D and 8 kilobar 1-D are shown along with the 8 kilobar hydrostat for reference. The stress-stress response for the 1-D tests is shown in Figure 6.

Figure 7 shows the mean stress versus volume strain response during hydrostatic and triaxial compression loading for the crushed material. The differential stress versus strain response from these tests is shown in Figure 8. Grain size distributions were also conducted on the material before and after the hydrostatic compression phase of the triaxial compression tests. These distributions are shown in Figure 9. As a note, the data point in Figure 3 at 0.1 kilobars confining pressure was obtained by WES[3] and is shown here for reference.

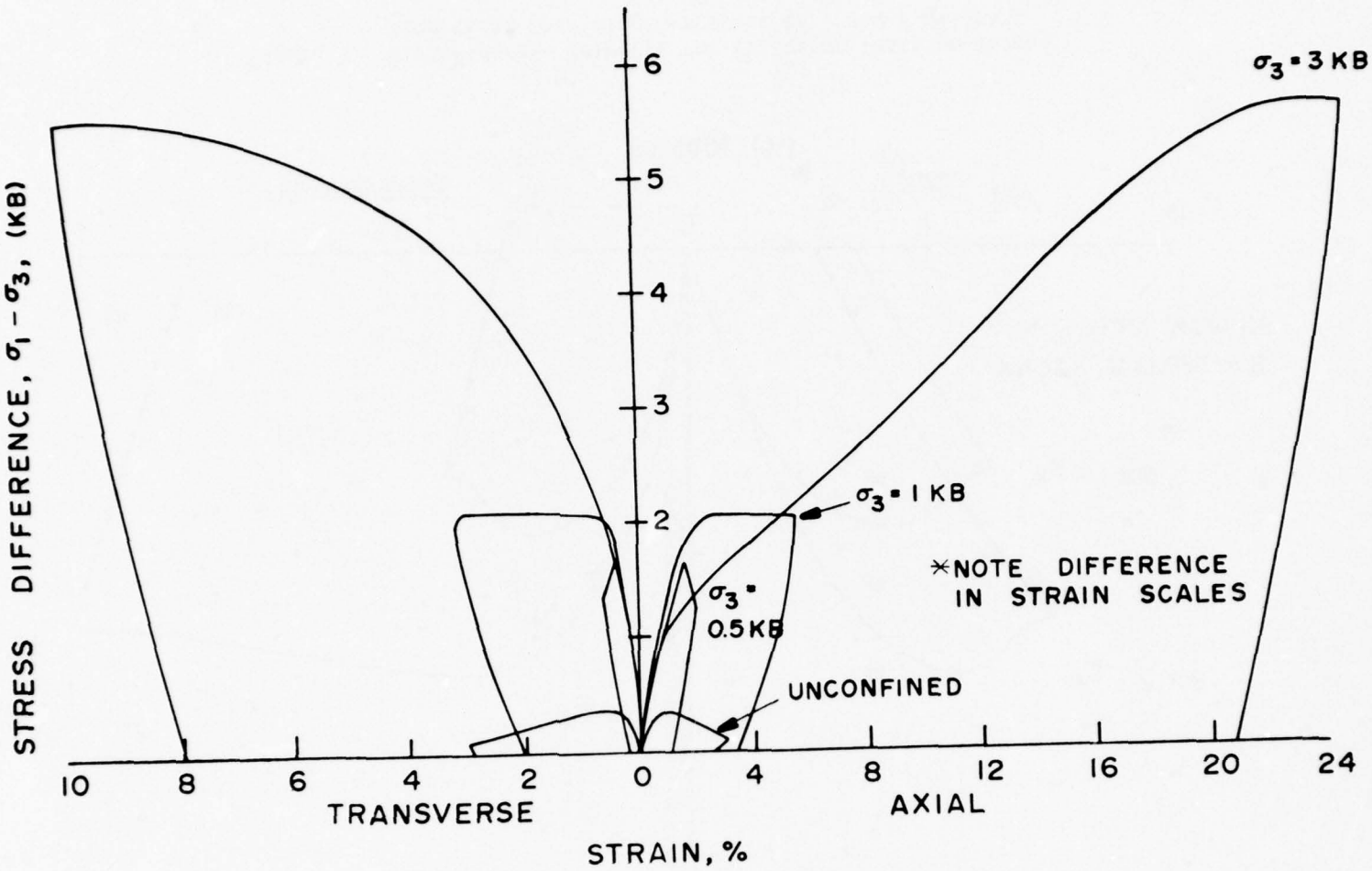

Figure 1. Stress-Strain Response for Triaxial Compression Tests on Intact Samples at Various Confining Pressures.

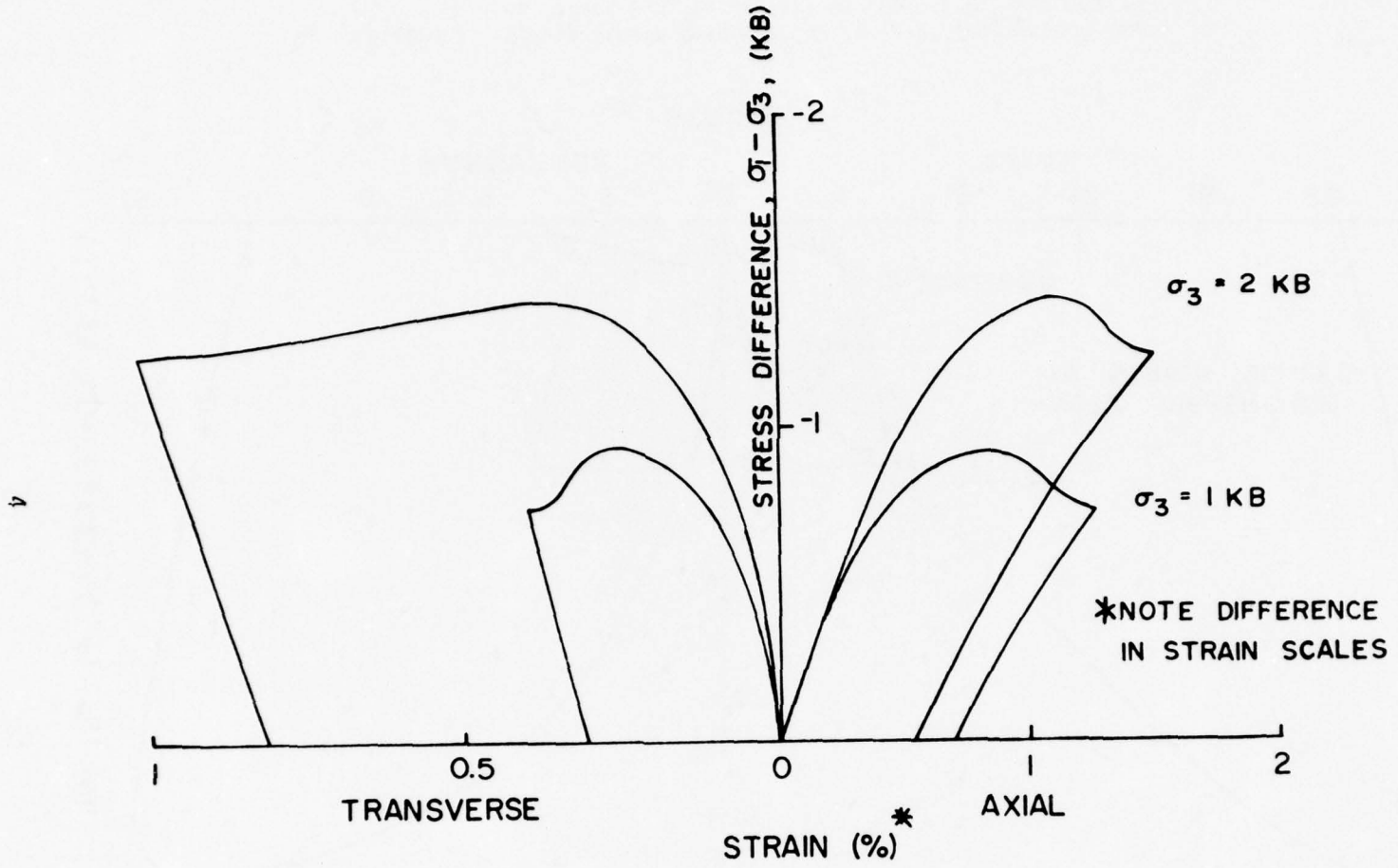

Figure 2. Stress-Strain Response for Extension Tests on Intact Samples at Confining Pressures of 1 and 2 Kilobars.

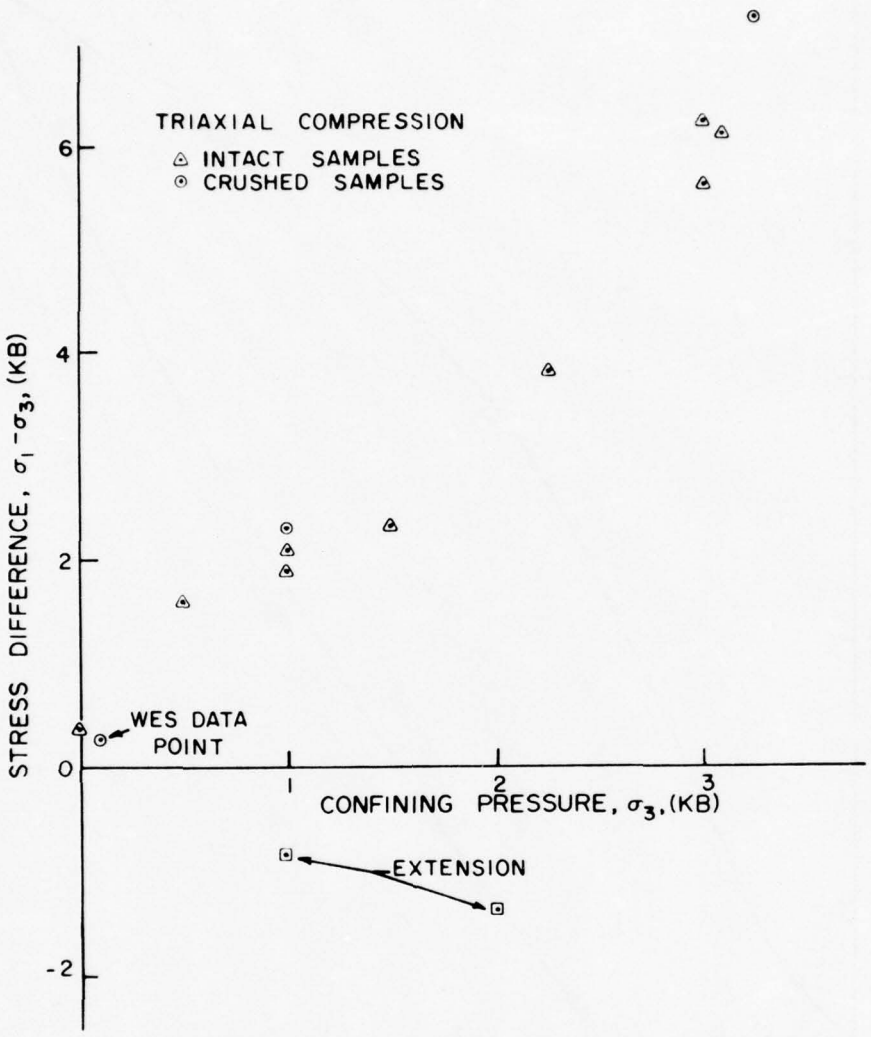

Figure 3. Failure Envelopes Based on Triaxial Compression and Extension Tests.

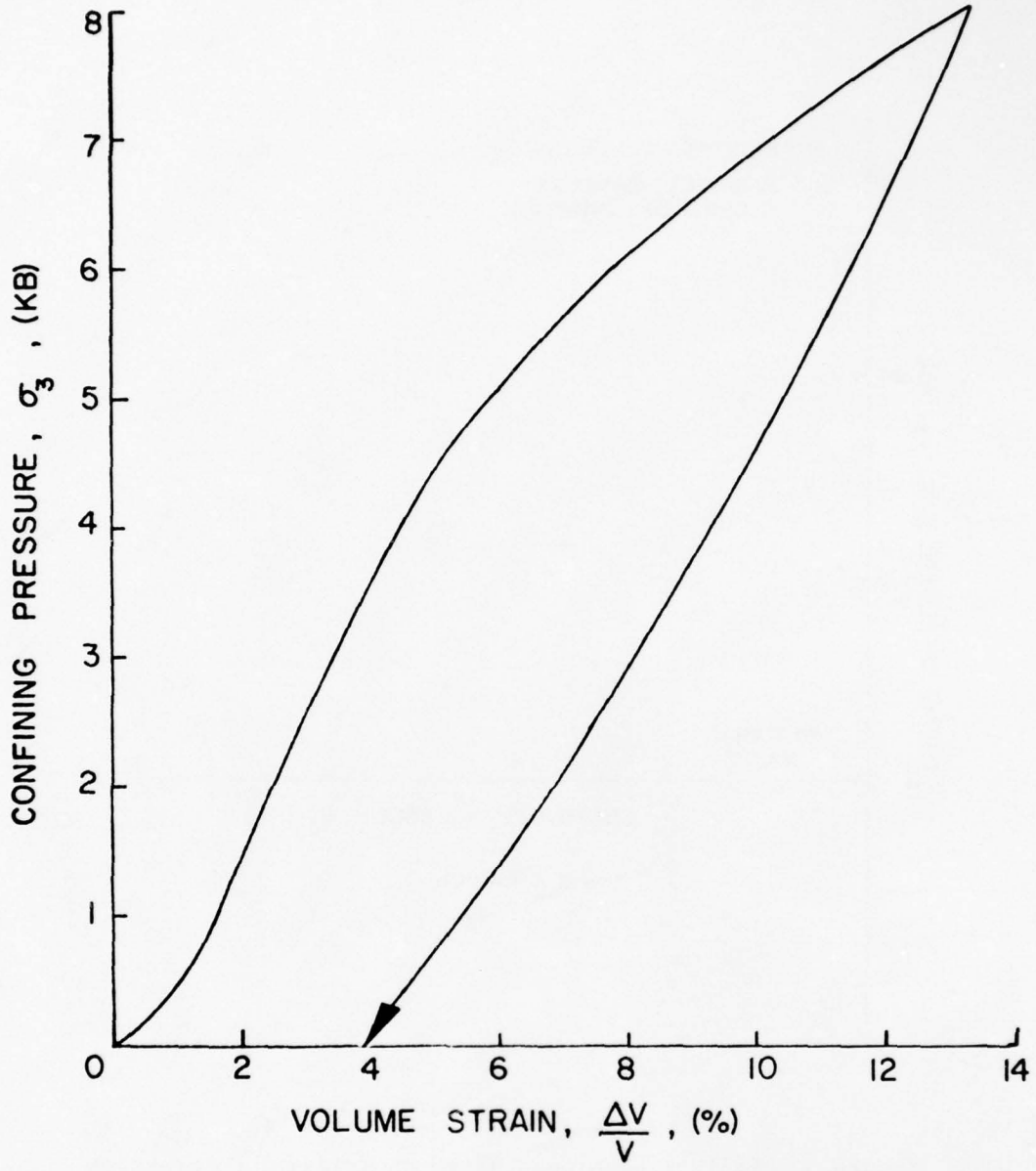

Figure 4: Response of a Typical, Intact Sample to Hydrostatic Pressure.

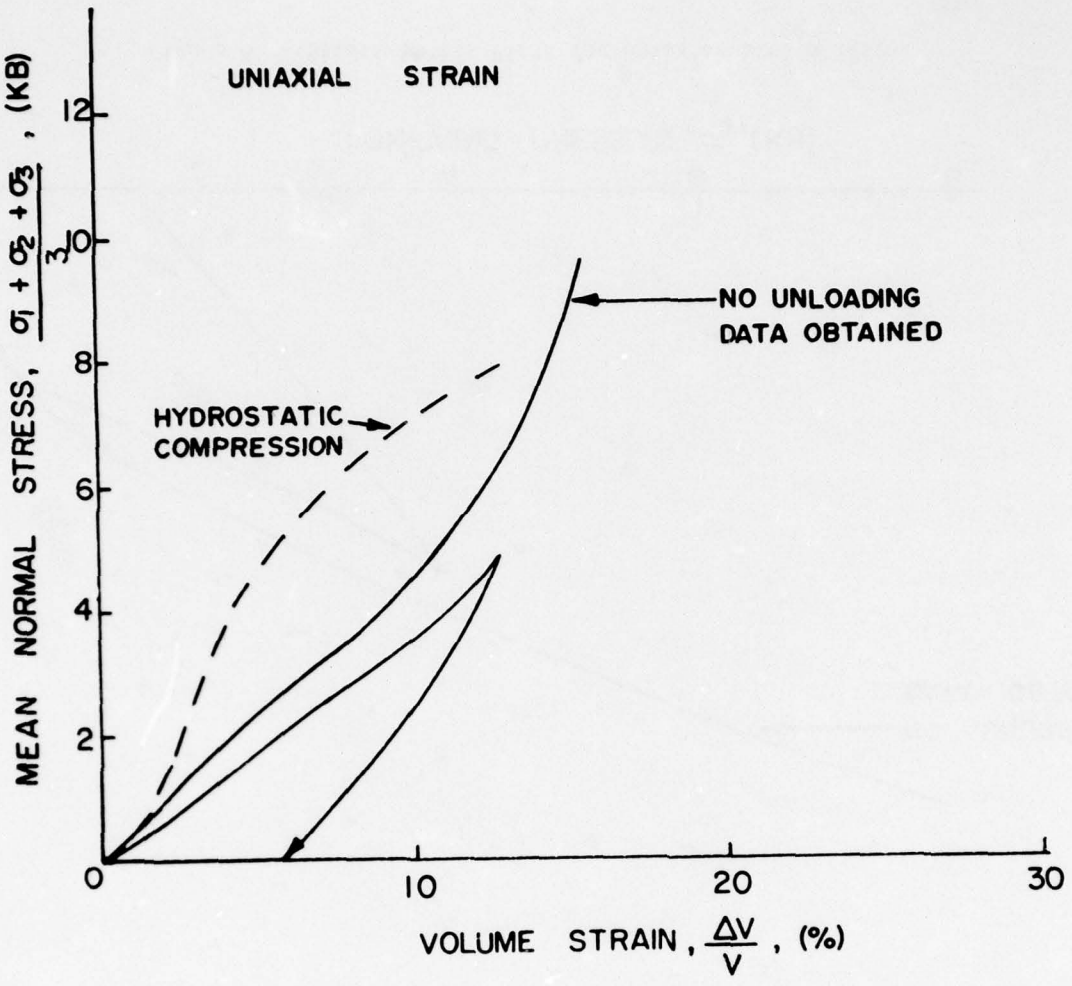

Figure 5. Volume Strain as a Function of Mean Normal Stress for Uniaxial Strain and Hydrostatic Compression Tests.

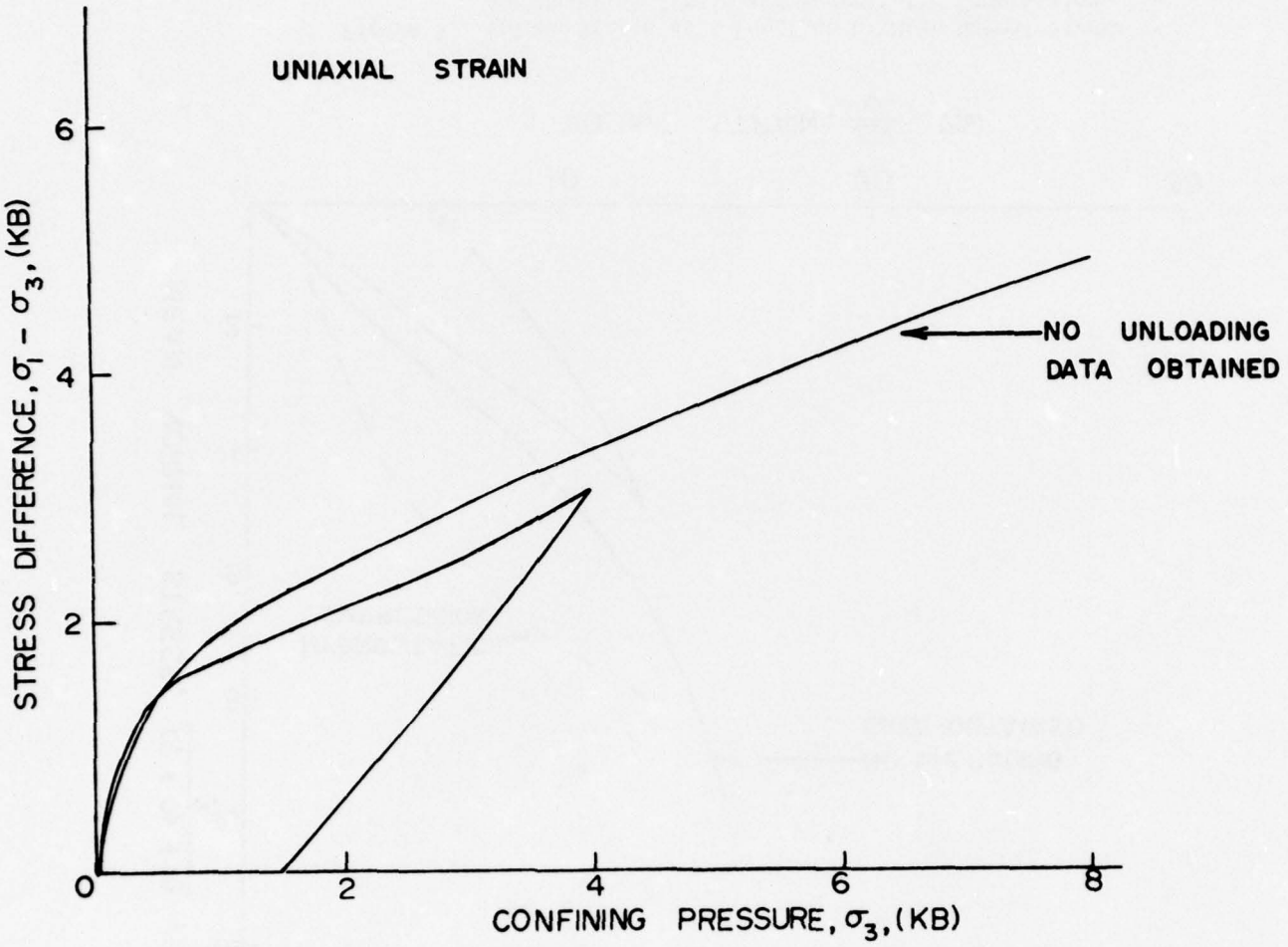

Figure 6. Stress-Stress Plots for Uniaxial Strain Tests.

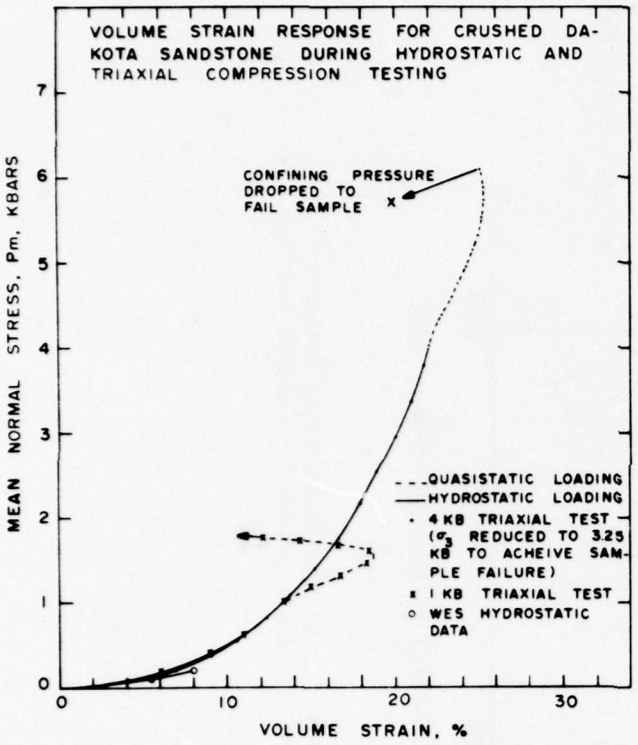

Figure 7. Crushed Dakota sandstone mean stress versus volume strain response during hydrostatic and quasi-static traixial compression loading.

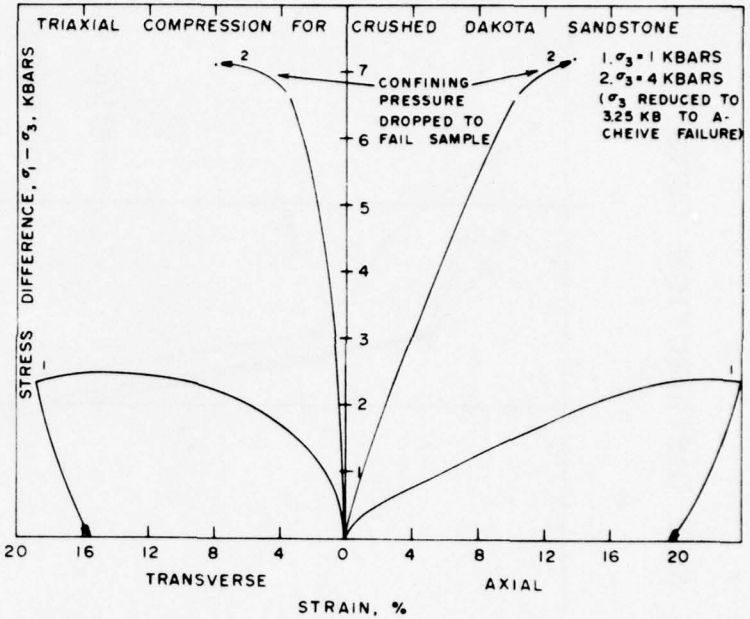

Figure 8. Differential stress versus strain response for triaxial tests conducted at 1 and 4 kilobars on crushed Dakota sandstone. Note that the confining pressure (σ_3) was dropped to 3.25 kilobars at 8 percent axial strain during the 4 kilobar triaxial test in order to fail the sample.

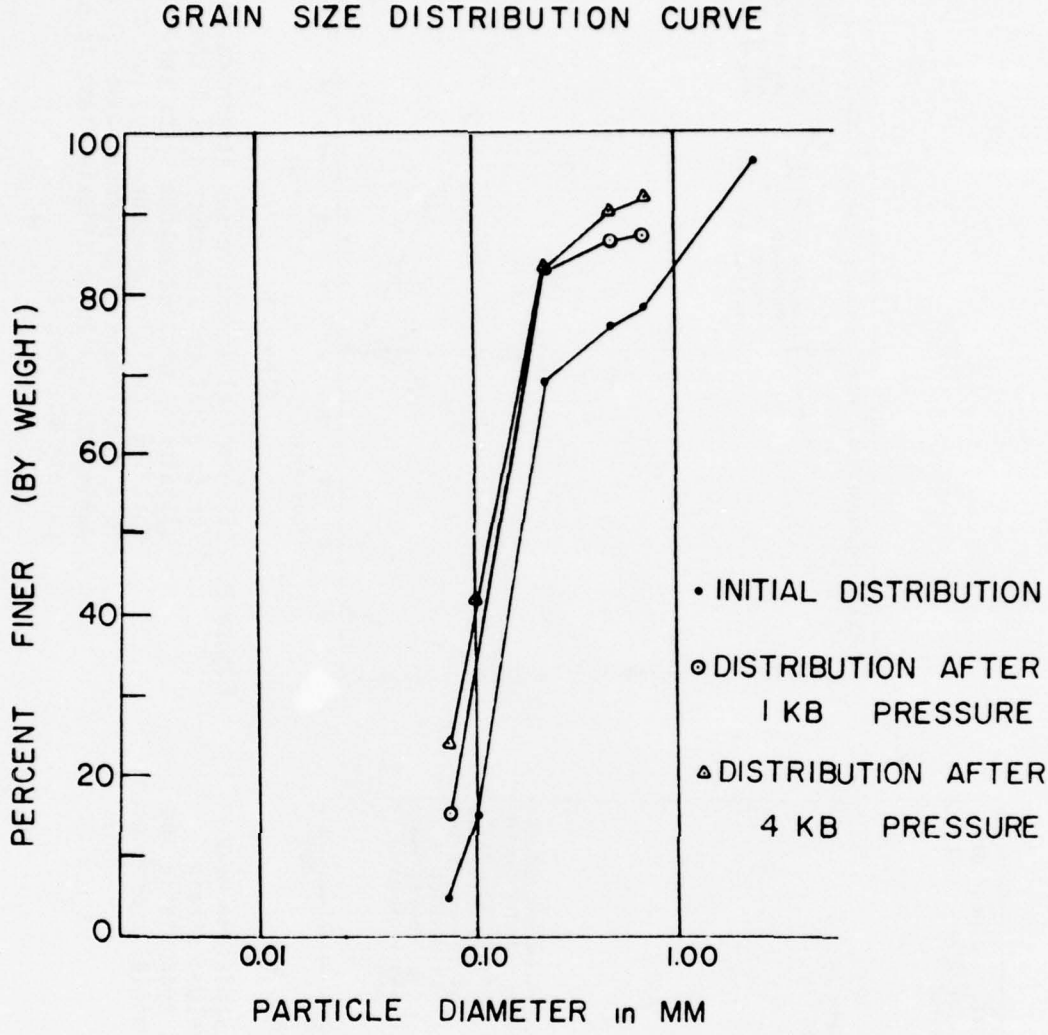

Figure 9: Effects of Hydrostatic Pressure on the Grain Size Distribution for Crushed Sandstone.

DISCUSSION AND CONCLUSIONS

The individual stress-strain curves indicate Young's Modulus doubles as the confining pressure is increased from 0 to 0.5 Kbar as shown in Figure 1. Subsequent increases in confining pressure above 0.5 Kbars show little effect on the Modulus. The data also indicates compaction prior to dilation.

Figure 3 indicates the failure strength increases by a factor of 10 (from 0.5 Kbar to over 5 Kbar) when confining pressure is increased from 0 to 3 Kbar. The shape of the failure surface (as shown in Figure 3) is not typical but repeated tests indicate it is indeed correct.

The failure strength for the crushed material is less than that of the intact material at a confining pressure of 0.1 kilobars (WES data) while at pressures of 1.0 and 3.25 kilobars the failure strengths are equivalent to that of the intact material. This would suggest considerable recompaction of the crushed material during the hydrostatic portion of the tests to the extent that all of the frictional strength of the intact material is regained.

During the hydrostatic compression tests and the uniaxial strain tests on the intact samples, there was considerable volume compaction (hysteresis). This compaction would be expected, however, since the physical properties suggest approximately 20 percent air voids by volume in the material.

REFERENCES

1. Butters, S. W., Johnson, J. N., Swolfs, H. S., Jones, A. H., "Modeling and Properties for Welded Tuff from Mt. Helen - Sandia Test Range, Nevada," Terra Tek Report TR 75-9, January, 1975.

2. Butters, S. W., Dropek, R. K., Green, S. J., Jones, A. H., "Material Properties in Support of the Nevada Test Site Nuclear Test Program," Terra Tek Report TR 75-27, October, 1975.

3. Dr. Dwaine Butler, Waterways Experiment Station.

DISTRIBUTION LIST

Address	No. of Copies
DOD	
Assistant to the Secretary of Defense, Atomic Energy, Washington, D. C. 20301	
ATTN: Donald R. Cotter	1
Director, Defense Advanced Research Projects Agency, Architect Building, 1400 Wilson Blvd., Arlington,	
ATTN: NMRO	1
LTC M. Franklin	1
PMO	1
Technical Library	1
Defense Documentation Center, Cameron Station, Alexandria, Virginia 22314	
ATTN: TC/Myer B. Kahn	12
Director, Defense Intelligence Agency, Washington, D. C. 20301	
ATTN: DI-7E	1
DT-2, Weapons & Systems Division	1
DI-7D, Phys. Vul. Div., Edward O'Farrell	1
Technical Library	1
Defense Mapping Agency, Washington, D. C. 20305	
ATTN: H. Lindsey	1
Director, Defense Nuclear Agency, Washington, D. C. 20305	
ATTN: STSI (Archives)	1
STTL (Technical Library)	2
SPSS	15
DDST	1
Director of Defense Research and Engineering, Washington, D. C. 20301	
ATTN: Assistant Director, Strategic Weapons	1
Deputy Director, Strategic Systems	1
M. J. Minneman	1
George Barse	1
Craig W. Hartsell	1
R. Thorkildsen	1
Deputy Director, Tactical Warfare	1

Address	No. of Copies
DOD (Continued)	
Commander, Field Command, Defense Nuclear Agency, Kirtland Air Force Base, New Mexico 87115	
ATTN: FCPR	1
Interservice Nuclear Weapons School, Kirtland Air Force Base, New Mexico 87115	
ATTN: Technical Library	1
Director, Joint Strategic Target Planning Staff, JCS, Offutt Air Force Base, Nebraska 68113	
ATTN: Science and Technology Info Library	1
Army	
Assistant Chief of Staff for Force Development, Department of the Army, Washington, D. C. 20310	
Technical Library	1
Office, Chief of Engineers, Department of the Army, Washington, D. C. 20314	
ATTN: DAEN-ASI-L	2
DAEN-MCE-D	2
DAEN-RDL	1
Office, Chief of Research, Development, and Acquisition, Department of the Army, Washington, D. C. 20310	
ATTN: DAMA-CSM/LTC Edward V. DeBoesser, Jr.	1
Technical Library	1
Commander, Harry Diamond Laboratories, 2800 Powder Mill Road, Adelphi, Maryland 20783	
ATTN: AMXDO-NP	1
F. Vrateric	1
AMXDO-RBH/J. Gwaltney	1
Project Manager, Remotely Monitored Battlefield Sensor System, AMC, Fort Monmouth, New Jersey 07703	
ATTN: Chuck Higgins	1
Commanding Officer, Picatinny Arsenal, Dover New Jersey 07801	
ATTN: P. Angelloti	1
Technical Library	1
SMUPA-ND-S/E. Zimpo	1

Address	No. of Copies
Army (Continued)	
Ray Goldstein	1
Ray Moessner	1
Jerry Pental	1
SUMPA-AD-D-A-7	1
SUMPA-AD-D-A	1
SUMPA-AD-D-M	1
Director, U. S. Army Ballistic Research Laboratories, Aberdeen Proving Ground, Maryland 21005	
ATTN: AMXBR-X/J. J. Meszaros	1
AMXBR-TB/J. T. Frasier	1
W. J. Taylor	1
D. Dunn	1
G. Grabarek	1
G. Roecker	1
Technical Library/Edward Baicy	2
Commander/Director, U. S. Army Cold Regions Research and Engineering Laboratory, P. O. Box 282, Hanover, New Hampshire 03755	
ATTN: G. Swinzow	1
Division Engineer, U. S. Army Engineer Division, Huntsville, P. O. Box 1600, West Station, Huntsville, Alabama 35807	
ATTN: HNDED-CS/Michael M. Dembo	1
Division Engineer, U. S. Army Engineer Division, Ohio River, P. O. Box 1159, Cincinnati, Ohio 45201	
ATTN: ORDAS-L/Technical Library	1
Director, U. S. Army Engineer Waterways Experiment Station, P. O. Box 631, Vicksburg, Mississippi 39180	
ATTN: Mr. D. K. Butler	1
Mr. William J. Flathau	1
Mr. John Strange	1
Library	3
Dr. Paul Hadala	1
Dr. Guy Jackson	1
Dr. Behzad Rohani	1
Mr. R. S. Bernard	1
Mr. D. C. Creighton	1
Commander, U. S. Army Materials and Mechanics Research Center, Watertown, Massachusetts 02172	
ATTN: Technical Library	1

Address	No. of Copies
Army (Continued)	
Director, U. S. Army Material Systems Analysis Agency, U. S. Army Aberdeen R&D Center, Aberdeen Proving Ground, Maryland 21005	
ATTN: J. Sperazza	1
M. Reches	1
Commander, U. S. Army Mobility Equipment R&D Center, Fort Belvoir, Virginia 22060	
ATTN: STSFB-MW	1
STSFB-XS	1
Technical Library	1
Commandant, U. S. Army Engineer School, Fort Belvoir, Virginia 22060	
ATTN: S. Grazier	1
Commander, U. S. Army Materiel Development and Readiness Command, 5001 Eisenhower Avenue, Alexandria, Virginia 22333	
ATTN: Technical Library	1
DRCRD-BN	2
DRCRD-WN	2
Commander, U. S. Army Missile Command, Redstone Arsenal, Alabama 35809	
ATTN: Technical Library	1
F. Fleming	1
AMCPM-PE-X (William K. Jann)	1
Commander, U. S. Army Nuclear Agency, Fort Bliss, Texas 79916	
ATTN: Document Control	1
Technical Library	1
COL Quinn	1
MAJ F. P. Weichel	1
Commander, U. S. Army Armament Command, Rock Island Arsenal, Rock Island, Illinois 61201	
ATTN: Technical Library	1
COL C. Treat	1
Division Engineer, U. S. Army Engineer Division, Missouri River, P. O. Box 103, Downtown Station, Omaha, Nebraska 68101	
ATTN: Library	1

Address	No. of Copies
Navy	
Chief of Naval Research, Department of the Navy, Arlington, Virginia 22217	
ATTN: Technical Library	1
Officer in Charge, Civil Engineering Laboratory, Naval Construction Battalion Center, Port Hueneme, California 93043	
ATTN: R. J. Odello	1
Technical Library	1
Director, Naval Research Laboratory, Washington, D. C. 20375	
ATTN: Code 2027/Tech Library	1
Commander, Naval Surface Weapons Center, White Oak, Silver Spring, Maryland 20910	
ATTN: Mr. Kasdorf	1
Technical Library, Code 730	1
Code 1224 Navy Nuc Prgms Off	1
L. Roslund	1
G. Briggs	1
Commander, Naval Surface Weapons Center, Dahlgren Laboratory, Dahlgren, Virginia 22448	
ATTN: Technical Library	1
William Wisherd	1
Ted Williams	1
Commander, Naval Weapons Center, China Lake, California 93555	
ATTN: Code 603, Dr. Carl Austin	1
Code 533, Technical Library	1
Commander, Naval Weapons Evaluation Facility, Kirtland Air Force Base, Albuquerque, New Mexico 87117	
ATTN: Technical Library	1
Air Force	
Air Force Armament and Testing Laboratory, AFSC, Eglin Air Force Base, Florida 32542	
ATTN: Technical Library	1
MAJ Thomas Tomasetti	1
Mr. John Collins	1

Address	No. of Copies
Air Force (Continued)	
ATTN: Mr. Masey Valentine	1
Mr. William Cramer	1
Dr. Kulp	1
Commander, Air Force Weapons Laboratory, AFSC, Kirtland Air Force Base, New Mexico 87117	
ATTN: SUL, Technical Library	1
DEV	1
Headquarters, Air Force Systems Command, Andrews Air Force Base, Washington, D. C. 20331	
ATTN: Technical Library	1
Project Manager, Gator Mine Program, Eglin Air Force Base, Florida 32542	
ATTN: E. J. Lindsey	1
Oklahoma State University, Field Office for Weapons Effectiveness, P. O. Box 1925, Eglin Air Force Base, Florida 32542	
ATTN: Ed Jackett	1
Commander, Armament Development and Test Center, Eglin Air Force Base, Florida 32542	
ATTN: Technical Library	1
Commander, Foreign Technology Division, AFSC, Wright-Patterson Air Force Base, Ohio 45433	
ATTN: TD-BTA Library	1
Space and Missile Systems Organization, Norton Air Force Base, California 92409	
ATTN: DEB	1
U. S. Energy Research and Development Administration	
U. S. Energy Research and Development Administration, Albuquerque Operations Office, P. O. Box 5400, Albuquerque, New Mexico 87115	
ATTN: Doc Control for Technical Library	1
U. S. Energy Research and Development Administration, Nevada Operations Office, P. O. Box 14100, Las Vegas, Nevada 89114	
ATTN: Doc Control for Technical Library	1

Address	No. of Copies
U. S. Energy Research and Development Administration (Continued)	
Los Alamos Scientific Laboratory, P. O. Box 1663, Los Alamos, New Mexico 87544	
ATTN: Doc Control for Reports Library	1
Doc Control for Tom Dowler	1
Doc Control for C. Cremer	1
Doc Control for G. Dials	1
Sandia Laboratories, Livermore Laboratory, P. O. Box 969, Livermore, California 94550	
ATTN: Doc Control for T. Gold	1
Doc Control for Technical Library	1
Sandia Laboratories, P. O. Box 5800, Albuquerque, New Mexico 87115	
ATTN: Doc Control for Dr. Walter Herrmann	1
Doc Control for John Colp	1
Doc Control for John Keizur	1
Doc Control for William Patterson	1
Doc Control for William Caudle	1
Doc Control for 3141 Sandia Rpt Coll	1
Doc Control for W. Altsheimer	1
Director, Lawrence Livermore Laboratory, P. O. Box 808, Livermore, California 94550	
ATTN: Technical Information Division, Technical Library	1
Larry Woodruff, L-125	1
Doc Control for W. Scanlin	1
Frank Walker	1
Mark Wilkins	1
Other Government Agencies	
Electric Power Research Institute, 3412 Hillview Avenue, Palo Alto, California 94303	
ATTN: Dr. George Sliter	1
Office of Nuclear Reactor Regulation, Nuclear Regulatory Commission, Division of Technical Review, Washington, D. C. 20555	
ATTN: Dr. Robert Heineman, Director	1
Mr. Lawrence Shao, Chief, Struc Engrg Br	1

Address	No. of Copies
DOD Contractors	
Aerospace Corporation, P. O. Box 92957, Los Angeles, California 90009	
ATTN: Technical Information Services	
Applied Theory Incorporated. 1010 Westwood Boulevard, Los Angeles, California 90024	
ATTN: Dr. John G. Trulio	2
AVCO, Government Products Group, 201 Lowell Street, Wilmington, Massachusetts 01887	
ATTN: David Henderson	1
Research Library A830, Room 7201	1
Bell Telephone Laboratories, Inc., Mountain Avenue, Murray Hill, New Jersey 07974	
ATTN: Technical Report Center	1
Boeing Company, P. O. Box 3707, Seattle, Washington 98124	
ATTN: Aerospace Library	1
Reynold Atlas	1
California Research and Technology, Inc., 6269 Variel Avenue, Woodland Hills, California 91364	
ATTN: Dr. K. N. Kreyenhagen	1
Technical Library	1
Civil/Nuclear Systems Corporation, 1200 University N.E., Albuquerque, New Mexico 87102	
ATTN: Robert Crawford	1
General Dynamics Corporation, Pomona Operation, P. O. Box 2507, Pomona, California 91766	
ATTN: Keith Anderson	1
General Electric Company, TEMPO-Center for Advanced Studies, 816 State Street, Santa Barbara, California 93102	
ATTN: DASIAC	1
IIT Research Institute, 10 West 35th Street, Chicago, Illinois 60616	
ATTN: Technical Library	1
Institute for Defense Analyses, 400 Army-Navy Drive, Arlington, Virginia 22202	
ATTN: IDA Librarian Ruth S. Smith	1

Address	No. of Copies
DOD Contractors (Continued)	
Consulting and Special Engineering Services, Inc., P. O. Box 1206, Redlands, California 92373	
ATTN: Dr. J. L. Merritt	1
Kaman Avidyne, Division of Kaman Sciences Corp., 83 Second Avenue, Northwest Industrial Park, Burlington, Massachusetts 01803	
ATTN: Technical Library	1
Lockheed Missiles and Space Company, 3251 Hanover Street, Palo Alto, California 94304	
ATTN: Tech Info Center D/Coll	1
Lockheed Missiles and Space Company, Inc., P. O. Box 504, Sunnyvale, California 94088	
ATTN: Technical Library	1
Martin Marietta Aerospace, Orlando Division, P. O. Box 5837, Orlando, Florida 32805	
ATTN: M. Anthony	1
Gerbert E. McQuaig (MP-81)	1
University of New Mexico, Dept of Campus Security and Police, 1821 Roma N.E., Albuquerque, New Mexico 87106	
ATTN: *G. E. Triandafalidis*	1
Physics International Company, 2700 Merced Street, San Leandro, California 94577	
Doc Control for Technical Library	1
Doc Control for Mr. Larry Behrman	1
R&D Associates, P. O. Box 9695, Marina Del Rey, California 90291	
ATTN: Dr. Harold L. Brode	1
Dr. H. F. Cooper, Jr.	1
Technical Library	1
Dr. C. P. Knowles	1
Mr. J. G. Lewis	1
Systems, Science and Software, P. O. Box 1620, La Jolla, California 92037	
ATTN: Dr. Donald R. Grine	1
Dr. E. W. Gaffney	1
Technical Library	1

Address	No. of Copies
DOD Contractors (Continued)	
Terra Tek, Inc., University Research Park, 420 Wakara Way, Salt Lake City, Utah 84108	
ATTN: Mr. S. J. Green	1
Technical Library	1
Mr. S. W. Butters	10
Texas A&M University, c/o Texas A&M Research Foundation, P. O. Box 3222, Bryan, Texas 77801	
ATTN: Harry Coyle	1
Texas A&M University, Department of Civil Engineering, College Station, Texas 77843	
ATTN: Prof. L. J. Thompson	1
Braddock, Dunn, & McDonald, Inc., 1920 Aline Ave., Vienna, Virginia 22180	
ATTN: Technical Library	1
TRW Systems Group, One Space Park, Redondo Beach, California 90278	
ATTN: Tech Info Center/S-1930	1
Weidlinger Associates, Consulting Engineers, 110 East 59th Street, New York, New York 10022	
ATTN: Dr. Melvin L. Baron	1
Weidlinger Associates, Consulting Engineers, 2710 Sand Hill Road, Suite 230, Menlo Park, California 99025	
ATTN: Dr. J. Isenberg	1
Lowell Technical Institute, Department of Civil Engineering, Lowell, Massachusetts 01854	
ATTN: L. W. Thigpen	1
Georgia Institute of Technology, Department of Aerospace Engineering, Atlanta, Georgia 30332	
ATTN: S. V. Hanagud	1
L. N. Rehfield	1
Pacifica Technology, Inc., P. O. Box 148, Del Mar, California 92014	
ATTN: G. I. Kent	1
R. L. Bjork	1

Address	No. of Copies

Domestic Exchange

Tennessee Valley Authority, 400 Commerce Avenue, W9D224, Knoxville, Tennessee 37902 ATTN: Ronald G. Domer, Chief, Civil Engineering Branch	1

In accordance with ER 70-2-3, paragraph 6c(1)(b), dated 15 February 1973, a facsimile catalog card in Library of Congress format is reproduced below.

Butler, Dwain K

Constitutive property investigations in support of full-scale penetration tests in Dakota sandstone, San Ysidro, New Mexico, by D. K. Butler, R. R. Nielsen, R. K. Dropek, [and] S. W. Butters. Vicksburg, U. S. Army Engineer Waterways Experiment Station, 1977.

1 v. (various pagings) illus. 27 cm. (U. S. Waterways Experiment Station. Technical report S-77-3)

Prepared for Defense Nuclear Agency, Washington, D. C., under DNA Subtask SB211, Work Unit 11, Field Firing Material Testing, and Contract No. DNA 001-75-C-0177.

Appendix D: Terra Tek, Inc., TR 75-60, Some properties of sandstone from the penetrator test site, San Ysidro, New Mexico.

Includes bibliography.

1. Constitutive models. 2. Projectile penetration. 3. Sandstones. 4. Soil penetration tests. 5. Stress-strain relations (Rock). I. Butters, S. W., joint author. II. Dropek, R. K., joint author. III. Nielsen, R. R., joint author. IV. Defense Nuclear Agency. V. Terra Tek, Inc. (Series: U. S. Waterways Experiment Station, Vicksburg, Miss. Technical report S-77-3)
TA7.W34 no.S-77-3